

UC Davis

UC Davis Electronic Theses and Dissertations

Title

Physical dynamics influencing dissolved oxygen over the shelf in the central and northern California Current System

Permalink

<https://escholarship.org/uc/item/6jh4s3gp>

Author

Hewett, Kathryn M.

Publication Date

2022

Peer reviewed|Thesis/dissertation

Physical dynamics influencing dissolved oxygen over the shelf in the central and northern
California Current System

By

KATHRYN M. HEWETT
DISSERTATION

Submitted in partial satisfaction of the requirements for the degree of

DOCTOR OF PHILOSOPHY

in

Hydrologic Sciences

in the

OFFICE OF GRADUATE STUDIES

of the

UNIVERSITY OF CALIFORNIA

DAVIS

Approved:

John L. Largier, Chair

Alexander L. Forrest

Sarah N. Giddings

Committee in Charge

2022

Copyright © by

Kathryn M. Hewett

2022

Table of Contents

List of Figures	v
List of Tables	xiii
Abstract	xiv
Dedication	xx
Acknowledgments	xxi
1 Introduction	1
1.1 Eastern Boundary Upwelling Systems	2
1.2 The California Current System	4
1.2.1 Winds and Regions	4
1.2.2 Shelf water mass properties and currents	5
1.2.3 Productivity and DO	8
1.2.4 Hypoxia thresholds	12
1.3 Outline	13
2 Observations of shelf hypoxia off northern California	17
2.1 Introduction	17
2.2 Data sources and processing	22
2.2.1 Mooring data	22
2.2.2 Buoy data – wind and temperature	23
2.2.3 Seasonality of coastal upwelling	24
2.2.4 Bottom DO and wind stress	25
2.2.5 Marine heatwave conditions and the California drought	26
2.3 Results	27
2.3.1 Coastal upwelling seasonality	27
2.3.2 Mid-shelf site, Gulf of the Farallones, GF (54 m)	31
2.3.3 Inner shelf sites, BH (30 m) and RP (18 m)	35
2.4 Discussion	37

2.4.1	Upwelling source waters	38
2.4.2	Upwelling seasonality and relaxation events	42
2.4.3	Oxygen uptake over the shelf	43
2.4.4	The 2012 – 2016 California drought	46
2.4.5	2015 marine heatwave conditions	48
2.5	Conclusions	48
3	Seasonality of near-bottom dissolved oxygen over a submarine bank off northern California	53
3.1	Introduction	53
3.2	Data sources and processing	54
3.2.1	Mooring data	54
3.2.2	Satellite chlorophyll concentrations	56
3.2.3	Atmospheric data	56
3.2.4	Hypoxia thresholds	60
3.3	Results	60
3.3.1	Cordell Bank Mooring Data	60
3.3.2	Winds and satellite chlorophyll concentration	62
3.4	Discussion	66
3.4.1	Regional productivity and DO levels	69
3.4.2	Winds and DO levels	71
3.4.3	Synthesis of winds, productivity and DO	73
3.4.4	Source Water Variability	79
3.5	Conclusions	82
4	Interannual variability in shelf hypoxia off the Washington coast	84
4.1	Introduction	84
4.1.1	The California Current System	86
4.2	Data and methods	91
4.2.1	Oceanographic data	91
4.2.2	River data	95
4.2.3	Atmospheric data	100
4.3	Observations	102
4.3.1	OCNMS hypoxia observations across 2011 - 2020	102
4.3.2	Anomalous hypoxia in 2017: winds, rivers and mooring data	105
4.3.3	Columbia and Fraser River discharge	109
4.4	Discussion	114
4.4.1	Stratification and DO	114
4.4.2	Anomalous summertime T-S-DO conditions	119
4.4.3	Variability of bottom water T-S-DO	124
4.4.4	Timing of spring transition and river flow	127
4.5	Conclusions	133
5	Summary	136
	<i>Reference List</i>	144

List of Figures

1.1	Map of the California Current System	This figure presents major currents and water mass locations, and is based on content presented in Checkley and Barth (2009); Thomson and Krassovski (2010); and Talley et al. (2011). Water mass descriptions are in Table 1.1 and approximate location shown on in this figure. Surface currents (gold arrows) and undercurrents (black arrows) shown include the (1) Alaskan Stream; (2) Alaska Current; (3) North Pacific Current; (4) California Current (shown as 2 arrows); (5) California Undercurrent; (6) North Equatorial Current; (7) North Equatorial Countercurrent; and (8) Equatorial Undercurrent. Coastal jets (9) form on the shelf and shown as red arrows. Freshwater input (10) (blue arrows at the Salish Sea and Columbia River) is greater in the northern CCS than the central and southern CCS. The strongest upwelling-favorable winds occur in the central CCS (off Bodega Head near N13 and south of Point Sur; see Figure 2.1). Approximate boundaries for the three CCS regions are shown by white lines. CCS region text is placed offshore and in the North Pacific Gyre, but the regions are physically located to the east of each text label, adjacent to the west coast and include (4), (5) and (9).	6
2.1	Site map	Mooring locations shown (blue triangles); CTD+DO cast locations (small red circles); Wind buoy NDBC46013 (N13) and 46026 (N26) marked by yellow circles. Contours shown on both maps: 40, 80, 130, 200, 500, 1000 m. Bold contour is 200 m.	21
2.2	Cross-correlation of hourly alongshore wind stress at N13 and bottom DO at BH, showing the results of correlations between filtered alongshore wind stress (W_k) and near-bottom DO at BH. Data used were collected between February – October 2015. The correlation coefficient, R, shown is normalized so that the autocorrelation at zero lag equals 1. A range of k values were analyzed between 1 hour - 240 hours (10 days). Max R for each k-value is shown. Wind data were collected at hourly intervals; therefore, we sampled the DO time-series at hourly increments prior to comparison. If only upwelling dominated months April – May are considered, k is still 2-days but R increases from 0.56 (February – October) to 0.67 (April – May).	26	

2.3	2015 alongshore wind stress, SST and mooring bottom temperature time-series	This figure presents (a) low-pass filtered alongshore wind stress at N13 (grey) and W_2 (red, downwelling favorable; blue upwelling favorable). Approximate seasonal transitions shown above subplot (a): the storm season (purple bar), upwelling season (yellow bar); and relaxation season (green bar). (b) SST at N13 (black line) shown with MHW presence flagged following Sanford et al. (2019). Shading, either grey or red, marks periods where the 2015 temperature at N13 exceeded the 90th percentile based on a 30-year record at N13 (1981 – 2011) for ≥ 5 days. Red shading represents one of 10 most intense events since 1981. For reference, the mean SST for 2015 is shown by a dashed horizontal line (13.15°C) and 9°C is also shown. (c) time-series of bottom temperature for each mooring site are shown: BH (gold) and RP (blue) on left y-axis, and GF (dark grey) on right y-axis. Using left y-axis as a reference, dashed horizontal lines are shown at 10.5°C (max right y-axis) and 9°C . Vertical black lines mark the first of each month in all subplots (a-c). Temperature and τ are low-pass filtered. Both asterisks on (a) denote relaxation events discussed in the Results section. Date tick marks are spaced at 8-day increments.	28
2.4	BH ($\sim 30\text{ m}$) and RP ($\sim 18\text{ m}$) mooring data.	This figure presents time-series of bottom DO (a) and temperature (b) at RP (blue line) and BH (yellow line). Alongshore wind stress at N13 (grey) and W_2 (blue upwelling favorable) are shown in (c). Approximate seasonal transitions shown above upwelling season (yellow bar); and relaxation season (green bar). All data presented, except W_2 , is low-pass filtered. Hypoxic thresholds are shown in subplot (a) mark severe (darkest grey); intermediate (grey); mild (lightest grey) hypoxia. Duration of intermediate hypoxia BH $\sim 1\text{-}2$ days. (a). Brown shading is provided to aid discussion of upwelling events (shaded). Relaxation events are not shaded, but generally follow upwelling events and feature decelerating winds (W_2 approaching zero). Trend arrows are shown on one upwelling/relaxation event (in April/May).	29
2.5	Gulf (GF 54 m) mooring data.	This figure presents time-series of bottom DO (black line, a); spiciness (black line) and sigma-theta (right axis, blue) (b); temperature at 1m, 15m and 54m from the GF mooring site. $\Delta T \Delta Z^{-1}$ (using surface and bottom temperature) is shown (grey line, a) for comparison with DO. Alongshore wind stress at N13 (grey) and W_2 (blue upwelling favorable) are shown in (d). Approximate seasonal transitions shown above upwelling season (yellow bar); and relaxation season (green bar). All data presented, except W_2 , is low-pass filtered. Hypoxic thresholds are shown in subplot (a) mark severe (darkest grey); intermediate (grey); mild (lightest grey) hypoxia. Duration of intermediate hypoxia: ~ 3.5 days; ~ 4 days; ~ 8.2 days; and ~ 3.6 days (in order of occurrence) (a). Pink shading across each subplot highlights a relaxation event discussed in the results section.	32

2.6	Spiciness – DO relationship for outer shelf and slope water. This figure shows spiciness (π) and DO data collected over the outer shelf and slope during ACCESS cruises (2014 – 2015). Depth-averaged CTD data were used to calculate spiciness. 45 casts are shown collected during June, July and September 2014 – 2015. Locations shown on Figure 1. Depths shallower than 50m are not shown. Max depth 200m. Salinity range: 33.3 - 34.3 $g\ kg^{-1}$. Temperature range: 8.5 - 11.7 °C.	41
3.1	Site map and Cordell Bank mooring coverage. (a) Cordell Bank mooring locations shown (triangles); Wind buoy NDBC46013 (N13) marked by yellow circle. Contours shown on both maps: 40, 80, 130, 200, 500, 1000 m. Bold contour is 200 m. Approximate location satellite chlorophyll data were clipped to include the shaded green region, see section 3.2.2). (b) Coverage for mooring data shown. Color corresponds to each mooring location, CB2 (blue) and CB1 (yellow). DO and temperature are available for each ‘.’ in the coverage plot, and salinity is available (in addition to DO-T) for years 2016 - 2018 at CB2.	57
3.2	Near-bottom DO and temperature at Cordell Bank. Mirrored histograms of observed bottom DO and temperature for years 2014 – 2018 binned by month are presented for both mooring locations CB1 (a & c: ~ 80 m; yellow) and CB2 (b & d: ~ 100 m; blue). Data coverage for each site is provided in Figure 3.1. Bin widths for each mirrored histogram are 0.1 $mL\ L^{-1}$ between 1 and 7 $mL\ L^{-1}$ and 0.1 °C between 8 and 13°C. The 25th/50th/75th percentiles are marked with black lines. Mild hypoxia is shaded light grey; intermediate hypoxia shaded dark grey. Data presented are all low-pass filtered with a cutoff period of 33 hours (see section 3.2.1).	61
3.3	Time-series of near-bottom DO and temperature at Cordell Bank. Temperature and DO data from CB1 (a & c: ~ 80 m) and CB2 (b & d: ~ 100 m) across deployments (2014 - 2018) are shown. Mild hypoxia is shaded light grey; intermediate hypoxia shaded dark grey. A horizontal line marks 8.5°C water in c & d. Data presented are all low-pass filtered with a cutoff period of 33 hours (see section 3.2.1).	63
3.4	Winds and satellite chlorophyll concentration. This figure presents the 8-day upwelling index, W_8 , for alongshore wind stress calculated from winds at N13 (a). Negative values (blue W_8) are upwelling favorable winds while positive values (red W_8) are downwelling favorable. The natural log of the median chlorophyll-a (chl-a) concentration are shown (b). Chl-a values shown represent median values calculated for each 4km section of shelf between 37°N and 39°N and to a distance of 100 km offshore from the coastline. If coverage was < 60% a median value is not presented.	64
3.5	Surface boundary layer depth summary statistics estimated from hourly N13 wind data using the Ekman layer scale, $\delta_{Et} \propto \delta_s$. Summary statistics represent the 10th, 90th, 75th, 25th and 50th percentiles grouped by month including data during the period 2014 - 2018.	74

3.6	Surface boundary layer depth - monthly	This figure shows summary statistics for the surface boundary layer depth, estimated from hourly N13 winds using the Ekman layer scale, $\delta_{Et} \propto \delta_s$. Summary statistics represent the 25th & 75th percentiles (thin black lines) and 50th percentile (thicker yellow line). Data are grouped by month and year (2014 - 2019). Median values are shaded yellow. The median Ekman layer scale is $\sim 30\text{m}$ (across all months and years), which is provided for reference as a black dashed line in each subplot.	75
3.7	2015 alongshore wind stress, SST and CB mooring bottom temperature time-series	This figure presents (a) low-pass filtered alongshore wind stress at N13 (grey) and W_2 (red, downwelling favorable; blue upwelling favorable). Approximate seasonal transitions shown above subplot (a): the storm season (purple bar), upwelling season (yellow bar); and relaxation season (green bar). (b) SST at N13 (black line) shown with MHW presence flagged following Sanford et al. (2019). Shading, either grey or red, marks periods where the 2015 temperature at N13 exceed the 90th percentile based on a 30-year record at N13 (1981 – 2011) for ≥ 5 days. Red shading represents one of 10 most intense events since 1981. For reference, the mean SST for 2015 is shown by a dashed horizontal line (13.15°C) and 9°C is also shown. (c) time-series of bottom DO for each mooring site are shown: CB1 (gold) and CB2 (blue). Hypoxia thresholds are shaded (c) light grey (mild) and dark grey (intermediate). Vertical black lines mark the first of each month in all subplots (a-c). Temperature and τ and are low-pass filtered. Date tick marks are spaced at 8-day increments.	79
3.8	T-S diagram showing CB2 mooring data (100m) collected during 2016 – 2018.	(a) Seasons are colored dark grey "Upwelling season"; light grey "relaxation season"; and white "storm season" in accordance with thresholds described in section 2.3. DO concentration are provided (b) in mLL^{-1} . Black contours are constant potential density and gray contours are constant spiciness. Potential salinity is presented here.	80

4.1	Site map and summary of subsurface DO at OCNMS from 2011 – 2020), showing 10 OCNMS mooring locations (a). This study used moorings with available DO data (filled triangles); CA042 was excluded due to a gap in DO data from 2016 – 2018. Wind buoy NDBC46041 (N41) marked with a blue/purple circle. Contours shown: 40, 80, 130, 200 m. In this work, Salish Sea rivers (light green) include: the Duckabush, Skokomish, Deschutes, Nisqually, Puyallup, Duwamish, Cedar, Snohomish, Stillaguamish, Skagit, SanJuan, Elwha, Dungeness, Clowhom, Squamish, Tsolum, Oyster, Englishman, Cowichan, Nanaimo, Nooksack rivers and the Fraser River (dark green). Coastal Washington (light blue) include: the Calawah, Hoh, Queets, Quinault, Chehalis, Willapa, Naselle rivers. The Columbia River (mid blue) is in a group alone. Coastal Oregon (dark blue) include: the Nehalem, Wilson, Nestucca, Siletz, Alsea, Siuslaw, Umpqua and Coquille rivers. (b-e): Mirrored histograms of observed DO for years 2011 – 2020 binned by month are presented for mooring locations from north to south: The northern-most site MB042 (b) to southern-most sites CE042/CE015 (e and f). There is less data coverage across years for (May) and (October), indicated by parentheses see Figure 4.2. Approximate DO data coverage for each site is provided in Figure 4.2. Bin widths for each mirrored histogram are 0.1 mL L ⁻¹ between 0 and 8 mL L ⁻¹ . The 25th/50th/75th percentiles are marked with black lines. Mild hypoxia is marked with a dashed black line; intermediate hypoxia is shaded light grey; severe hypoxia shaded dark grey. Anoxic/suboxic thresholds are not distinguished. Sites CE042, TH042, MB042 are all at the same approximate depth (42m), while KL027 is 27m and CE015 15m.	92
4.2	OCNMS coastal mooring coverage of DO data from 2001 - 2020 Black vertical and horizontal lines are shown to help visualize the first of each month (vertical lines) and different mooring years (horizontal at 2011; -15 and -19). CA042 is excluded because of DO data gap from 2016 - 2018. Approximate coverage for CA042 can be seen in Figure 4.5c.	94
4.3	Summary statistics of flow for the Columbia and Fraser Rivers and winds at N41. Median values marked with a horizontal sea green line; boxes represent the upper and lower quartiles (25th and 75th percentiles). The 90th and 10th percentiles are shown as whiskers with dashed ends. Summary statistics of flow data (a & b) and N41 winds (c) are shown for each month of the reference period (1991 – 2020). In subplot (c) upwelling-favorable winds are negative; downwelling-favorable positive. .	97

4.4	30-year summary of discharge at the Columbia and Fraser Rivers. Multivariate ENSO index (MEI) v2 (a) shown together with PDO cycle (b) and river discharge (c & d). (a) Light pink and light blue shading represent neutral conditions ($-0.5 < \text{MEI v2} < 0.5$). Mean monthly and peak monthly discharge are each shown for the Fraser (c) and Columbia (d). Both stem and marker are colored for mean monthly discharge, while the stem is grey and marker colored for each peak monthly discharge. Below normal flow conditions are less than the lower quartile (red); above normal if greater than the upper quartile (blue), and within normal range if between the upper and lower quartiles (sea green). High flow events of interest discussed in text are labeled. Quartiles for each river are presented in Figure 4.3. A closer look of 2011 – 2020 (dashed box A) shown in Figure 4.8.	99
4.5	Interannual hypoxia at OCNMS coastal moorings showing binned subsurface DO levels for 2011 – 2020. Data are classified by observed DO level: (blue) $\text{DO} > 2.45 \text{ ml } L^{-1}$; "mild hypoxia" $\text{DO } 1.4 - 2.45 \text{ ml } L^{-1}$; "intermediate hypoxia" $\text{DO } 0.5 - 1.4 \text{ ml } L^{-1}$; "severe hypoxia" $\text{DO } 0.2 - 0.5 \text{ ml } L^{-1}$; "suboxia" $\text{DO} \leq 0.2 \text{ ml } L^{-1}$ with "anoxia" zero DO. Each bar represents the number of days between 1 May to 31 October for each deployment year (180 days; 2011 – 2020). White space indicates no observations. Colored triangles next to each subplot title relate to their color designation on Figure 4.1. CA042 does not have DO data for 2016 – 2018. Anoxia observed in 2017* at KL027 and CE042.	104
4.6	Cumulative discharge for the Columbia and Fraser Rivers. Cumulative discharge is shown for each river: Columbia River (a) and Fraser River (b) across 10 water years (2011 - 2020). The three largest values at the end of each year are flagged in each legend with a dashed box and marked on the figure. Water years with below normal cumulative discharge at the end of each water year are marked with an asterisk. The median cumulative discharge for the reference period (1991 – 2020) is shown as a black dashed line in both plots. Note the y-axis are not the same, and a dashed line in subplot (a) marks the max y-axis value of subplot (b). IQR = interquartile range = upper - lower quartile(s) and the IQR for 1991 - 2020 is shaded grey in each subplot.	110

4.7	<p>2017 spring/summer: N41 winds, discharge and OCNMS coastal mooring data This figure presents low-pass filtered alongshore wind stress (a) calculated from N41 winds (grey) with the 8-day upwelling index, W_8, overlain in color. Negative values (blue for W_8) are upwelling favorable winds while positive values (red for W_8) are downwelling favorable. Discharge data for the Columbia River (blue) and rivers that empty to the Salish Sea (including the Fraser River; sea green) are shown (b) on the left y-axis, while coastal rivers off Oregon (white) and Washington (black) are shown on the right y-axis. The river locations, names and groupings are shown on Figure 2.1. Temperature plots created using low-pass filtered temperature sensors moored through the water column are shown for MB042 (c); TH042 (d); KL027 (e); CE042 (f), with depth on the left y-axis. In the same subplots, the buoyancy frequency (N^2; blue line) is shown using the right y-axis. Low pass filtered near-bottom DO data are shown for MB042 (yellow) and TH042 (orange) (g); and KL027 (red) and CE042 (dark red) (h). Hypoxia thresholds are shaded grey (mild, intermediate, severe and suboxic; anoxia is zero oxygen). Data shown (except for W_8) were filtered using the PL33 filter described by Rosenfeld (1983) with a 33 hour cutoff period, to remove higher frequency signals.</p>	111
4.8	<p>Summary of discharge at the Columbia and Fraser Rivers (2011 – 2020). A closer look at years 2011 - 2020 from Figure 4.4 dashed box A.</p>	112
4.9	<p>OCNMS mid-shelf sites subsurface DO and stratification. This figure presents daily averages of observed DO and calculated buoyancy frequency (N^2). Data shown represents times when top-bottom density and bottom DO were available, at the same time, for all four sites (CE042, KL027, TH042 and MB042). This requirement yields 786 days of data per site, with the coverage shown in (b). Statistics for the daily averages of DO and N^2 are presented for each mooring (a): the median (white circle), the 25th - 75th percentile (thick lines); and 10th/90th percentile (end dashes). Sites CE042 (dark red), TH042 (orange), MB042 (yellow) are all at the same approximate depth (42m), while KL027 (red) is shallower (27m).</p>	117
4.10	<p>CE042 subsurface DO and stratification. This figure presents summary statistics of observed DO and calculated buoyancy frequency (N^2) at CE042. Data shown represents times when top-bottom density and bottom DO were available, at the same time, at CE042 with coverage shown in (b). Summary statistics were calculated using N^2 and DO at 8-day increments for all deployments, which provides a total of $N = 134$ (sets of 8-day data). Each N^2 and DO set are colored by median surface salinity during the 8-day span (a). Summary statistics are the same as Figure 4.9. Mild and intermediate hypoxia are marked with a vertical dashed line; severe hypoxia is shaded light grey and suboxia shaded dark grey.</p>	118

4.12	Summary statistics for CE042 bottom data. This figure presents August data for years 2011 – 2020 (yellow, notched-boxes). Baseline summary statistics (grey, notched-boxes) represent August data for 2007 – 2013. Baseline summary statistics are also stretched across each subplot for reference: grey dashed lines represent the 90th/10th percentiles; dark grey lines represent the 50th percentile; and light grey shading represents 75th/25th percentiles. Vertical, yellow shading marks groups with mean ranks that tested significantly different than the baseline.	121
4.11	Near-bottom temperature and salinity. This figure presents daily averaged data for near-bottom temperature and Salinity at CE042. Black contours represent constant sigma-theta (dotted) and constant (dashed) spiciness. Data were separated by month: June (a), July (b), August (c) and September (d) and colored by year (see subplot c for legend). Grey shading in (d) highlights the difference in x- and y-axis scale from other subplots (a-c).	122
4.13	August near-bottom DO and salinity. This figure presents time-series data for DO (a) and Salinity (b) at MB042 and CE042. Each August of every year (2011 – 2020) have 744 hours of data included except for: (1) MB042/2011 (n = 0); (2) CE042/2015 (n = 612/ 25.5 days of hourly data); and (3) CE042/2020 (n = 705; 29.4 days of hourly data). Statistics for each year are presented: 10th/25th/50th/75th/90th percentiles. The notched-mean is white, while the median is marked with a dash (CE042) or a circle (MB042).	125

List of Tables

- 1.1 Relative Comparison of CCS Water Masses 8
- 1.2 Hypoxic Thresholds 13

Abstract

Physical dynamics influencing dissolved oxygen over the shelf in the central and northern California Current System

by

Kathryn M. Hewett

Eastern Boundary Upwelling Systems (EBUS) are highly productive biomes, which provide benefit to society and support local ecosystems. Although EBUS total area is small when compared to other pelagic ecosystems, a growing body of literature demonstrate that climate impacts on EBUS will have disproportionately large consequences for human society. Like other EBUS, the California Current System (CCS) is experiencing a number of inextricably linked stressors: acidification, oxygen stress (hypoxia), altered food webs, and warming temperatures. Each stressor has the potential to change species interactions; alter the abundance and distribution of organisms; and can even result in mortality for certain organisms. Wind forcing and freshwater input drive change in the coastal zone, and result in heterogeneous expression of multiple stressors in time and space. River-flow and winds are both anticipated to change in magnitude and timing due to human- and climate-induced changes, which drive associated impacts to physical and biogeochemical processes in estuaries and continental shelves. A step towards better understanding drivers of multiple stressor interactions includes analysis of subsurface observations to identify relationships and trends in shelf waters. In this work we focus on the physical dynamics which influence dissolved oxygen (DO) over

the shelf off northern California and Washington, to better understand the physical dynamics that influence hypoxia. In the CCS, and other EBUS, high productivity is supported by coastal wind-driven upwelling that supplies the shelf with nutrient-rich waters. However, high rates of productivity in the coastal zone may operate at the expense of (1) decreasing aragonite and calcite saturation states and decreasing dissolved oxygen (DO) concentrations because the water that is upwelled to the continental shelf also has reduced DO levels, lower pH, and higher concentrations of dissolved inorganic carbon (DIC); and (2) high productivity maintains a high standing stock of particulate organic carbon (POC), which builds a respiration signal in the water column and at the sediment/water interface and results in a decline in DO. These are two mechanisms that make EBUS, including the CCS, prone to hypoxia and acidification, which threaten ecosystems and the communities they support. The coastal waters of Washington (and southern British Columbia) have the highest primary productivity in the CCS, but this high productivity is not co-located with the strongest upwelling-favorable alongshore winds (which occur off northern California). This mismatch has been explored (e.g. by Hickey and Banas 2009), and results point to additional mechanisms that facilitate the region's high productivity beyond the traditional focus of the coastal wind field. The work presented in this dissertation, to explore the physical dynamics which influence DO over the shelf in two regions of the CCS, was motivated by (1) the link between productivity and hypoxia (and the mismatch of productivity/wind forcing); (2) reports of extreme low DO observed off Washington in the summers of 2017 - 2019; and (3) a lack of subsurface DO time-series observations off northern California (where peak up-

welling wind stress occurs). Two chapters of this dissertation focus on the central CCS (off northern California), a region for which which DO time-series are scarce; and one chapter addresses the northern CCS (off Washington) and is comprised of an analysis of a 10-year record of DO, temperature and salinity at multiple sites along with wind and river discharge data to better understand the timing and severity of shelf hypoxia.

Although the CCS is one of the most highly observed ocean regions in the world, there has been comparatively limited research on subsurface DO and carbonate system parameters in the central CCS off northern California (from 37°N to 42°N). Since long time-series of subsurface DO are relatively scarce, management decisions are made without a proper understanding of regional risk. Scientifically we are left wondering: (1) what DO levels occur in a section of the CCS that experiences the strongest upwelling favorable winds ($\sim 8x$ stronger than the Pacific Northwest)?; and (2) how DO levels respond to upwelling and relaxation events in this subregion? We collected time-series mooring data (temperature, salinity and DO), which are used to describe patterns and timing of hypoxia, and explore how DO levels respond to upwelling and relaxation events in the northern California coastal upwelling region. A deeper, mid-shelf site ($\sim 54m$) is located in the Gulf of the Farallones, offshore San Francisco Bay, and within the more stratified upwelling shadow south of Point Reyes. The lowest DO concentrations and most persistent hypoxia were present at the mid-shelf site. At the shallower sites, (~ 18 and $30m$), results show highly variable DO values with brief hypoxic events outside the core upwelling season (i.e., strongest winds and coldest water did not associate with the lowest DO levels). At the deeper, mid-shelf site, two distinct modes of

variability were observed. During the first mode, upwelling events related to DO decline and relaxation events to increasing DO. During the second mode, the opposite occurs: upwelling related to an increase in DO and relaxation events to declining DO. At the shallower inner-shelf sites, and for the entire time-series, upwelling generally relates to DO decline and relaxation events to increasing DO. The importance of source water is clear during the first half of the mid-shelf deployment, and the overall trend and second half shows the importance of local drawdown. We also explored the seasonality of DO over a submarine bank (Cordell Bank) located at the shelf-break off northern California. Results show a recurrent seasonal cycle in temperature and DO. The similarity of seasonal patterns of temperature across years (2014 - 2018) is interesting, especially given the diverse set of oceanographic conditions the CCS experienced from 2014 – 2019. Although the coolest water occurs over the bank early in the upwelling season, the DO minimum occurs later, towards the end of the upwelling season and often during the relaxation season. Deviations from the seasonal trend observed are likely attributed to a combination of physical and biogeochemical processes working together. Specifically, we hypothesize that the interplay of wind-driven mixing and surface productivity can explain interannual differences, but additional work is needed to fully understand the role of these drivers. At Cordell Bank, DO concentrations were often below the threshold of mild hypoxia (2.45 ml/L), but only one instance of intermediate hypoxia was observed (1.4 to 2.45 ml/L) during the relaxation season (July 2017). Overall DO off northern California appears higher (fewer hypoxic events) than those observed in the northern CCS, but the upwelling favorable winds are also eight times stronger off

northern California. Finally, observed DO is also lower than predicted using two source waters (PEW and PSUW) thus pointing to the likely importance of local drawdown (and potentially presence of more than two source water masses).

We focused on the physical dynamics which influence shelf DO in the northern CCS (off Washington), in attempt to better understand the physical dynamics that influenced the extreme low DO observed in the summers of 2017 - 2019. Mooring data (2011 - 2020) are used to describe the timing and severity of hypoxia off Washington. River and winds data (1991 - 2020) are also used to better understand the coastal environment and drivers of low DO. From this work we found significant interannual variability in DO. The 2016-2019 low DO period is statistically associated with spicier water, suggesting a link between source waters impacted by the El Niño, very, very low North Pacific Gyre Oscillation Index, marine heat wave presence and low DO over the shelf. When compared to historical DO records, summertime hypoxic exposure appears to have worsened on the Washington shelf. However, 2011 – 2020 shows significant interannual variability without a clear downward trend. We also observed a north-south trend with lower DO in the south, which can be explained by several hypotheses, ranging from shelf width to canyons to stratification. However, the relationship between stratification, surface salinity and DO is complex. Within periods with similar surface salinity, more stratification is related to lower DO, *but* overall higher stratification is caused by lower surface salinity and is associated with higher DO. This likely demonstrates a complex relationship between the presence of river water advected northward by downwelling-favorable winds and vertical mixing driven by downwelling. Additional

work to further assess the impact of timing of the Columbia and Fraser Rivers relative to wind events is important to understand DO and carbonate chemistry off Washington, and help make predictions for future climate conditions.

To Anne Marie, RiRi, Ana and Lyndsey.

Acknowledgments

My work on this dissertation took place on the unceded ancestral lands of the Ohlone, Me-wuk, Makah, Quileute, Quinault, and coast Salish people, past and present; I honor them and the land with my gratitude.

A portion of the work presented in this dissertation was funded by the California Sea Grant and various awards from the University of California (UC), including two Institute for the Study of Ecological and Evolutionary Climate Impacts Fund Awards; two Henry A. Jastro Graduate Research Awards; and a Van Alfen/MacDonald Graduate Student Award. A large portion support for my research and time came from a NOAA Dr. Nancy Foster Scholarship award with support from the Ocean Acidification Program (OAP). I would like to thank all the staff at Sanctuaries and the OAP for their continued support and friendship throughout my PhD. Special thanks to the staff at Cordell Bank, the Greater Farallones, and the Olympic Coast National Marine Sanctuaries. Thank you to John Armor, Libby Jewett, Seaberry Nachbar, Kate Thompson, Steve Gittings, Dani Lipski, Dan Howard, Jan Rotello, Jenny Waddell, and many others.

I would like to thank my advisor and the members of my dissertation committee. I am grateful for your time, patience, and guidance, scientific and otherwise. Thank you especially to my advisor, John Largier, for supporting my independence and growth as a researcher. I learned a lot about the coastal ocean from him - and through his support - I was able to often get out in the field and observe how the coast off California behaves. To my committee member, Alex Forrest, I thank for being supportive

and always making time for me. To Sarah Giddings, I admire your creativity and am thankful for your feedback and guidance. From figure suggestions to explaining coastal dynamics, I have learned so much from you! I'm a better scientist because of each of you. Thank you for the time put aside to meet with me as well as the pep talks you gave me when I needed it. Your advice on both my research and career have been invaluable.

During my PhD, I was fortunate enough to attend three summer school sessions on coastal and estuarine dynamics. This brought me to Heliogoland (Germany), Quintana Roo (Mexico) and Washington (USA). I would like to thank Hans Burchard, Götz Flöser, Arnoldo Valle-Levinson, Parker MacCready, and Rocky Geyer for organizing these courses and sharing your version of estuarine and coastal physics with us. I also appreciate the various guest lecturers who made time to teach us and share their science. Not only did I learn a lot, but I made a cohort of coastal oceanography colleagues/friends and learned the estuarine shuffle.

When I started my fieldwork and became interested in better understanding understand shelf oxygen, Francis Chan, Burke Hales, Ann Russell, Tom Connolly and Matt Robart were all very helpful. I am grateful for each for their support and time. A benefit from being at the Bodega Marine Laboratory (BML) is that students also receive mentoring from the other resident faculty. Special thanks to Tessa Hill, Brian Gaylord, Susan Williams, Ted Grosholz, Eric Sanford and Jackie Sones. I am a better scientist for being around each of you. BML is located on a unique section of the California coast with an equally great community of people. Thank you to my friends and colleagues at BML for ideas and collaboration through grad school. These included Dane, Brittany,

Jeff, Aaron, Erin, Jennifer, Grace, Sam, Kristen, Kristin, Katie, Gabe, Jordan, Helen, Mel, Hannah, Kate, Emily, Sarah, Chris, Dan, Dale, Marcel, Matt R., Robin, Matt W., Emily, Tallulah and many others.

I was fortunate to have the mentorship of Chris Edwards, Melanie Fewings, Simone Alin, Ian Phillips, Marisol Garcia-Reyes and Mary Miller during my PhD. Thank you, Chris, for teaching me how to use ROMS and challenging me to think about the ocean in different ways. Thank you also for giving me desk space and supporting me through the end of my PhD. Thank you, Melanie, for teaching me more about scientific writing and spending countless hours talking about cool science. Thank you Simone for including me in your research and connecting me with people to get my program collaboration (and fourth chapter) complete. Ian mentored me prior to graduate school while working as an engineer, and he has continued to mentor me through grad school. Thank you, Ian, for all your time and support! Thank you, Marisol, for taking time, whenever I have asked for help, to explain/read/trouble shoot. (T.y. to Keshi too). Thank you Mary, for helping me expand the broader impacts of my research by bringing me on as a scientist in residence at the ExplOration. Spending time at the ExplOration with Mary, Ron Hipschman and other staff was a great way to learn more about science communication.

Of course the support that I have received extends well past my academic and professional community. I owe my work ethic to my mom, and completing this dissertation would not have been possible without her support. She has read every single thing that I have written since primary school, and might be the only person

that reads my acknowledgements: hi, mom! Thanks for encouraging me, for believing in me, and for teaching me to care about the world and the people in it. Thank you to my family, especially Reezie, Hal and my brothers, for keeping me grounded and for celebrating all my milestones. Thank you also, obviously, to Dr. Duck. I owe a great deal to my friends. To all the toasts and frondly-friends, I love you so much. Thank you to Ana, Lyndsey, Robin, Butter, Jill, Davon, Tilden, Carson, Sam, Murphy, Mikey, Nate, Goto, Laura and all the other friends for keeping my days so splendid and full of life. Finishing a pandemic PhD would not have been possible without you! Thank you to my science friends, especially Jacki, Sam, Yui, Emily, Jasen, Mer, Alex and Sarah. And thank you to Dana, John, Jill, Claudia, Kim, Brian and Sabina for being there for me while I finish grad school. Thanks to Riley, Kenzie, Keith, Erin (+ Shea and Blue) for loving me and supporting me through my PhD. Thank you for getting me outside, which kept me sane through the end of my PhD. I am looking forward to spending much more time with each of you now that my dissertation is complete!

There is no way I can possibly express my gratitude enough for those I acknowledge here. I am lucky that so many people have played an integral part of my graduate school experience. It has been an incredible journey. Thank you for all of your unending support!

Chapter 1

Introduction

Motivated by an increase in both magnitude and persistence of low oxygen (hypoxia) in the coastal zone as well as open ocean oxygen decline (deoxygenation), increasing attention has been placed on monitoring dissolved oxygen (DO) levels and understanding physical dynamics that influence DO levels and biogeochemical change in and across estuarine to open ocean environments (see review by Levin and Breitburg 2015). This dissertation aims to expand current knowledge of physical dynamics influence on DO levels over the shelf through use of observational data from the central and northern California Current System (CCS). We synthesize findings from (1) a novel dataset of shelf DO collected off northern California and (2) a 10-year dataset off Washington with wind and river discharge data to better understand the timing and severity of shelf hypoxia. The remainder of this chapter provides basic background information on Eastern Boundary Upwelling Systems and anticipated climate impacts (section 1.1); the CCS and deoxygenation and hypoxia in the CCS, section 1.2. The

hypoxia thresholds we adopt for our analysis are described in subsection 1.2.4. Finally, section 1.3 outlines the chapters provided in this dissertation.

1.1 Eastern Boundary Upwelling Systems

The California Current System (CCS) is an eastern boundary upwelling system (EBUS), located in the North Pacific (Figure 1.1). EBUS are among the world's most productive ocean ecosystems (Kämpf and Chapman 2016), which provide wide benefit to society and directly support coastal communities (Garcia-Reyes et al. 2015; Levin and Le Bris 2015; Bindoff et al. 2019). Although EBUS total area is small when compared to other pelagic ecosystems, a growing body of literature demonstrate that climate impacts on EBUS will have disproportionately large consequences for human society, as summarized in the Fifth Assessment Report (AR5) of the United Nations (UN) Intergovernmental Panel on Climate Change (IPCC) (Chapter 5, AR5 Bindoff et al. 2019). While the ocean becomes warmer and more stratified (Capotondi et al. 2012; Talley et al. 2016), global biogeochemical change is occurring which includes increased levels of dissolved inorganic carbon (DIC), decreased levels of dissolved oxygen (DO) and increased oxygen stress (hypoxia), and changes in productivity and altered food webs (Bopp et al. 2002; 2013; Deutsch et al. 2006; Keeling et al. 2010; Doney et al. 2009; 2020; Feely et al 2004; 2009; Hoegh-Guldberg and Bruno 2010; Garcia-Reyes et al. 2015; Schmidtko et al. 2017; Breitburg et al. 2015; 2018; Levin et al. 2018; Pitcher et al. 2021). Natural variability inherent to EBUS alongside uncertainties in

present and future trends in upwelling seasonality, coastal warming and stratification, primary production and biogeochemistry of source waters each pose large challenges to the climate response across EBUS and within each system itself (Sydeman et al. 2014; Hickey et al. 2010; García-Reyes et al. 2015; Rykaczewski et al. 2015; Varela et al. 2015; Wang et al. 2015; Bindoff et al. 2019). Further, we are learning that rates of change in the coastal zone often outpace that of offshore waters; this mismatch is strongly influenced by coastal physical dynamics and respiration signals (Diaz and Rosenberg 2008; Rabalais et al. 2010; Booth et al. 2014; Chavez et al. 2017; Siedlecki et al. 2021). Across the latitudinal range of an individual EBUS, variations exist in winds (e.g., Sydeman et al. 2014; Wang et al. 2015; Rykaczewski et al. 2015; García-Reyes et al. 2015), freshwater input (e.g., in the CCS, Hickey and Banas 2008), coastline shape, bathymetry and shelf width (e.g., Allen et al. 1995; Barth et al. 2000; Pickett and Paduan 2003; Allen and Hickey 2010; Monterio et al. 2011), and presence of source waters for upwelling (Monteiro et al. 2011; Rykaczewski and Dunne 2010; Doney et al. 2012; Rykaczewski et al. 2015; Pozo-Buil 2015;2017; Bograd et al. 2015; 2019), which all drive biogeochemical variability. EBUS, like the CCS, experience both remote and local physical forcing (e.g., Jacox et al. 2015; Bograd et al. 2015), but often local winds and mesoscale oceanographic features are not resolved in global Earth System Models (ESMs) which can often limit our ability to understand their complicated physical dynamics which shape these valuable ecosystems. However, work to enhance representation of coastal winds and upwelling dynamics that shape EBUS ecosystems are underway in the modeling community (e.g., Machu et al. 2015; Echevin et al 2012;

Bruyère et al. 2014; Xiu et al. 2018; Arellano and Rivas 2019; Dussin et al 2019; Howard et al. 2020; Pozo-Buil et al. 2021; Siedlecki et al. 2021). While modeling efforts have the ability to produce climate projections and sharpen scientific questions, observations (especially subsurface) and a better understanding of physical dynamics that shape ecosystems within and across EBUS are each necessary to properly manage ecosystem services in a rapidly changing climate.

1.2 The California Current System

1.2.1 Winds and Regions

The CCS is an EBUS, located in the North Pacific that extends from $\sim 50^\circ\text{N}$ (where the east-flowing North Pacific Current approaches North America) to $\sim 15\text{-}25^\circ\text{N}$ (off Baja California, Mexico). With regional borders around Cape Mendocino and Point Conception, the CCS divides into three main regions: the northern, central and southern CCS (Hickey 1979; Checkley and Barth 2009) (see Figure 1.1). Wind forcing over the CCS varies from moderately strong, seasonally varying in the northern CCS, to persistently equatorward in the central and southern portions (Huyer 1983). However, the strongest upwelling favorable winds occur in the central CCS off Bodega Head (in the vicinity of N13; Figure 2.1) and another in region south of Point Sur (García-Reyes and Largier 2010; 2012) (Figure 1.1). North of Cape Mendocino winds are generally northward and downwelling favorable in the winter, while south of Cape Mendocino alongshore winds are generally equatorward and upwelling favorable year-round (Huyer

1983). Across the CCS, prevailing winds are upwelling-favorable during the spring and summer, on which weather-band fluctuations are superimposed (see review by Fewings et al. 2016). Off Washington, upwelling winds typically occur \sim half to two-thirds of the season with downwelling conditions present for the remainder (Hickey and Banas 2008). The efficiency and depth from which shelf water is derived during upwelling is dependent on the magnitude/persistence of upwelling winds (e.g. Hickey et al. 2006) and the local cross-shelf wind profile (Jacox and Edwards 2012), as well as other physical characteristics like local stratification, alongshore flow, bottom slope, shelf width (Allen et al. 1995) and coastline shape (Barth et al. 2000; Pickett and Paduan 2003). These factors combine to differentiate regions of the CCS (see review by Checkley and Barth 2009), and each region is strongly influenced by remote and local physical forcing (e.g., Jacox et al. 2015; Bograd et al. 2015). Finally, while upwelling favorable winds are much stronger (\sim 8x) off California (in the central CCS) than off Washington (in the northern CCS), the degree of freshwater input (by rivers, estuaries and associated energetic tidal flows) is significantly higher in the northern CCS (Hickey 1998; Hickey and Banas 2008).

1.2.2 Shelf water mass properties and currents

The CCS represents a union of different water masses that originate in the tropical, subtropical, and subarctic regions of the eastern Pacific Ocean; each defined by temperature, salinity, DO and nutrients at the time of entry to the CCS (Table 1.1; Lynn and Simpson 1987; Talley et al. 2011). Deep waters upwelled on to the shelf predominantly include two end-member source water masses: Pacific Subarctic Upper

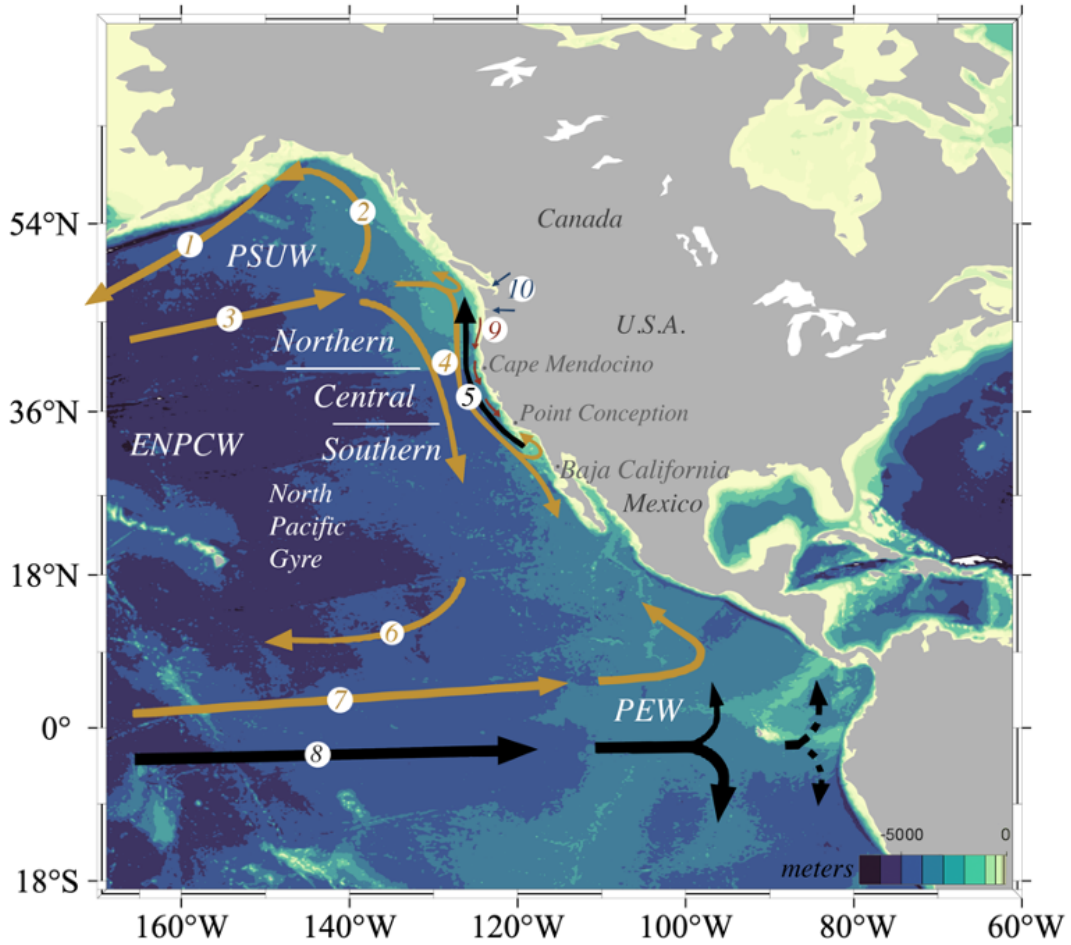


Figure 1.1: Map of the California Current System This figure presents major currents and water mass locations, and is based on content presented in Checkley and Barth (2009); Thomson and Krassovski (2010); and Talley et al. (2011). Water mass descriptions are in Table 1.1 and approximate location shown on in this figure. Surface currents (gold arrows) and undercurrents (black arrows) shown include the (1) Alaskan Stream; (2) Alaska Current; (3) North Pacific Current; (4) California Current (shown as 2 arrows); (5) California Undercurrent; (6) North Equatorial Current; (7) North Equatorial Countercurrent; and (8) Equatorial Undercurrent. Coastal jets (9) form on the shelf and shown as red arrows. Freshwater input (10) (blue arrows at the Salish Sea and Columbia River) is greater in the northern CCS than the central and southern CCS. The strongest upwelling-favorable winds occur in the central CCS (off Bodega Head near N13 and south of Point Sur; see Figure 2.1). Approximate boundaries for the three CCS regions are shown by white lines. CCS region text is placed offshore and in the North Pacific Gyre, but the regions are physically located to the east of each text label, adjacent to the west coast and include (4), (5) and (9).

Water (PSUW) and Pacific Equatorial Water (PEW) (Hickey 1979; Huyer et al 1989). Although, we are also learning that Eastern North Pacific Central Water (ENPCW) can contribute to biogeochemical variability (Bograd et al. 2019) and salinity anomalies (Ren and Rudnick 2021) in the CCS. The sluggish surface California Current typically transports PSUW equatorward, while the California Undercurrent transports PEW poleward (Hickey 1979; 1998) (Figure 1.1). The percentage of PEW in upwelled waters varies with season and with latitude (decreasing poleward) (Thomson and Krassovski 2010). As each upwelling season progresses, development of the California Undercurrent occurs which plays an important role in providing nutrients to (or removing nutrient-depleted waters from) the shelf (Hickey and Banas 2008). Further, increased advection of low-oxygen, PEW by the California Undercurrent has often been shown to cause a decline in coastal DO levels (e.g. Bograd et al. 2008; Pierce et al. 2012; Meinvielle and Johnson 2013), and the relative proportion of PEW present has been shown to impact community composition in the CCS (e.g., fish community composition as shown in McClatchie et al. 2010; Schroeder et al. 2019). The chemistry and character (T-S) of water brought to the shelf during upwelling is dependent on the source water origin, which is an active area of research (both understanding what water is present for upwelling and how the biogeochemistry of water masses are changing) (e.g., Bograd et al. 2015; Pozo-Buil and DiLorenzo 2015; Whitney et al. 2013).

Table 1.1: Relative Comparison of CCS Water Masses

Water Mass	Temperature	Salinity	DO	Nutrients
PSUW	<i>low</i>	<i>low</i>	<i>high</i>	<i>highly variable</i>
ENPCW	<i>high</i>	<i>high</i>	<i>low</i>	<i>low</i>
Coastal upwelled	<i>low</i>	<i>high</i>	<i>low</i>	<i>high</i>
PEW	<i>high</i>	<i>high</i>	<i>low</i>	<i>high</i>

Comparisons based on Lynn and Simpson (1987) and Talley et al. (2011).

"Coastal upwelled" waters represent a mixture of source waters present for upwelling.

1.2.3 Productivity and DO

The CCS is a highly productive biome because of wind-driven coastal upwelling; a process that supplies the continental shelf with deeper, nutrient-rich water (Smith, 1981; Hickey 1979; Huyer 1983) and supports high primary productivity and fisheries (e.g., Ryther 1969; Pauly and Christensen 1995). This efficient supply of deep oceanic nutrients to the coastal zone can operate at the expense of a decline in nearshore aragonite and calcite saturation states and DO concentrations, because the water that is upwelled to the shelf is also often oxygen-poor and high in DIC (Feely et al. 2004; 2009). Both observations and models highlight the rapid progression and biogeochemical sensitivity of the CCS to ocean acidification and hypoxia (OAH) (Feely et al. 2008; Gruber et al. 2012; Chan et al. 2017), which strongly affects present and future expression of OAH in the coastal zone (Feely et al. 2008; Gruber et al. 2012; Harris et al. 2013; Chan et al. 2017). High rates of productivity in the coastal zone may operate at the expense of (1) decreasing aragonite and calcite saturation states and decreasing DO concentrations because the water that is upwelled to the continental shelf also has reduced DO levels, lower pH, and higher concentrations of DIC; and (2) high productivity maintains a high standing stock of POC (e.g., Hales et al. 2006), which builds a

respiration signal in the water column and at the sediment/water interface and results in DO level declines (Diaz and Rosenberg 2008; Rabalais et al. 2010). We are learning that nearshore rates of change (e.g., lower pH, warmer water, lower DO) often outpace offshore estimates and observations, and the mismatch is due to coastal processes (Booth et al. 2014; Chavez et al. 2017; Siedlecki et al. 2021). Physical forcing mechanisms and regional topography and bathymetry can influence the composition of source and upwelled waters while shelf biogeochemical processes can further modify waters (either upwelled to the shelf or introduced by rivers/estuaries). This has the potential to drive spatial and temporal variability in nearshore OAH exposure within CCS regions and across regions at different rates.

The coastal waters of Washington and southern British Columbia (northern CCS) have the highest primary productivity in the CCS, but this high productivity is not co-located with the highest magnitude of upwelling-favorable alongshore winds (Ware and Thomson 2005). This mismatch has been addressed by Hickey and Banas (2008), who describe additional mechanisms that facilitate the region's high productivity beyond the traditional focus of the coastal wind field. First, the PNW shelf is wider than the California shelf (where peak winds occur), which promotes retention of upwelled nutrients (Strub et al. 1991). Second, energy from upwelling off northern California, in the form of coastal trapped waves contributes to upwelling in the northern CCS (Connolly and Hickey 2014). Third, the presence of shelf-break canyons are common across the CCS with a high density of canyons present off Washington (Hickey 1995). Canyon presence facilitates enhanced upwelling and allows water from deeper depths to

reach the shelf (Hickey 1997; Allen and Hickey 2010; Connolly and Hickey 2014), which contribute high rates of nutrients to the shelf (Hickey and Banas 2008; Crawford and Dewey 1989). Plus, canyons also experience intense mixing (Lueck and Osborn 1985; Kunze et al. 2002; Wain et al 2013; Zhao et al. 2012), which can impact source depth and modify water mass properties transiting the canyon sill (Alford and MacCready 2014). Fourth, freshwater-driven mechanisms play an important and complex role in coastal productivity which includes but is not limited to: modifying nutrient distributions across the shelf, shifting primary productivity offshore and/or deeper in the water column, and modifying retention time, estuarine exchange, and regional circulation in the cross- and along-shelf direction (Lohan and Bruland 2006; Hickey and Banas 2008; Banas et al. 2009; MacCready et al. 2009; Hickey et al. 2009; Kudela et al. 2010; Giddings et al. 2014; Davis et al. 2015).

Although the CCS is one the most highly observed ocean regions in the world, there has been comparatively limited research on subsurface DO and carbonate system parameters off central and northern California (from 37°N to 42°N). Currents and circulation south of Cape Mendocino and north of San Francisco Bay have been well studied through data obtained during several large projects in the 1980's and 1990's (CODE Beardsley and Lentz 1987; Super CODE Strub et al. 1987; CCCCS Chelton et al. 1987; NCCCS Magnell et al. 1991, Largier et al. 1993; SMILE Dever and Lentz

1994; Dever 1997a&b; STRESS Trowbridge and Lentz 1998)¹, and the impact of wind and current variability on productivity between 37.5 - 39°N and 122.5 - 124°N were studied during CoOP WEST (Largier et al. 2006)². However, time-series of subsurface DO are relatively scarce in this subregion, and we are left knowing little about the oxygen content of coastal waters over the shelf and specifically in the Gulf of Farallones, which feed San Francisco Bay and – at times – flow poleward past Point Reyes, a prominent headland that shelters the Gulf to the north (see Figure 1.1). This forces management decisions on hypoxic exposure to be made without a proper understanding of regional risk. Scientifically we are left wondering (1) what shelf hypoxia looks like in a section of the CCS that experiences the strongest upwelling favorable winds (~8x stronger than the Pacific Northwest); and (2) how subsurface DO responds to upwelling and relaxation events in this subregion. This gap in observational coverage has reduced our communities ability to predict the onset of corrosive events, validate existing OAH algorithms, and groundtruth models that predict subsurface water properties. This limitation also extends to impact regions (and communities) outside the central CCS, because although observational coverage is less lacking elsewhere, ecological impacts of hypoxia in the central CCS likely influence change in the northern and southern CCS.

Analysis of ocean observations from the 1980s to 2000s point to a significant decline in DO across the CCS: off Oregon and Washington (Grantham et al. 2004;

¹Coastal Ocean Dynamic Experiment (CODE) and super CODE acquired observations from 1981 to 1983; Central California Coastal Circulation Study (CCCCS) 1984-1985; Northern California Coastal Circulation Study (NCCCS) 1987-89; Shelf Mixed Layer Experiment (SMILE) 1988-89; and Sediment Transport Events over the Shelf and Slope (STRESS)

²Wind Events and Shelf Transport (WEST) was a Coastal Ocean Processes (CoOP) National Science Foundation project, which acquired field observations between 2000 - 2003.

Chan et al. 2004;2008; Pierce et al. 2012), in the Southern California Bight (Bograd et al. 2008; 2015), and off Monterey Bay (central California; Ren et al. 2018). Plus deoxygenation trends have been observed in the North Pacific (Emerson et al. 2001; 2004; Ono et al. 2001; Watanabe et al. 2001; Whitney et al. 2007; Mecking et al. 2008) and oxygen minimum zone expansion has been observed in the tropical eastern Pacific (Stramma et al. 2008; Moffitt et al. 2015; Schmidtko et al. 2017). These large-scale trends in offshore DO content intensify hypoxic events, especially over the continental shelf (e.g., Grantham et al. 2004; Bograd et al. 2008; Chan et al. 2008; Booth et al. 2012; 2014; Levin and Breitburg 2015). An important question is whether nearshore hypoxic events are worsening over time. Before long-term impacts can be adequately predicted, it is necessary to better understand physical processes that contribute to low DO events. To accomplish this, subsurface observations are required across each region of the CCS.

1.2.4 Hypoxia thresholds

While many thresholds are used for hypoxia (Table 1.2), most commonly it is defined as ≤ 1.4 milliliters O_2 per liter ($ml L^{-1}$) in aquatic systems. However, DO concentrations above and below this limit can alter the structure and function of communities (see reviews by Levin et al. 2009 and Hofmann et al. 2011). In this analysis we employ classification thresholds of hypoxia to visualize the spatial and interannual expression of hypoxia, which we define as “mild hypoxia” between 1.4-2.45 $ml L^{-1}$; “intermediate hypoxia” $\leq 1.4 ml L^{-1}$; “severe hypoxia” $\leq 0.5 ml L^{-1}$; “suboxia” ≤ 0.2

$ml L^{-1}$; and anoxia (zero oxygen).

Table 1.2: Hypoxic Thresholds

Category	$ml L^{-1}$	$mg L^{-1}$	$umol kg^{-1}{}^a$	O_2 sat a	pO_2 kPa a
<i>Mild</i> ^b	2.45	3.5	106.6	38	8.0
<i>Intermediate</i> ^c	1.4	2.0	60.9	21.7	4.5
<i>Severe</i> ^d	0.5	0.71	21.6	7.7	1.6
<i>Suboxia</i> ^e	0.2	0.07	–	–	–
<i>Anoxia</i>	0	–	–	–	–

^a unit conversions for DO follow García and Gordon 2012 and Enns et al. 1965.

and assume a salinity of 33.5, temperature of 9.5°C.

^b Sensitive species behavior impacted and may exhibit avoidance reactions (Hofmann et al. 2011).

Survival and metabolism can be affected dependent on taxa (Levin et al. 2009; Chan et al. 2019).

^c Conventional threshold for biological impacts.

^d Only highly specialized species survive extended exposure below this threshold.

Severe hypoxia is also the operational threshold in the CCS for impacts to Dungeness crab mortality and reduced catch (Chan et al. 2019).

^e biogeochemical processes are altered, including oxygen consumption rather than nitrate during denitrification processes (Giorgio and Williams 2005).

1.3 Outline

This dissertation aims to expand current knowledge of physical dynamics influence on DO levels over the shelf through use of observational data from the central CCS (off California) and northern CCS (off Washington). Chapters 2 and 3 address the central CCS, a region for which which time-series of DO data are scarce. Chapter 4 addresses the northern CCS and is comprised of an analysis of a 10-year record of DO, temperature and salinity at multiple sites along with wind and river discharge data to better understand the timing and severity of shelf hypoxia. Each chapter is described below. Chapter 5 summarizes conclusions from chapters 2-4.

In Chapter 2 uses time-series mooring data (temperature, salinity and DO) to describe patterns and timing of hypoxia, and explore how DO levels respond to upwelling

and relaxation events in the northern California coastal upwelling region. The deeper, mid-shelf site ($\sim 54\text{m}$) is located in the Gulf of the Farallones, offshore San Francisco Bay, and within the more stratified upwelling shadow south of Point Reyes. The lowest DO concentrations and most persistent hypoxia were present at the mid-shelf site. At the shallower sites, (~ 18 and 30m), results show highly variable DO values with brief hypoxic events outside the core upwelling season (e.g., strongest winds and coldest water did not associate with the lowest DO levels). Overall DO levels off northern California appear higher (and less hypoxic) than those observed in the northern CCS, but the upwelling favorable winds are also $\sim 8\text{x}$ stronger off northern California. At the deeper, mid-shelf site, two distinct modes of variability were observed. During the first mode, upwelling events related to DO decline and relaxation events with increasing DO levels. During the second mode, the opposite occurs: upwelling relates to an increase in DO levels; relaxation events to declining DO levels. At the shallower inner-shelf sites, and for the entire time-series, upwelling generally relates to DO level decline and relaxation events with increasing DO levels. The importance of source water is clear in the first half at during the first half of the mid-shelf deployment, and the overall trend and second half shows the importance of local drawdown.

Chapter 3 uses a 5-year record of near-bottom DO, temperature and salinity to explore the seasonality of DO levels over a submarine bank (Cordell Bank) located at the shelf-break off northern California. Results show a recurrent seasonal cycle in temperature and DO. The similarity of seasonal patterns of temperature across years (2014 - 2018) is interesting, especially given the unique set of oceanographic conditions the

CCS experienced from 2014 – 2019. Overall, with the onset of upwelling, near-bottom water becomes cooler and saltier, and DO levels decrease. The coolest water occurs earlier than the minimum DO level. The seasonal cycle in DO is thought to be a response to interacting seasonal cycles in wind, surface warming, and productivity. Deviations from the seasonal trend are observed when strong wind forcing is present during the relaxation season (resulting in elevated DO levels) and when increased productivity is present (resulting in lower DO levels). At Cordell Bank, DO concentrations were often below the threshold of mild hypoxia (2.45 ml/L), but only one instance of intermediate hypoxia was observed (1.4 to 2.45 ml/L) during the relaxation season (July 2017). Observed DO is also lower than predicted using two source waters (PEW and PSUW) thus pointing to the likely importance of local drawdown (and potentially presence of more than two source water masses).

Chapter 4 focuses on the physical dynamics which influence shelf DO in the northern CCS (off Washington), in attempt to better understand the physical dynamics that influenced the extreme low DO observed in the summers of 2017 - 2019. Mooring data (2011 - 2020) are used to describe the timing and severity of hypoxia off Washington. River and winds data (1991 - 2020) are also used to better understand the coastal environment and drivers of low DO. From this work we found significant interannual variability in DO, with the 2016-2019 low DO period is statistically associated with spicier water potentially suggesting a link between source waters impacted by the El Niño, a very, very low North Pacific Gyre Oscillation (NPGO) index and marine heat wave presence and DO levels over the continental shelf. When compared to historical

DO records, summertime hypoxic exposure appears to have worsened on the Washington shelf. However, 2011 – 2020 shows significant interannual variability without a clear downward trend. We also observed a north-south trend with lower DO in the south, which can be explained by several hypotheses, ranging from shelf width to canyons to stratification. However, the relationship between stratification, surface salinity and DO is complex. Within periods with similar surface salinity, more stratification is related to lower DO, *but* overall higher stratification is caused by lower surface salinity and is associated with higher DO. This likely demonstrates a complex relationship between the presence of river water and mixing driven by downwelling.

Chapter 5 summarizes the dissertation conclusions.

Chapter 2

Observations of shelf hypoxia off northern California

2.1 Introduction

The California Current System (CCS) is a highly productive biome because of wind-driven coastal upwelling; a process that supplies the continental shelf with deeper, nutrient-rich water (Smith, 1981; Hickey 1976; Huyer 1983) and supports high primary productivity and fisheries (e.g., Ryther 1969; Pauly and Christensen 1995). This efficient supply of deep oceanic nutrients to the coastal zone can operate at the expense of a decline in nearshore aragonite and calcite saturation states and DO concentrations, because the water that is upwelled to the shelf is also often oxygen-poor and high in DIC (Feely et al. 2004; 2009). Both observations and models highlight the rapid progression and biogeochemical sensitivity of the CCS to ocean acidification and hypoxia (OAH)

(Feely et al. 2008; Gruber et al. 2012; Chan et al. 2017), which strongly affects present and future expression of OAH in the coastal zone (Feely et al. 2008; Gruber et al. 2012; Harris et al. 2013; Chan et al. 2017). High rates of productivity in the coastal zone may operate at the expense of (1) decreasing aragonite and calcite saturation states and decreasing DO concentrations because the water that is upwelled to the continental shelf also has reduced DO levels, lower pH, and higher concentrations of DIC; and (2) high productivity maintains a high standing stock of POC (e.g., Hales et al. 2006), which builds a respiration signal in the water column and at the sediment/water interface and results in DO level declines (Diaz and Rosenberg 2008; Rabalais et al. 2010). We are learning that nearshore rates of change (e.g., lower pH, warmer water, lower DO) often outpace offshore estimates and observations, and the mismatch is due to coastal processes (Booth et al. 2014; Chavez et al. 2017; Siedlecki et al. 2021). Physical forcing mechanisms and regional topography and bathymetry can influence the composition of source and upwelled waters while shelf biogeochemical processes can further modify waters (either upwelled to the shelf and introduced by rivers/estuaries). This has the potential to drive spatial and temporal variability in nearshore OAH exposure within CCS regions and across regions at different rates.

Although the CCS is one of the most highly observed ocean regions in the world, there has been comparatively limited research on subsurface dissolved oxygen (DO) and carbonate system parameters on the continental shelf between Cape Mendocino and San Francisco Bay (Figure 2.1). Currents and circulation south of Cape Mendocino and north of San Francisco Bay have been well studied through data ob-

tained during several large projects in the 1980's and 1990's (see section 1.2.3), and the impact of wind and current variability on productivity between 37.5 - 39°N and 122.5 - 124°N were studied during CoOP WEST (Largier et al. 2006). However, time-series of subsurface DO are relatively scarce in this subregion, and we are left knowing little about the oxygen content of coastal waters in the Gulf, which feed San Francisco Bay and – at times – flow poleward past Point Reyes, a prominent headland that shelters the Gulf to the north (see Figure 2.1). This forces management decisions on low oxygen (hypoxic) exposure to be made without a proper understanding of regional risk. Scientifically we are left wondering: (1) what DO levels occur in a section of the CCS that experiences the strongest upwelling favorable winds ($\sim 8x$ stronger than the Pacific Northwest); and (2) how DO levels respond to upwelling and relaxation events in this subregion?

The The Gulf of the Farallones ("the Gulf") represents a unique section of the California coast. It is situated on a wide section of continental shelf and sits at the entrance to San Francisco Bay (Figure 2.1). Therefore, the Gulf interacts with the estuary, adjacent coastal ocean, and water off the steep, continental slope. While much of the continental shelf from Oregon to Point Conception is relatively narrow, and typically $\leq 20\text{km}$ wide, the Gulf represents a wider section of shelf, $\sim 50\text{km}$. The Gulf is also considered a retentive zone for San Francisco Bay outflow and newly upwelled water (near Drakes Bay and $\sim 30\text{ km}$ south of Point Reyes; Wing et al. 1998; Largier 2004; Vander Woude et al. 2006), and the embayment extends immediately north of Point Reyes can also be retentive at times (Figure 2.1; Vander Woude et al. 2006).

Not only does the Gulf represent source water to San Francisco Bay, Drakes Bay, and other small coastal lagoons, but it is also connected to coastal and estuarine waters north of Point Reyes (and vice versa; Figure 2.1). Equatorward shelf flow is driven by persistent upwelling favorable winds (Halle and Largier 2011; Kaplan et al. 2009), and during wind relaxation events, poleward flow on the shelf is observed which is driven by a poleward pressure gradient (Gan and Allen 2002a&b;2005; Hickey and Pola 1983; Largier et al. 1993). The biological importance of these circulation patterns is well documented for this connected Farallones–Reyes–Arena region (e.g., Wing et al 1995a&b; 1998; Largier 2003; Botsford et al. 2003;2006; Largier et al. 2006; Roughan et al. 2006; Kudela et al. 2008; Krause et al. 2020). This region features (1) high rates of productivity, (2) retentive embayments, and (3) is located on a wide shelf section. The combined impact of prolonged retention with a strong respiration signal typically facilitates coastal hypoxia, with the severity, persistence and spatial pattern reflected by the degree of water column ventilation (Diaz Rosenberg 2001; Monterio et al. 2011 Levin and Breitburg 2015).

Scarcity of subsurface DO observations off northern California (from 37°N to 42°N) previously limited our ability to characterize the occurrence of hypoxia in this subregion of the CCS. In this chapter, we use time-series mooring data collected in the Gulf and north of Point Reyes, off Bodega Head (Figure 2.1), to describe patterns and timing of hypoxia, and explore how DO levels respond to upwelling and relaxation events. We first describe the mooring data (section 2.2). Then, in sections 2.3 and 2.4, we use mooring and wind data to describe (1) the timing and severity of hypoxia, and

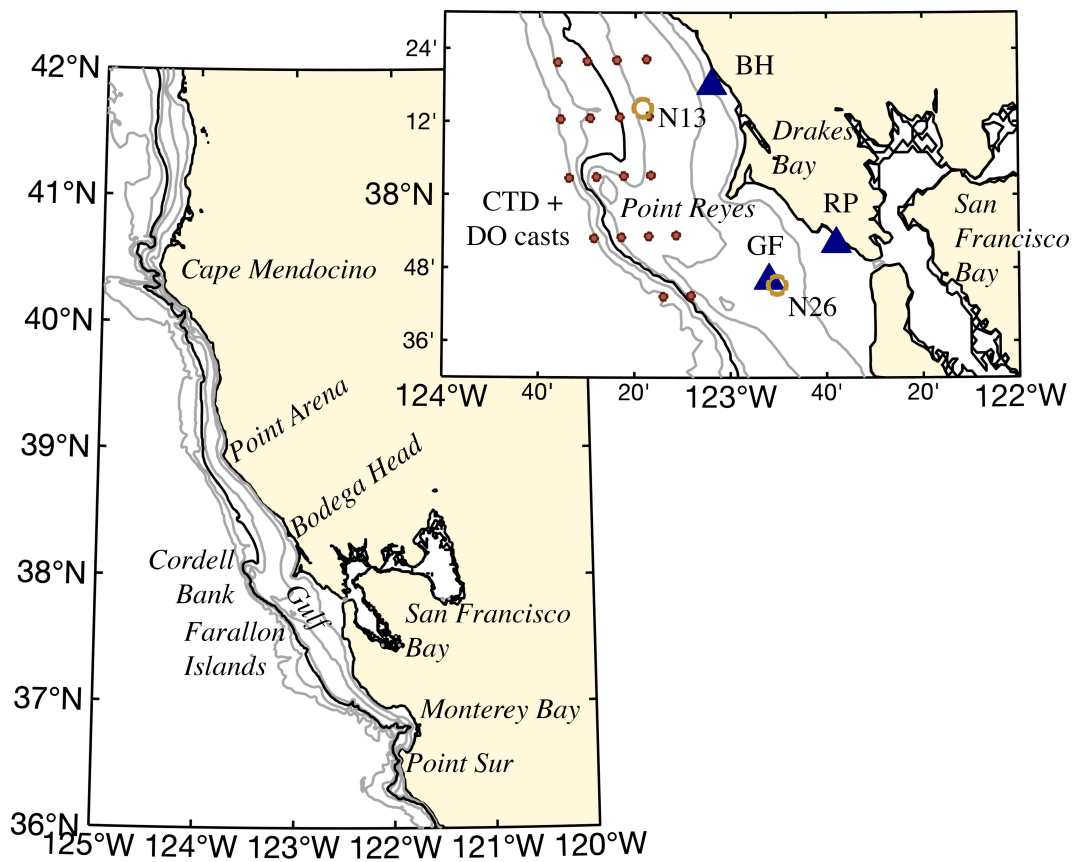


Figure 2.1: Site map Mooring locations shown (blue triangles); CTD+DO cast locations (small red circles); Wind buoy NDBC46013 (N13) and 46026 (N26) marked by yellow circles. Contours shown on both maps: 40, 80, 130, 200, 500, 1000 m. Bold contour is 200 m.

(2) the response to upwelling and relaxation events.

2.2 Data sources and processing

2.2.1 Mooring data

During 2015, moored sensors are deployed on the California shelf: Two sites in the Gulf of the Farallones (GF; RP) and one site located north of Point Reyes, off Bodega Head (BH) (Figure 2.1).

Two moorings were deployed in the Gulf of Farallones from 28 March – 20 July 2015 (GF and RP; Figure 2.1) as part of a California Sea Grant project investigating the potential for hypoxic intrusions into San Francisco Bay. One mooring was deployed east of the Farallon Islands at about $\sim 54\text{m}$ depth; the other deployed at $\sim 18\text{m}$ (Figure 2.1). At both sites a Sea-Bird Electronics (SBE) 37 MicroCAT conductivity and temperature (C-T) recorder and Precision Measurement Engineering (PME) DO and temperature logger (MiniDOT) collected data at $\sim 1\text{m}$ above bottom. At the deeper Gulf mooring, GF, a SBE-39 temperature sensor was deployed at $\sim 15\text{m}$ and an Onset HOBO 12-bit temperature logger (TidbiT) was deployed $\sim 1\text{m}$ below surface to provide an estimate of sea surface temperature. TidbiT sensors provide a rough estimate of temperature, as their accuracy is $\pm 0.2^\circ\text{C}$. The northern site (BH) is located approximately 1.2 km off Bodega Head (Figure 2.1), and was located next to a semi-permanent mooring maintained by the University of California, Davis - Bodega Marine Laboratory (BML). In 2015 a PME MiniDOT logger was deployed at BH ($\sim 30\text{m}$ depth) from February

through October 2015.

Instruments were serviced before the field season for GF and RP mooring locations, and field validated at the beginning and end of each deployment using a SBE 19plus V2 SeaCAT Profiler equipped with a DO auxiliary sensor, which measures conductivity, temperature, and depth (CTD) and DO. Density and other seawater properties were calculated using the Thermodynamic Equation of Seawater 2010 standard, using the Gibbs-SeaWater Oceanographic Toolbox (McDougall et al. 2012). To that end, unless otherwise specified, salinity in this manuscript is reported as Absolute Salinity (SA; $g\ kg^{-1}$). Sigma-density values, $\sigma_\theta = \rho(S, T, P) - 1000$ and spiciness, π , presented were calculated using SA, conservative temperature, and pressure. In this chapter, "low-pass filtered data" refers to a time-series variable that had a 33-hour low-pass filter applied using the PL33 filter described by Rosenfeld (1983).

2.2.2 Buoy data – wind and temperature

We used wind and sea surface temperature (SST) data from the National Data Buoy Center (NDBC) meteorological monitoring buoy located off Bodega Head (46013; N13) and in the Gulf of the Farallones, California (46026; N26; Figure 2.1), which are available at: ndbc.noaa.gov. Small gaps (< 3 hours) in the buoy record were gap filled using linear interpolation. We filled a 5-hour gap at N13 on 29 July 2015 with data from N26 using coefficients determined from a regression of 2015 data between N13 and N26 (wind speed $R^2 = 0.81$). We used hourly wind speed and direction data from 2015 and calculated equivalent 10m wind velocity and wind stress (Edson et al. 2013).

Wind data were rotated into local coordinate systems based on the principal axes of wind variability and are referred to as \sim alongshore (positive poleward; downwelling-favorable) and cross-shore (positive onshore, orthogonal to the major axis) winds. Both hourly stress and wind were low-pass filtered, using the PL33 filter described by Rosenfeld (1983) with a 33 hour cutoff period, to remove higher frequency signals. Principal axis wind ellipses obtained for 2015 were like those calculated by Dorman and Winant (1995) and Garcia-Reyes and Largier (2012). The filtered alongshore wind stress measured at N13 is denoted simply as τ (without subscript). Unless otherwise specified, reference to “low-pass filtered data” hereafter indicates time-series data that were filtered with a 33-hour cutoff period.

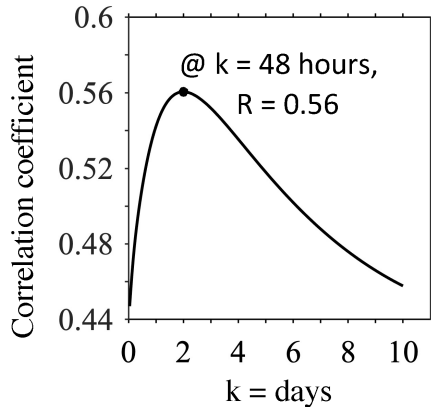
2.2.3 Seasonality of coastal upwelling

Wind forcing is one of the features that divides the CCS into sub-regions (see Figure CCS; section 1.2). Off northern California three seasons are recognized (Largier et al. 1993; Garcia-Reyes and Largier 2012). Specifically, Garcia-Reyes and Largier (2012) use monthly mean and standard deviation of buoy wind stress to describe these seasons: an upwelling season (April - June), a relaxation season (July - September), and a storm season (December - February). Here we employ a simple set of thresholds to estimate seasonal transitions using wind data from N13. The spring transition marks an increase in equatorward wind stress and persistence, here flagged when the median of the past 30 days $\tau \leq -0.04 \text{ N m}^{-2}$ and confirmed by inspection of near-bottom temperature values off Bodega Head. Soon after the spring transition, winds strengthen

and typically exceed $\sim 0.1 N m^{-2}$ through the upwelling season. Relaxation events are common throughout the upwelling season and identified by periods of time when wind velocity drop below its mean value after being strongly upwelling favorable (see also Fewings et al. 2016 and Melton et al. 2009). The start of the relaxation season is marked by a persistent decrease in mean wind stress and flagged when the median of the past 30 days $\tau \geq -0.04 N m^{-2}$. The storm season represents a transition to weak mean winds and flagged when the median of the past 30 days $\tau \geq -0.02 N m^{-2}$.

2.2.4 Bottom DO and wind stress

To investigate the response of subsurface DO to wind forcing, we applied an exponential decay filter to hourly alongshore wind stress at N13 (see Figure 2.2). This index was based of work described in Austin and Barth (2002) and was applied as a filter following Giddings et al. (2014). The response time scale was determined by finding the filter width, k , that maximizes correlations between filtered wind stress (W_k) and near-bottom DO, here $k = 48$ hours (2 days). In this analysis we used instantaneous hourly, alongshore wind stress from N13 and subsurface DO from BH. Mooring data from BH was used in this analysis because it has the longest DO record from 2015 (February – October; see Figure 2.3c). Filtered wind stress, “ W_2 ”, is used in our analysis alongside low-pass filtered alongshore wind stress.



$$W_k = \frac{1}{k} \int_0^t \tau e^{(t'-t)/k} dt'$$

τ is alongshore wind stress at N13
 k is a filter time scale
and t is time

Figure 2.2: Cross-correlation of hourly alongshore wind stress at N13 and bottom DO at BH, showing the results of correlations between filtered alongshore wind stress (W_k) and near-bottom DO at BH. Data used were collected between February – October 2015. The correlation coefficient, R , shown is normalized so that the autocorrelation at zero lag equals 1. A range of k values were analyzed between 1 hour - 240 hours (10 days). Max R for each k -value is shown. Wind data were collected at hourly intervals; therefore, we sampled the DO time-series at hourly increments prior to comparison. If only upwelling dominated months April – May are considered, k is still 2-days but R increases from 0.56 (February – October) to 0.67 (April – May).

2.2.5 Marine heatwave conditions and the California drought

The 2015 mooring data used in this study were collected during the 2012 – 2016 California drought and feature periods of time when strong warm water anomalies (marine heat waves, [MHWs]) were present in coastal waters of the CCS. Notably, in 2015, one of the largest MHWs on record in the northeast Pacific extended to the central and southern CCS (Gentemann et al. 2017; Zaba and Rudnick 2016). We use dates identified by Sanford et al. (2019) to flag times when MHW conditions were present in coastal waters of our study. Sanford et al. (2019) followed Hobday et al. (2016) definitions for MHW presence to classify temperature anomaly conditions, which included using a 30-year record (1981 – 2011) of SST from N13 (Figure 2.1). Coastal

conditions were flagged when 2015 SST at N13 exceed the 90th percentile based on the 30-year record for ≥ 5 days.

Although freshwater input to estuarine and coastal regions is typically low off California during the upwelling and relaxation season, it would be remiss to ignore the severe drought conditions that affected California in 2015. Implications of the drought on shelf hypoxia and retention are addressed in our discussion.

2.3 Results

2.3.1 Coastal upwelling seasonality

Although upwelling favorable winds are present throughout the year in the central CCS (also shown in Figure 2.3a), the spring transition marks the first month dominated by upwelling-favorable conditions (Strub et al. 1987; Lentz 1987; Lynn et al. 2003). We estimate the 2015 spring transition to occur between 20 March (based on the wind conditions) and 5 April (based on the arrival of cold bottom water at BH and reduced SST at N13) (vertical dashed lines flag transitions in Figures 3a and b). Although the deeper Gulf mooring (GF) was deployed on 26 March 2015, we still observe a strong decline in bottom water temperature associated with the strong upwelling event on 1 April (peak $W_2 > 0.3 \text{ N m}^{-2}$) (Figure 2.3b). In addition to decreasing temperatures, we also observe a net decline in subsurface DO at BH between February and April (median DO levels drop from 4.7 ml L^{-1} to 3.5 ml L^{-1}) (Figure 2.4a). Both Gulf moorings (RP and GF) were deployed on 26 March 2015, so we cannot include

trends of subsurface DO across the 2015 transition to the upwelling season. However, from ~ 5 April through ~ 9 May the coldest, near-bottom water is observed at the mooring sites (GF, RP and BH), and overall, at all three sites the lowest DO conditions are observed outside 5 April - 9 May 2015.

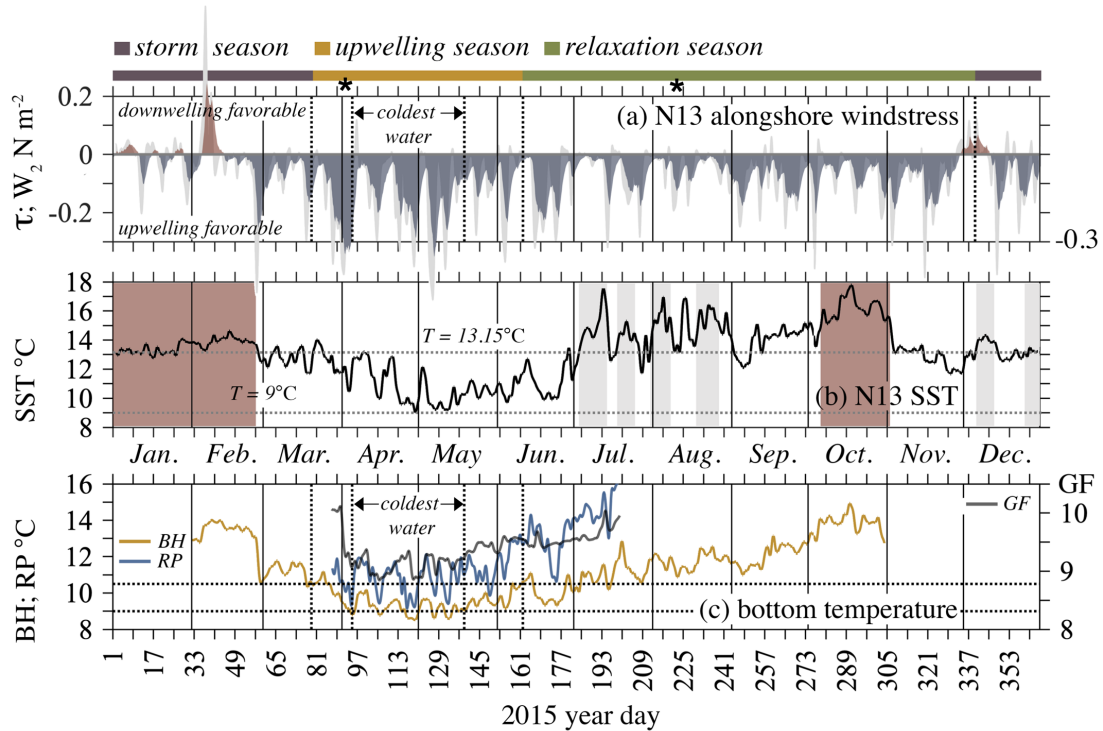


Figure 2.3: 2015 alongshore wind stress, SST and mooring bottom temperature time-series This figure presents (a) low-pass filtered alongshore wind stress at N13 (grey) and W_2 (red, downwelling favorable; blue upwelling favorable). Approximate seasonal transitions shown above subplot (a): the storm season (purple bar), upwelling season (yellow bar); and relaxation season (green bar). (b) SST at N13 (black line) shown with MHW presence flagged following Sanford et al. (2019). Shading, either grey or red, marks periods where the 2015 temperature at N13 exceed the 90th percentile based on a 30-year record at N13 (1981 – 2011) for ≥ 5 days. Red shading represents one of 10 most intense events since 1981. For reference, the mean SST for 2015 is shown by a dashed horizontal line ($13.15^\circ C$) and $9^\circ C$ is also shown. (c) time-series of bottom temperature for each mooring site are shown: BH (gold) and RP (blue) on left y-axis, and GF (dark grey) on right y-axis. Using left y-axis as a reference, dashed horizontal lines are shown at $10.5^\circ C$ (max right y-axis) and $9^\circ C$. Vertical black lines mark the first of each month in all subplots (a-c). Temperature and τ and are low-pass filtered. Both asterisks on (a) denote relaxation events discussed in the Results section. Date tick marks are spaced at 8-day increments.

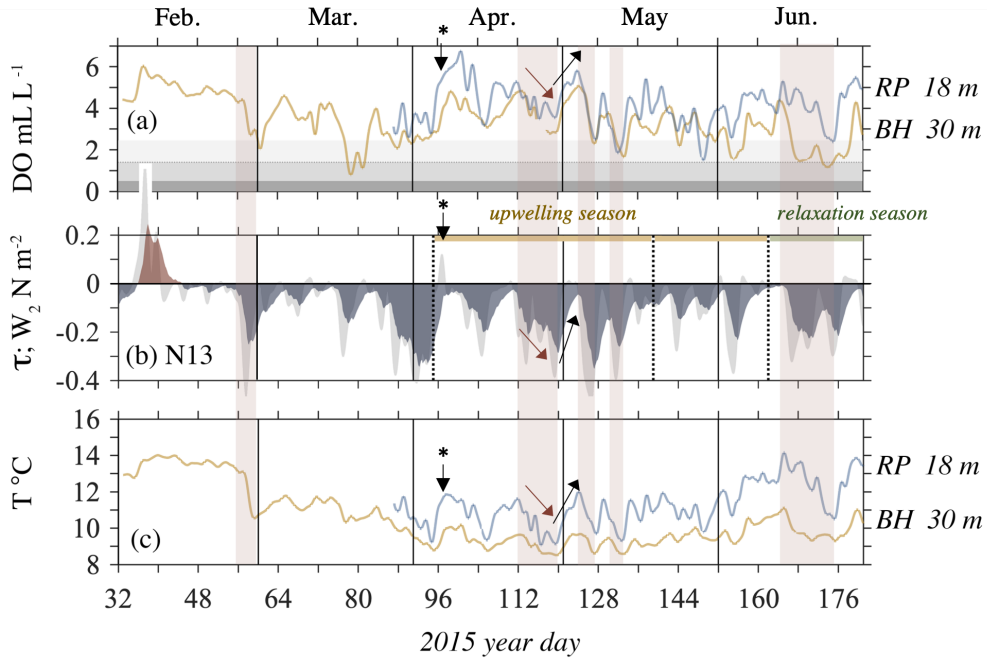


Figure 2.4: BH (~ 30 m) and RP (~ 18 m) mooring data. This figure presents time-series of bottom DO (a) and temperature (b) at RP (blue line) and BH (yellow line). Alongshore wind stress at N13 (grey) and W_2 (blue upwelling favorable) are shown in (c). Approximate seasonal transitions shown above upwelling season (yellow bar); and relaxation season (green bar). All data presented, except W_2 , is low-pass filtered. Hypoxic thresholds are shown in subplot (a) mark severe (darkest grey); intermediate (grey); mild (lightest grey) hypoxia. Duration of intermediate hypoxia BH ~ 1 -2 days. (a). Brown shading is provided to aid discussion of upwelling events (shaded). Relaxation events are not shaded, but generally follow upwelling events and feature decelerating winds (W_2 approaching zero). Trend arrows are shown on one upwelling/relaxation event (in April/May).

As expected, we observe a strong relationship between temperature and wind stress, which is characterized by strong upwelling-favorable winds (and cooling temperatures) and frequent wind relaxations (which associate with warming temperatures). Downwelling events (e.g., early February 2015) are rare and associate with increases in both temperature and subsurface DO concentrations (Figures 2.3 & 2.4a). Across all three mooring sites we observe lowest DO conditions during the relaxation season

(Figure 2.4a & 2.5). Further, at the deeper Gulf mooring (GF ~ 54 m) we observe a net decline in subsurface DO levels during relaxation events (Figure 2.5). In contrast, we generally observe an increase in DO levels at the shallower sites (BH 30m and RP 18 m) during relaxation events, and declines during upwelling events (Figure 2.4).

As typical for this region, winds weaken at N13 between June and July 2015, and the system switches to a relaxation season on ~ 11 June 2015 (a vertical dashed line flags this transition in Figure 2.3a and c). In the relaxation season, we still observe some strong upwelling events (e.g., late June; September and November in Figure 2.3a). However, the relaxation season features (1) overall weaker equatorward winds at N13; and (2) a smaller change between peak upwelling favorable and weak winds during relaxation events. For illustration, an upwelling event in August peaks with $W_2 \approx 0.12 \text{ N m}^{-2}$, while an event in April peaks with $W_2 \approx 0.34 \text{ N m}^{-2}$ (see Figure 2.3a*). Both events relax to $W_2 \approx 0.04 \text{ N m}^{-2}$ (August) and $W_2 \approx 0.03 \text{ N m}^{-2}$ (April) over a span of 4-5 days. Most relaxation events feature decelerating winds over a similar timescale of ~ 3 -10 days in both the upwelling and relaxation season(s), but the change in wind stress is generally larger in the upwelling season when compared with the relaxation season.

During the relaxation season, we observe an increasing trend in SST at N13 (starting late June, Figure 2.3b), and the arrival of strong SST anomalies which coincide with relaxation events in July and August (grey shading; Figure 2.3b), a time when the MHW conditions were present nearshore (e.g., Genteman et al. 2017; Sanford et al. 2019). Stronger upwelling favorable winds return in September (and November)

2015, which coincide with an ~ 1 month respite (each) from elevated SST (Figure 2.3b). However, as winds relax at N13, severe MHW conditions also return in October (red shading; Figure 2.3b). Although it occurs outside the dates when the Gulf and BH moorings were deployed, storm season conditions return between 5-6 December 2015 (a vertical dashed line flags this transition in Figure 2.3a). The Gulf mooring deployments ended on 20 July 2015. Based off a 30-year record at N13 by Sanford et al. 2019 (see section 2.5), elevated SST anomalies were not present at N13 during most of the Gulf mooring deployments (from 26 March - 3 July 2015) (Figure 2.3b).

2.3.2 Mid-shelf site, Gulf of the Farallones, GF (54 m)

The Gulf mooring was deployed on 26 March 2015 during a lull in upwelling favorable winds. Although the spring transition was not fully captured, we observe a strong decline in bottom water temperature associated with the strong upwelling conditions present in late March and early April (peak $W_2 > 0.3 N m^{-2}$) (Figure 2.3b). After this event, subsurface temperature at GF (and the other 2 moorings) remains low through ~ 19 May (Figures 3c and 4c). Coincident to this strong spring upwelling event, we observe reduced subsurface DO just above the threshold for mild hypoxia at GF. Winds transition to downwelling favorable on (~ 5 April) and we observe an increase in subsurface DO and a decrease in spiciness (Figure 2.5a and b).

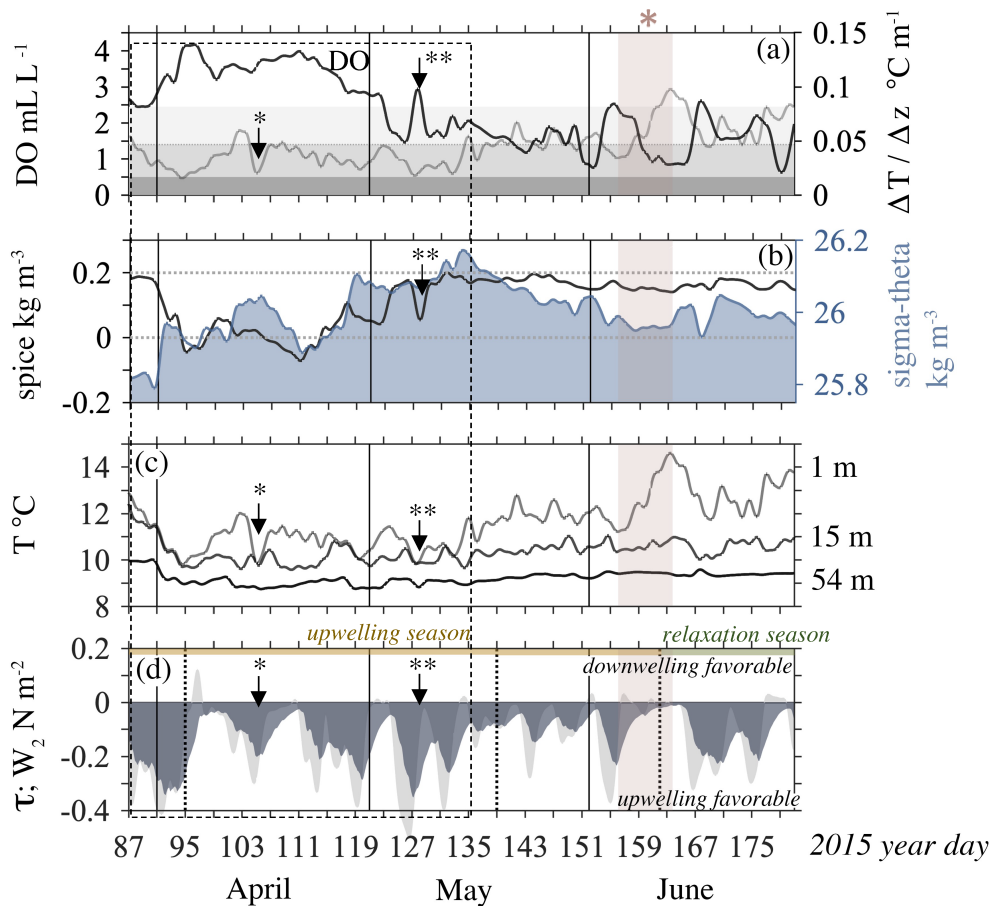


Figure 2.5: Gulf (GF 54 m) mooring data. This figure presents time-series of bottom DO (black line, a); spiciness (black line) and sigma-theta (right axis, blue) (b); temperature at 1m, 15m and 54m from the GF mooring site. $\Delta T \Delta Z^{-1}$ (using surface and bottom temperature) is shown (grey line, a) for comparison with DO. Alongshore wind stress at N13 (grey) and W_2 (blue upwelling favorable) are shown in (d). Approximate seasonal transitions shown above upwelling season (yellow bar); and relaxation season (green bar). All data presented, except W_2 , is low-pass filtered. Hypoxic thresholds are shown in subplot (a) mark severe (darkest grey); intermediate (grey); mild (lightest grey) hypoxia. Duration of intermediate hypoxia: ~ 3.5 days; ~ 4 days; ~ 8.2 days; and ~ 3.6 days (in order of occurrence) (a). Pink shading across each subplot highlights a relaxation event discussed in the results section.

As shown in Figure 2.5a and b, subsurface DO at GF exhibits two modes of variability. During the first part of the GF deployment (outlined by a dashed line, Figure 2.5), a strong relationship between DO and water type, as indexed by spiciness,

is observed prior to ~ 14 May 2015. Prior to 14 May 2015, decreasing DO correlates with increasing spiciness, and vice versa (adj R^2 0.9; RSME 0.15). Then after ~ 14 May 2015, the variability in spiciness we observe is small and DO levels fluctuate with changes in stratification and wind events. At the Gulf mooring, for discussion purposes, hereinafter we refer to the time prior to 14 May 2015 as "first mode" and afterwards as "second mode". During this second mode, strong increasing upwelling conditions (indexed by W_2 becoming more negative) corresponds to a decrease in stratification and an increase in DO content. While relaxation events (decelerating winds; W_2 trending towards zero) coincide with an increase in stratification and a decline in DO content (see brown shading in Figure 2.5 for illustration of relaxation event). Fluctuations in density are superimposed on a longer density trend (see Figure 2.5b): during the first mode an increasing trend in σ_θ is evident and peaks at ($\sim 26.17 \text{ kg m}^{-3}$). Afterwards, during the second mode, a decreasing trend in σ_θ is evident through the end of the deployment (through July as well, not shown). It is during the second mode that the lowest DO levels are observed.

During the first mode (prior to 14 May), we observe an event where subsurface DO changes relatively fast (~ 6 May; Figure 2.5a**) concurrent with a changing temperature and salinity. This event coincides with strong upwelling favorable winds at N13 (peak $\tau \sim -0.5 \text{ N m}^{-2}$) (Figure 2.5d), which explain the fast change in water type (Figure 2.5b**) and deepening of the mixed layer (Figure 2.5c**). Prior to this event, there was a net decline in DO during a relaxation event ($\sim 5-6$ days in length). Strong upwelling winds likely interrupted the decline to intermediate hypoxia, and re-

duced stratification which is a mechanism that helps alleviate hypoxia across the shelf. However, we attribute the sudden change (in DO and water type) at the mooring to be dominated by advection of a water mass from a different location to the mooring site. Weaker upwelling events (e.g., ~ 14 April with peak $\tau \sim -0.3 \text{ N m}^{-2}$) also result in deepening of the mixed layer (Figure 2.5c*) and reduced stratification (Figure 2.5a*) but the change in water type is not as rapid (Figure 2.5b). While advection is important in this event, a more gradual increase in subsurface DO observed at the mooring, which may be attributable to an increase in vertical mixing allowed by a breakdown in stratification.

Subsurface DO levels at GF declined to mild hypoxia in early May 2015, and a trend for declining subsurface DO is evident through May and June (Figure 2.5a). Upwelling events alleviate hypoxia (e.g., ~ 6 May; ~ 3 June, $\sim 15 - 23$ June; Figure 2.5a and d), while DO levels decline during relaxation events (e.g., ~ 30 May – 1 June; $\sim 4 - 14$ June (brown shading); $\sim 24 - 28$ June; Figure 2.5a and d). The lowest DO is present from mid-May to mid-June during relaxation events, with four intermediate hypoxia events lasting ~ 3.5 - to 8.2-days. In low-pass filtered data, the range of minimum DO levels are 1.2 mL L^{-1} (mid-May) to 0.6 mL L^{-1} (late June), and during the prolonged period of intermediate hypoxia ($\sim 8 - 15$ June) the minimum DO level is $\sim 0.8 \text{ mL L}^{-1}$. In hourly averaged data, there are two events where DO levels decline to the upper threshold of severe hypoxia: on 2 June (minimum 0.60 mL L^{-1}) and 28 June (minimum 0.57 mL L^{-1}). Both events are coincident with $\sim 9.5^\circ\text{C}$ water, decelerating winds and enhanced stratification.

2.3.3 Inner shelf sites, BH (30 m) and RP (18 m)

The first significant upwelling event in 2015 occurred at the end of February, which also aligns with a break from severe MHW conditions (present from December 2014 – February 2015; Figure 2.3a) and a drop in subsurface DO at BH (Figure 2.4). The response of subsurface temperature at BH in February 2015 reflects the (relatively quick) transition from strong downwelling (peak on 6 February, $0.5 N m^{-2}$) to strong upwelling (peak on 26 March, $-0.47 N m^{-2}$) (Figure 2.3a and c). The spring transition does not occur until 20 March (based on the wind conditions) and 5 April (based on the arrival of cold bottom water at BH and reduced SST at N13) (vertical dashed lines flag transitions in Figures 3a and b). We observe a net decline in subsurface temperature and DO at BH between February and April; Median subsurface DO levels(temperatures) drop from $4.7 mL L^{-1}(13.5^{\circ}C)$ to $3.2 mL L^{-1}(11^{\circ}C)$ and after the spring transition April median values are: $3.6 mL L^{-1}(9.2^{\circ}C)$ (Figure 2.4).

The inner shelf, Gulf mooring (RP) and was deployed on 26 March 2015, so we cannot include trends of subsurface DO across the 2015 transition to the upwelling season. However, from ~ 5 April through ~ 9 May the coldest, near-bottom water is observed at the mooring sites (GF, RP and BH), but overall the lowest DO is observed outside the period of coldest temperatures and strongest winds (i.e., not during the months of April and May) (Figure 2.4 & 2.5). Interestingly, and although the two moorings are separated by Point Reyes (Figure 2.1), DO at RP and BH followed markedly similar trends in 2015 (Figure 2.4). The relationship between the two moorings appears

to be the tightest in the upwelling season (during strongest winds). Although during downwelling winds just after the spring transition (see Figure 2.4*), an increase at the shallower site RP (18 m) has a larger increase in DO as compared to the deeper mooring BH (30 m). As the mean wind stress declines towards the end of the upwelling season, and the bottom water starts to warm, we observe a bigger difference in DO between the two mooring locations. However, they both follow similar trends through the end of June (Figure 2.4).

Subsurface DO levels at both moorings exhibits high variability. Between 28 March and 30 June 2015, DO values range from 1.2(1.5) $mL L^{-1}$ to 5(6.8) $mL L^{-1}$ at BH(RP). This DO variability correlates well with fluctuations in water temperature, which in turn are correlated with wind forcing. By applying an exponential decay filter to instantaneous, hourly alongshore wind stress at N13, we find that the response time scale that maximizes correlations between filtered wind stress and subsurface DO to be ~ 2 days (see section 2.2.4; Figure 2.2). By only using the W_2 metric and subsurface DO, we can explain a large majority of the variability in DO at BH and RP: we observe reduced DO values with cold, upwelled water brought to the inner shelf sites during upwelling events, and DO concentrations increase during relaxation events. Illustration of these events are shown in Figure 2.4, with select upwelling events shaded brown and subsequent relaxation events follow the shaded bars. This trend is opposite to the response in DO we observe during the first mode at the deeper Gulf mooring (GF).

We observe the lowest DO levels in June at GF (Figure 2.5 and in May/June at RP and BH (Figure 2.4). Low DO levels are also present at BH during March 2015,

prior to the arrival of cold water (Figure 2.4), but the GF and RP were not deployed at the time of this observation. A few short observations of intermediate hypoxia events lasting ~ 1 - 2-days are also present. In low-pass filtered data, we observe minimum DO levels during intermediate hypoxic events of 0.8 mL L^{-1} (March/BH; note RP not deployed yet) and $\sim 1.2 \text{ mL L}^{-1}$ (June/BH). At RP, we observe lowest DO levels ($\sim 1.5 \text{ mL L}^{-1}$) in late May that approach intermediate hypoxia. However, values below 1.4 mL L^{-1} are only present in hourly data at RP.

2.4 Discussion

This work was motivated by a need to better understand how this subregion off northern California fits with current understanding of shelf hypoxia in the CCS. We are interested in understanding (1) what shelf hypoxia looks like in a section of the CCS that experiences the strongest upwelling favorable winds; and (2) how subsurface DO responds to upwelling and relaxation events in this subregion. To answer these questions, we monitored DO levels over the shelf to the north and south of a major headland (Point Reyes) in the northern California coastal upwelling region. Two sites (RP and GF) were located south (and typically downwind) of Point Reyes, and the third site (BH) was located to the north of the headland (Figure 2.1). The deeper Gulf site (GF ~ 54 m) is located within the more stratified upwelling shadow downwind of Point Reyes. We observed lowest DO concentrations and most persistent hypoxia at GF. At the shallower sites, BH (~ 30 m) and RP (~ 18 m), we observed highly variable DO values

with short hypoxic events outside the upwelling season. Data collected in 2015 also represents an extreme year for the California coastal zone in terms of freshwater input (largest drought on historical record), and warm temperature anomalies (as a MHW was present in the CCS). The weakness of the freshwater flux from San Francisco Bay during these mooring deployments was somewhat convenient in that it allowed observations of stratification and hypoxia related entirely to upwelling and surface warming, in contrast to conditions in the northern CCS (e.g., in the northern CCS where freshwater input is large, as discussed in Chapter 4 of this dissertation). The presence of MHW conditions and high surface temperatures are anomalous for this location (and across the CCS), but the strength of thermal stratification is comparable with many other classical upwelling bay locations (Largier 2020).

2.4.1 Upwelling source waters

The CCS represents a union of different water masses that originate in the tropical, subtropical, and subarctic regions of the eastern Pacific Ocean; each defined by temperature, salinity, DO and nutrients at the time of entry to the CCS (Lynn and Simpson 1987). The source of the deeper waters upwelled onto the shelf (“source waters”) varies by latitude due to basin-scale circulation and varies due to regional differences in upwelling processes. The efficiency and depth from which shelf water is derived during upwelling is dependent on the magnitude/persistence of upwelling winds, the alongshore structure of upwelling winds (e.g. Hickey et al. 2006), and the local cross-shelf wind profile (Jacox and Edwards 2012), as well as physical characteristics like local

stratification, bottom slope, and shelf width (Allen et al. 1995) and coastline shape (Barth et al. 2000; Pickett and Paduan 2003). These factors combine to differentiate regions of the CCS (see review by Checkley and Barth 2009), and each region is strongly influenced by remote and local physical forcing (Jacox et al. 2015; Bograd et al. 2015).

Deep waters upwelled on to the shelf predominantly include two end-member source water masses: Pacific Subarctic Upper Water (PSUW) and Pacific Equatorial Water (PEW) (Hickey 1979). But we are also learning that Eastern North Pacific Central Water (ENPCW) can contribute to salinity anomalies in the CCS (e.g., Ren and Rudnick 2021) and oceanic change in interior waters may drive regional variability in EBUS, including the CCS (e.g. Bograd et al. 2019; Monterio et al. 2011). The sluggish surface California Current transports PSUW equatorward, while the California Undercurrent transports PEW poleward (Hickey 1979). Further, increased advection of low-oxygen, PEW by the California Undercurrent has often been shown to cause a decline in coastal DO levels (e.g. Bograd et al. 2008; Pierce et al. 2012; Meinvielle and Johnson 2013), and the relative proportion of PEW present has been shown to impact community composition in the CCS (e.g., fish community composition as shown in McClatchie et al. 2010; Schroeder et al. 2019). On isopycnal surfaces, PEW and PSUW can be identified by temperature and salinity (Davis et al 2008; Thomson and Krassovski 2010), or “spiciness”, which combines these two conservative variables into one variable (Flament 2002). The percentage of PEW in upwelled waters varies with season and with latitude (decreasing poleward). Prior work estimates a range of 20% (Schroeder et al. 2019) to 50% (Thomson and Krassovski 2010) off northern California.

For analysis of water beneath ~ 100 m depth, end member analysis can be performed (e.g., Thomson and Krassovski 2010). Above that depth, and as we approach the coast, the mixture of PSUW, PEW and – sometimes ENPCW – is often modified. At depths shallower than 100m, deep upwelled water can mix with surface water, and downward fluxes of carbon likely contributes to modification of water chemistry. The chemistry and character (T-S) of water brought to the shelf during upwelling is dependent on the source water origin, which is an active area of research (both understanding what water is present for upwelling and how the biogeochemistry of water masses are changing).

To better understand the upwelling source water present during our mooring deployments we used conductivity, temperature, and depth (CTD)+DO casts collected over the outer shelf and slope as part of Applied California Current Ecosystem System Services (ACCESS) cruises (Figure 2.1). We included depth-averaged ACCESS CTD+DO data between 50 and 200m during years from 2014 and 2015. Data were collected only in June, July and September. Although data are not available in spring, we can see that there is a relationship between spiciness and DO. As expected, higher spice coincides with lower DO (and vice versa; Figure 6). This makes sense as ENPCW and PEW each associate with higher positive spice (warm and salty) and lower DO. While PSUW is typically characterized by a negative to low positive spiciness (“bland”) with high DO levels. Prior work suggests that the water upwelled to the shelf is oxygen-poor but above the threshold for intermediate hypoxia (e.g., off Oregon and Washington; Connolly et al. 2010; Adams et al. 2013). Typically the lowest DO levels present in cast data are just above the $1.4 \text{ mL } L^{-1}$ threshold, however a few observations fall

below (Figure 2.6).

While oxygen uptake, retention time and stratification over the shelf are drivers of shelf hypoxia, DO levels in upwelling source waters are also important. The amount of oxygen removed from a water mass on the shelf does not depend on the initial DO concentration. Given the same oxygen uptake and stratification across the shelf, a decrease in upwelling source water DO would drive deoxygenation trends that would result in lower DO levels over the shelf. Even small DO decreases in upwelling source waters will increase oxygen stress over the shelf, e.g., if DO levels in source waters supplied to the shelf were 0.1 mL L^{-1} lower during 2015, two severe hypoxic events would have occurred at GF (6 hours and 16 hours) instead of a single 2-hour event.

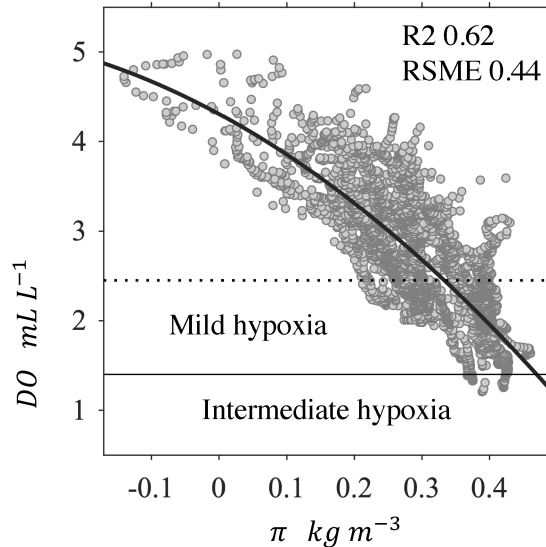


Figure 2.6: Spiciness – DO relationship for outer shelf and slope water. This figure shows spiciness (π) and DO data collected over the outer shelf and slope during ACCESS cruises (2014 – 2015). Depth-averaged CTD data were used to calculate spiciness. 45 casts are shown collected during June, July and September 2014 – 2015. Locations shown on Figure 1. Depths shallower than 50m are not shown. Max depth 200m. Salinity range: $33.3 - 34.3 \text{ g kg}^{-1}$. Temperature range: $8.5 - 11.7 \text{ }^\circ\text{C}$.

2.4.2 Upwelling seasonality and relaxation events

Although transition from the storm to the upwelling season coincides with a net drop in DO, the lowest DO is observed outside the period of coldest temperatures and strongest winds (i.e., not during the months of April and May) at all three sites (Figure 2.4 & 2.5). During the first mode at GF (deeper, mid-shelf site) and the entire time-series at RP and BH (inner-shelf sites), upwelling relates to DO decline and relaxation events with increasing DO levels. However, during the second mode at GF, the opposite occurs: upwelling relates to an increase in DO levels; relaxation events to declining DO levels. These observations paired with the relationship between spice and DO levels during the first mode at GF suggest water mass variability is driving DO trends (at least over the deeper sections of shelf, i.e., GF). During the second mode at GF, we hypothesize that either: (1) a local respiration signal was established and, during the second mode, shelf waters are lower in DO level than source waters, but the signal is still dominated by advection; (2) weaker winds lend to upwelling from shallower depths. It is clear that the DO-spice covariance over the first mode is strong, and then DO-stratification vary over the second mode at GF.

The direction of shelf flow is also important during upwelling and relaxation events. It has been shown that relaxation phases advect warm water poleward (Send et al. 1987; Send 1989; Largier et al. 1993; Gan and Allen 2002a&b; Kaplan and Largier 2006). Following Send and Nam (2012), we expect that relaxation events will modify subsurface DO. Oxygen-depleted waters can be advected from regions with strong

respiration signals to other sites over the shelf. We hypothesize mid-shelf waters are often advected northward during relaxation events which may have originated in the vicinity of GF (or areas where lower DO levels are present). However, our data set could not fully explore that hypothesis. Later in the spring/summer, during the relaxation season, DO levels on the shelf are likely be lower than the water being upwelled to the shelf. In this scenario, when upwelling circulation starts, the near-bottom, the mid-shelf environment may freshened by higher-DO water advected to the shelf during upwelling, while the lower-DO water present at the mid-shelf may be advected shoreward. This would result in a drop in DO values at inner-shelf sites (e.g., BH) but increasing DO levels at mid-shelf sites like (GF).

More work is necessary to unpack these observations. Additional, data from RP and BH may be available to explore whether these observations hold in other years (during other deployments), and securing funding for an additional mooring on the mid-shelf in the Gulf of the Farallones would be helpful to better understand shelf biogeochemistry as well as the source waters for San Francisco Bay (and other adjacent estuaries and lagoons).

2.4.3 Oxygen uptake over the shelf

The coastal waters across the CCS have high primary productivity, but this highest productivity (off Washington/southern British Columbia) is not co-located with the highest magnitude of upwelling-favorable alongshore winds (this region; off northern California) (Ware and Thomson 2005). This mismatch has been addressed by Hickey

and Banas (2008), who describe additional mechanisms that facilitate the region's high productivity beyond the traditional focus of the coastal wind field. First, the PNW shelf is wider than the California shelf (where peak winds occur), which promotes retention of upwelled nutrients (Strub et al. 1991). Second, energy from upwelling off northern California, in the form of coastal trapped waves contributes to upwelling in the northern CCS (Connolly and Hickey 2014). Third, the presence of shelf-break canyons are common across the CCS with a high density of canyons present off Washington (Hickey 1995). Canyon presence facilitates enhanced upwelling and allows water from deeper depths to reach the shelf (Allen and Hickey 2010; Connolly and Hickey 2014), which contribute high rates of nutrients to the shelf (Hickey and Banas 2008; Crawford and Dewey 1989). Plus, canyons also experience intense mixing (Lueck and Osborn 1985; Kunze et al. 2002; Wain et al 2013; Zhao et al. 2012), which can impact source depth and modify water mass properties transiting the canyon sill (Alford and MacCready 2014). Fourth, freshwater-driven mechanisms play an important and complex role in coastal productivity which includes but is not limited to: modifying nutrient distributions across the shelf, shifting primary productivity offshore and/or deeper in the water column, and modifying retention time, estuarine exchange, and regional circulation in the cross- and along-shelf direction (Lohan and Bruland 2006; Hickey and Banas 2008; Banas et al. 2009; MacCready et al. 2009; Hickey et al. 2010; Kudela et al. 2008; Giddings et al. 2014; Davis et al. 2014). As discussed in section 2.1, high rates of productivity in the coastal zone may operate at the expense of decreasing DO levels because high productivity maintains a high standing stock of POC (e.g., Hales et al.

2006), which builds a respiration signal in the water column and at the sediment/water interface and results in DO level declines (Diaz and Rosenberg 2008; Rabalais et al. 2010). In the northern CCS, August and September typically experience the most severe hypoxia as a respiration signal builds after the spring transition (Connolly et al. 2010; Adams et al. 2013; Siedlecki et al 2015). Our mooring time-series also does not extend to August/September, and therefore it is unclear how subsurface DO acts for the remainder of the relaxation season. However, based on the mooring data we explored, it seems like DO levels off northern California are higher than those observed off Washington. However, it is not yet clear why hypoxia off northern California is less severe than in the PNW. Is shelf hypoxia less severe off northern California because it is more readily flushed by stronger upwelling? Or because surface productivity is lower in the central CCS and therefore standing stocks of POC are smaller? Or if the presence of more freshwater input in the Northern CCS contributes to stronger stratification and the retention of POC? Or does the high density of canyons in the PNW facilitate worse hypoxic conditions? It is likely a combination of forcing that results in the mismatch. Although, we also hypothesize that the wind strength likely plays a role in alleviating the respiration signal by: (1) reducing the respiration signal on the shelf; (2) shifting carbon export to the outer shelf/slope; and (3) changing retention time and ventilation of shelf waters (e.g., Botsford et al. 2006; Yokomizo et al. 2010; Stone et al. 2020). Each would in turn have potential to alleviate shelf hypoxia across the shelf represented by mooring locations (BH, RP and GF). During the core upwelling season had oxygen-poor waters present, but the lowest DO levels and excursions to hypoxia were not observed

when the strongest, persistent upwelling favorable winds were present. The magnitude of upwelling-favorable winds observed at N13 (this study region) are not typically observed at N41 (off Washington); the winds following spring transition in the PNW more resemble the winds observed in the relaxation season in this subregion of the the central CCS.

While newly upwelled waters may exhibit mild hypoxia, intermediate hypoxia is rare and severe hypoxia is not expected (e.g., Figure 6). Intermediate and severe hypoxia are facilitated by oxygen uptake over the shelf. The lowest DO concentrations were observed in the Gulf of Farallones during relaxation events, when stratification is strong and surface phytoplankton blooms occur. Stratification can be expected to suppress downward mixing of DO from the surface layer while net or even enhanced respiration continues to deplete oxygen from subsurface waters. Given that the Gulf of Farallones is recognized as an upwelling shadow with enhanced stratification and surface plankton blooms (Largier 2004, VanderWoude et al 2006, Largier 2020), situated on a wide section of shelf, and given that sediments in this region are muddy with a significant organic fraction (USGS 2006), it can be expected that there is a marked oxygen demand and also that sub-thermocline waters are retained long enough for the effect of local drawdown to result in hypoxic conditions.

2.4.4 The 2012 – 2016 California drought

The CCS is experiencing several inextricably linked stressors. In the coastal zone, stressor conditions are impacted by large-scale changes observed in the North

Pacific as well as land-based changes in timing and volume of freshwater input. At the same time that the 2014 – 2016 MHW impacted the Pacific, California was also experiencing one of its deepest, longest, and warmest droughts in historical record (from 2012 – 2016; Lund et al. 2018). Although freshwater input to estuarine and coastal regions is typically low off California during the upwelling and relaxation season, it would be remiss to ignore the severe drought conditions that disrupted California in 2015. The cause of this drought has been largely attributed to the formation of a high-pressure system (ridging) in the Pacific Ocean off California. Although the climatological cause of the ridge is still being determined (Swain 2015; Singh et al. 2016; Swain et al. 2017), the documented impacts across California were severe with dismal snowpack volumes (e.g., Belmecheri et al. 2016), very low precipitation, and critically dry flows and water delivery (see review by Lund et al. 2018). Further, regulatory Delta outflows were reduced by the State Water Board which reduced environmental outflows by 1.4 billion m^3 thus allowing the salinity gradient zone in the Delta to move eastward; and from May - October 2015 barriers were placed in the western Delta to reduce the need for additional freshwater flow to the San Francisco Bay (see review by Lund et al. 2018).

Although drought conditions were present, San Francisco Bay outflow likely may still contribute to changes in shelf stratification and chemistry. The increasing trend in σ_θ observed in subsurface water at GF during the first half of the deployment may be explained by a building amount of dense water present on the shelf as the upwelling season progresses. However, it is unclear how this relates to a reduction in Delta outflow volume and change in outflow water type. The 2015 water temperature

and salinity at Fort Point, inside Golden Gate, increased in May and June and continued to increase throughout the summer. Part of this is likely attributable to the drought conditions and flow restrictions, and part due to warming coastal waters present in July (when MHW conditions were present at N13)(Figure 2.1). Although freshwater input was extremely low in 2015, warm water was still introduced to the Gulf from San Francisco Bay outflow. These data represent shelf DO dynamics during drought conditions. Collection of additional mooring data during large freshwater flow years (and non-drought years) would be helpful to determine if reduced freshwater inputs (and reduced Delta flows) act to modify shelf DO by modifying exchange with central San Francisco Bay and thus the shelf.

2.4.5 2015 marine heatwave conditions

At the same time land-based flow modifications were present, MHW conditions were present offshore. We used a flagging system developed by Sanford et al. (2019) to identify MHW conditions on the shelf. For the majority of our deployments MHW conditions were not present on the shelf. It has been shown that MHW conditions substantially modified subsurface waters (e.g., Scannell et al. 2020). It is unclear how MHW conditions modified subsurface water type present on the shelf and/or slope.

2.5 Conclusions

Moorings placed over the central CCS shelf from the mid- to inner- shelf exhibit complex and temporally varying DO trends. At the deeper, mid-shelf site, GF,

two distinct modes of variability are seen where upwelling relates to DO decline and relaxation events with increasing DO levels. During the second mode at GF, it seems like the opposite occurs: upwelling relates to an increase in DO levels; relaxation events to declining DO levels. These observations paired with the relationship between spice and DO levels during the first mode at GF suggest water mass variability is driving DO trends (at least over the deeper sections of shelf, i.e., GF). During the second mode at GF, we hypothesize that either: (1) a local respiration signal was established and, during the second mode, shelf waters are lower in DO level than source waters, but the signal is still dominated by advection; (2) weaker winds lead to upwelling from shallower depths. It is clear that the DO-spice covariance over the first mode is strong, and then DO-stratification vary over the second mode at GF. At the shallower inner-shelf sites, and for the entire time-series, upwelling relates to DO decline and relaxation events with increasing DO levels.

Stratification reduces vertical mixing, precluding diffusive fluxes of DO from the surface layer. As the upwelling season continues and shifts to the relaxation season, a respiration signal likely builds up across the shelf and may explain why the lowest DO levels occur later in the summer. The spatial variations in hypoxia that we observed in this study region, and differences between this region and other upwelling regions, is likely to be explained by differences in oxygen demand (sediment demand plus delivery of POC to sub-thermocline waters), differences in stratification (surface heating, freshwater influences, wind stress), and flow-path history of waters at that site. We hypothesize that later in the spring/summer (during the relaxation season) DO levels on the shelf

are likely be lower than the water being upwelled to the shelf. In this scenario, when upwelling circulation starts, the near-bottom mid-shelf environment may be freshened by higher-DO water advected to the shelf during upwelling, while the lower-DO water present at the mid-shelf may be advected shoreward. This would result in a drop in DO values at inner-shelf sites (e.g., BH) but increasing DO levels at mid-shelf sites like (GF). The importance of source water is clear in the first half at GF and the overall trend and second half shows the importance of local drawdown. These are consistent with other parts of the CCS. For example Adams et al. (2013) found later in the upwelling season shelf DO levels were lower than DO levels in newly upwelled water. The inner-shelf on the other hand shows less clear trends and more temporal variability pointing to a complex mosaic of shelf DO levels. Future work should involve velocity measurements to better understand the direction of flow during upwelling and relaxation events.

Based on the mooring data we explored, it seems like DO levels off northern California are higher than those observed off Washington. It is not yet clear why hypoxia off northern California is less severe than in the PNW, but it likely relates to a combination of forcing mechanisms that explain the mismatch in productivity. We hypothesize that the wind strength likely plays a role in alleviating the respiration signal by: (1) reducing the respiration signal on the shelf; (2) shifting carbon export to the outer shelf/slope; and (3) changing retention time and ventilation of shelf waters (e.g., Botsford et al. 2006; Yokomizo et al. 2010; Stone et al. 2020). This idea is corroborated by the lowest DO levels at all three sites were observed outside the core upwelling season (e.g., the period of coldest water temperatures and strongest

upwelling-favorable winds; not during the months of April and May). We also think the role of river plumes may play an important role in the expression of hypoxia in different regions of the CCS (and during different freshwater input scenarios within a subregion). For instance, lower freshwater to San Francisco Bay would result in less extreme density anomalies and thus weaker shelf stratification. However, more work is needed to explore the mismatch between shelf DO levels observed in the central versus northern CCS.

Our study region features a characteristic strong upwelling season and, in 2015, negligible freshwater influence. During the upwelling season, low runoff is typical but the freshwater input was exacerbated by drought conditions in 2015. With literature pointing to an increase in warming that will magnify the frequency of both droughts and floods in California, these data present one bookend of the shelf hypoxia story for this subregion. Although discharge from San Francisco Bay (and the Sacramento-San Joaquin Delta) is already a particularly complex puzzle with several end users, a better understanding of freshwater impacts to shelf chemistry may help with ecosystem management in the coastal zone. In a system like San Francisco Bay, where freshwater discharge is heavily regulated (from the Delta and from industrial and municipal discharge sources), managers may have a lever to help modulate coastal hypoxia and acidification. Although, a development of this metric would require collection of additional time-series observations and require a modeling study to further quantify the impact of San Francisco Bay outflow on retention within the Gulf.

While open-ocean waters are experiencing deoxygenation, at present upwelling source waters hover near the threshold for intermediate hypoxia and are often below

the threshold for mild hypoxia. The presence of more persistent hypoxia and intermediate to severe hypoxic events over the shelf is achieved by local oxygen uptake over the shelf. At the deeper site, GF, the lowest DO levels were observed after the upwelling season and during relaxation events, pointing to an important role of local DO draw-down. Upwelling regions with broader shelves and stronger stratification may be prone to more severe and/or persistent hypoxia (e.g., Monterio et al. 2011) – and within these regions, it has been suggested that most severe hypoxia has potential to occur within bays (e.g., Largier 2020). Linking observations with numerical modeling has the potential to describe the mosaic of oxygen variability more fully across upwelling shelves and may elucidate how short duration hypoxic events may be exacerbated by global deoxygenation. This is critical to assessment, evaluation, and management responses to increased occurrences of hypoxia due to deoxygenation of source waters.

Chapter 3

Seasonality of near-bottom dissolved oxygen over a submarine bank off northern California

3.1 Introduction

Motivated by an increase in both magnitude and persistence of low oxygen (hypoxia) in the coastal zone as well as open ocean oxygen decline (deoxygenation), increasing attention has been placed on monitoring dissolved oxygen (DO) levels and understanding physical dynamics that influence DO levels and biogeochemical change in and across estuarine to open ocean environments (see review by ?). The California Current System (CCS) is a highly productive Eastern Boundary Upwelling System characterized by wind-driven coastal upwelling that delivers oxygen-poor, carbon-dioxide-rich waters to the shelf. Regional models and observations in the CCS highlight sensitivity

to the progression of ocean acidification (OA) and deoxygenation, and suggest regionally varying exposure to hypoxia and OA effects (Chan et al. 2017). Although it is one of the most highly observed ocean regions in the world, there has been limited research on the subsurface DO and carbonate system parameters over the central CCS shelf, off northern California, north of Monterey Bay (from 37°N to 42°N). Since time-series of subsurface DO in this region are scarce, the magnitude and persistence of regional shelf hypoxia remains unknown. In this paper we report observations of near-bottom DO obtained at the shelf-edge over a submarine bank (Cordell Bank, Figure 3.1), and characterize the seasonal variation in DO and water type. We discuss reasons for the observation that the seasonal DO minimum lags the temperature minimum by a couple of months, including the role of wind-driven mixing and near-surface phytoplankton productivity.

3.2 Data sources and processing

3.2.1 Mooring data

Observations of near-bottom DO concentration were obtained at the shelf-edge over a submarine bank, ~ 37 km west of Point Reyes (Cordell Bank, Figure 3.1). Here we focus on time series of near-bottom DO, temperature, and salinity data collected using moored sensors deployed from 2014 to 2018. Two moorings were deployed on Cordell Bank (CB1 and CB2; Figure 3.1) as part of a collaborative project between the University of California, Bodega Marine Laboratory (BML) and National Oceanographic and

Atmospheric Administration (NOAA) Cordell Bank National Marine Sanctuary (CB-NMS) to monitor DO concentrations in the sanctuary. Temperature and DO data were collected near-bottom at 80 m (CB1) and 100 m (CB2) using Precision Measurement Engineering (PME) DO and temperature (MiniDOT) loggers from 2014 to 2018. In 2016, a Sea-Bird Electronics (SBE) 37 MicroCAT conductivity and temperature (C-T) recorder was added to the CB2 mooring configuration to obtain near-bottom conductivity for salinity data. Mooring deployments ranged from 3 to 5 months, at which time sensors were swapped and moorings re-deployed. Sensors collected data at 10 minute increments.

Density and other seawater properties were calculated using the Thermodynamic Equation of Seawater 2010 standard, using the Gibbs-SeaWater Oceanographic Toolbox (McDougall and Barker, 2011). To that end, unless otherwise specified, salinity reported in this manuscript is Absolute Salinity ($g\ kg^{-1}$). Sigma-density values, $\sigma_\theta = \rho(S, T, P) - 1000$ and spiciness, π , were calculated using Absolute Salinity, conservative temperature, and pressure. In this chapter, "low-pass filtered data" refers to a time-series variable that had a 33-hour low-pass filter applied using the PL33 filter described by Rosenfeld (1983).

3.2.2 Satellite chlorophyll concentrations

We use a merged chlorophyll product from the European Node for Global Ocean Colour (GlobColour). GlobColour provides a merged product¹ of near-surface chlorophyll concentration, which we use as a proxy for phytoplankton biomass. Although the GlobColour product only provides near-surface chlorophyll, Frolov et al. 2012 reports depth-integrated chlorophyll is highly correlated with near-surface chlorophyll off California ($R^2 = 0.9$). We extracted a merged product for 8-day composites of chlorophyll concentration at a 4km spatial resolution for the years 2014 - 2018. The 8-day chlorophyll concentration value was selected because it represents an appropriate response time for an upwelling event (3 - 10 days) (Wilkerson et al. 2006). We clipped the chlorophyll data such that it is bound to the south and north by 37°N and 39°N, and extends across the shelf (and slope) to a distance of 100 km offshore from the coastline (Figure 3.1).

3.2.3 Atmospheric data

3.2.3.1 Buoy Winds

We used two types of wind data. The first type is from the National Data Buoy Center (NDBC) meteorological monitoring buoy located off Bodega Head, California

¹GlobColour provides a merged product from SeaWiFS (NASA), MERIS (ESA), MODIS (NASA), VIIRS NPP (NASA), (ESA), VIIRS JPSS-1 (NASA) and OLCI-B (ESA). Additional information can be found at www.globcolour.info/. Acronyms listed: SeaWiFS (Sea-viewing Wide Field-of-view Sensor); NASA (National Aeronautics and Space Administration); MERIS (MEdium Resolution Imaging Spectrometer); ESA (European Space Agency); MODIS (Moderate Resolution Imaging Spectroradiometer); VIIRS NPP (Visible Infrared Imaging Radiometer Suite onboard the Suomi National Polar-orbiting Partnership satellite platform); OLCI (Ocean and Land Colour Instrument).

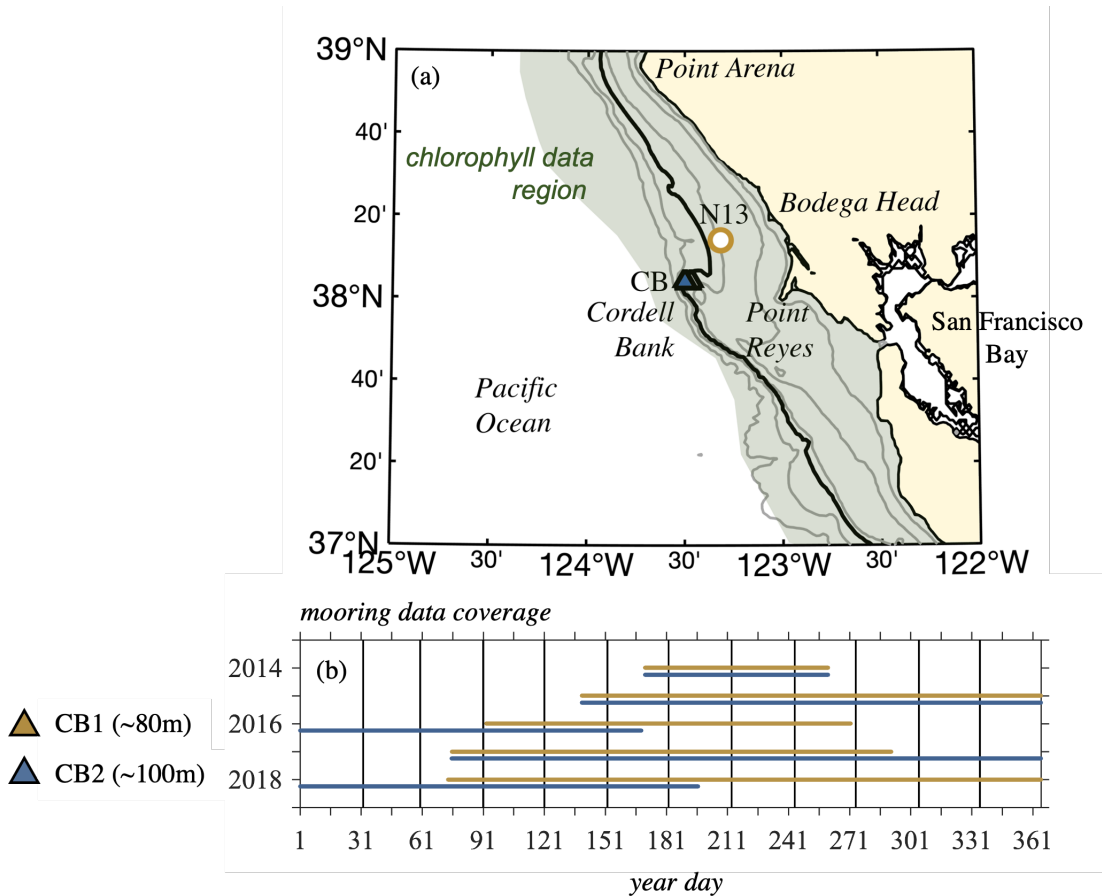


Figure 3.1: Site map and Cordell Bank mooring coverage. (a) Cordell Bank mooring locations shown (triangles); Wind buoy NDBC46013 (N13) marked by yellow circle. Contours shown on both maps: 40, 80, 130, 200, 500, 1000 m. Bold contour is 200 m. Approximate location satellite chlorophyll data were clipped to include the shaded green region, see section 3.2.2). (b) Coverage for mooring data shown. Color corresponds to each mooring location, CB2 (blue) and CB1 (yellow). DO and temperature are available for each '.' in the coverage plot, and salinity is available (in addition to DO-T) for years 2016 - 2018 at CB2.

(46013; N13; Figure 3.1); data are available at: ndbc.noaa.gov. A 5-year record of wind (2014 - 2018) was selected to match the temporal coverage of our mooring deployments as discussed in section 3.2.1. Small gaps in the buoy record were gap filled using linear interpolation; gaps larger than 3 hours were filled using hourly estimates of wind data from the ERA5 dataset described below.

3.2.3.2 ERA5 reanalysis data for winds

Our second source of wind data is a reanalysis product from the European Centre for Medium-Range Weather Forecasts (ECMWF), which combines model data with observations from across the world. We used ERA5, which is the fifth generation of ECMWF reanalysis for the global climate and weather. Atmospheric reanalysis data are available on a regular 0.25 degree grid and are available at cds.climate.copernicus.eu. We extracted the 10m northward (v-) and eastward (u-) wind components from the ERA5 reanalysis point closest to the N13 buoy location from 2014 to 2018. For the wind record we analyzed, the correlation coefficient between the N13 buoy and ERA5 extracted wind data sets is 0.64 and 0.82 for the 10m u- and v- wind components, respectively. Gap-filling occurred for ~ 1.5 % of the record, with the longest stretch being ~ 27 days long (30 June to 27 July 2016).

3.2.3.3 Wind stress, time history and Ekman layer scale

We used hourly wind speed and direction data from 2014 - 2018 and calculated equivalent 10m wind velocity and wind stress (Edson et al. 2013). Wind data were

rotated into a local coordinate system based on the principal axes of wind variability and are referred to as alongshore (positive poleward; downwelling-favorable) and cross-shore (positive onshore) winds, where only the former is used in this manuscript. Both hourly wind and wind stress were low-pass filtered, using the PL33 filter described by Rosenfeld (1983) with a 33 hour cutoff period, to remove higher frequency signals.

To account for the cumulative effect of wind, we used an upwelling index based on a weighted mean of instantaneous (hourly, not-filtered) wind stress in the alongshore direction. This upwelling index is based on work described in Austin and Barth (2002) and is applied as a filter following Giddings et al. (2014) to retain the units of wind stress (τ):

$$W_k = \frac{1}{k} \int_0^t \tau e^{(t'-t)/k} dt'$$

where k is a filter time scale, either 8 days (to match the timescale of the chlorophyll data (see section 3.2.2) or 2 days (to maximize correlations between filtered wind stress (W_k) and near-bottom DO, see Chapter 2 section 2.2.4), and t is time.

To estimate the depth of wind mixing, we calculated the Ekman layer scale, δ_{Et} , using hourly wind stress, τ , calculated from N13 wind data over the reference period 2014 - 2018. Using a turbulent eddy-viscosity solution (Thomas 1975, Poon and Madsen 1991, Lentz 1995) to Ekman's solution (1905) for a continental shelf, we can estimate the Ekman layer scale, $\delta_{Et} \sim \kappa u_* / f$, where $\kappa \approx 0.4$ is von Kármán's constant, f is the Coriolis parameter, and $u_* = \sqrt{|\tau|/\rho_0}$ is the shear velocity (Madsen 1977). We then applied a 33-hour low-pass filter to the calculated Ekman layer scale using the PL33

filter described by Rosenfeld (1983), and calculated summary statistics.

3.2.4 Hypoxia thresholds

We employ classification thresholds of hypoxia to visualize the spatial and interannual expression of hypoxia, which we define as “mild hypoxia” between 1.4 and 2.45 $ml L^{-1}$ and “intermediate hypoxia” $\leq 1.4 ml L^{-1}$. DO levels diminished to “severe hypoxia” $\leq 0.5 ml L^{-1}$ were not observed. A summary of these thresholds are provided in subsection 1.2.4, with alternate units (Table 1.2).

3.3 Results

3.3.1 Cordell Bank Mooring Data

We observe seasonal variability in DO levels at Cordell Bank (Figure 3.2). Lowest DO levels occur in July, after the seasonal temperature minimum in May (Figure 3.2). Mild hypoxia was observed at both moorings, during each deployment (2014 to 2018). However, outside the months of May - September, DO levels typically remain above the threshold for mild hypoxia (Figure 3.2 a&b). Near-bottom DO levels at CB1 (80m) vary in parallel with CB2 (100m) (Figure 3.2 b&c), with DO levels typically higher at the shallower CB1 mooring (Figure 3.2 a&b).

While seasonal cycles in temperature and DO levels were similar across most deployment years, interannual variability was also present and specifically higher DO levels were observed at both moorings in 2018 starting in early May lasting through

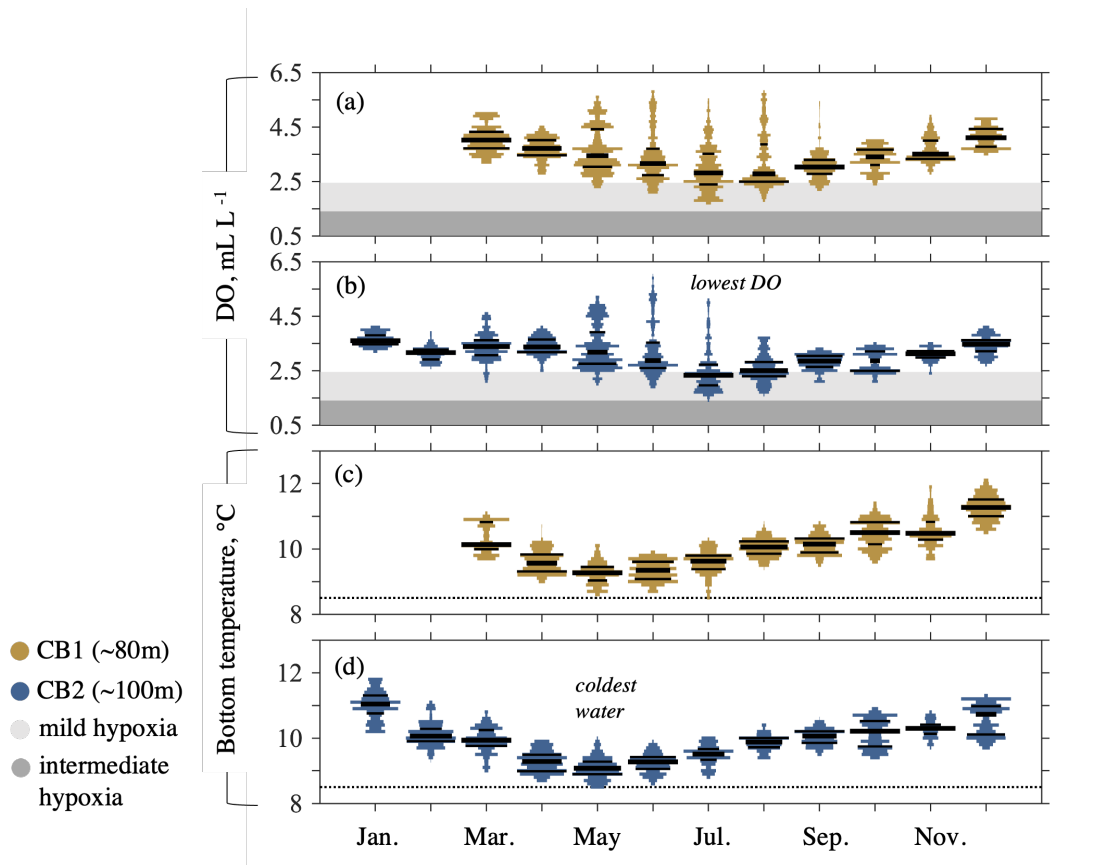


Figure 3.2: Near-bottom DO and temperature at Cordell Bank. Mirrored histograms of observed bottom DO and temperature for years 2014 – 2018 binned by month are presented for both mooring locations CB1 (a & c: ~ 80 m; yellow) and CB2 (b & d: ~ 100 m; blue). Data coverage for each site is provided in Figure 3.1. Bin widths for each mirrored histogram are 0.1 mL L^{-1} between 1 and 7 mL L^{-1} and $0.1 \text{ }^\circ\text{C}$ between 8 and $13 \text{ }^\circ\text{C}$. The 25th/50th/75th percentiles are marked with black lines. Mild hypoxia is shaded light grey; intermediate hypoxia shaded dark grey. Data presented are all low-pass filtered with a cutoff period of 33 hours (see section 3.2.1).

August (Figure 3.3). 2018 DO levels did not exhibit prolonged mild hypoxia at CB2 as in other summers, but the seasonal cycle of temperature at both moorings was similar to other years (Figure 3.3). Across deployments, the lowest DO levels were observed in July 2014 and July/August 2017 (Figure 3.3). During both deployments (2014 and 2017), DO levels declined to just above the threshold for intermediate hypoxia. In 2014, hourly DO levels dropped below 1.4 mL L^{-1} on 16-17 July 2014 for ~ 20 hours at CB2. In both 2014 and 2017, relaxation events were present at N13 (not shown) while DO levels at CB2 declined. We did not observe severe hypoxia in the 5-year record of DO levels from CB2 and CB1 (2014 - 2018).

3.3.2 Winds and satellite chlorophyll concentration

We use near-surface chlorophyll concentration as a proxy for phytoplankton biomass. In the region bound by 37°N and 39°N , median values obtained to a distance of 100 km offshore from the coastline (Figure 3.4), show higher 8-day chlorophyll levels south of 38°N , with highest levels typically present between 37.75°N and 38.25°N (Figure 3.4), within and offshore of the Gulf of Farallones and immediately south of Cordell Bank. At times, high chlorophyll values are present north of Cordell Bank (e.g., north of 38°N). A noteworthy example includes the spring of 2014, where high chlorophyll values are present north of 38°N . Seasonally, the highest chlorophyll levels south of 38°N align with the strongest upwelling winds in spring and early summer. This result is consistent with prior observations in this region, as reported in Largier et al. 2006. A widespread, unprecedented, harmful algal bloom (HAB; Pseudo-

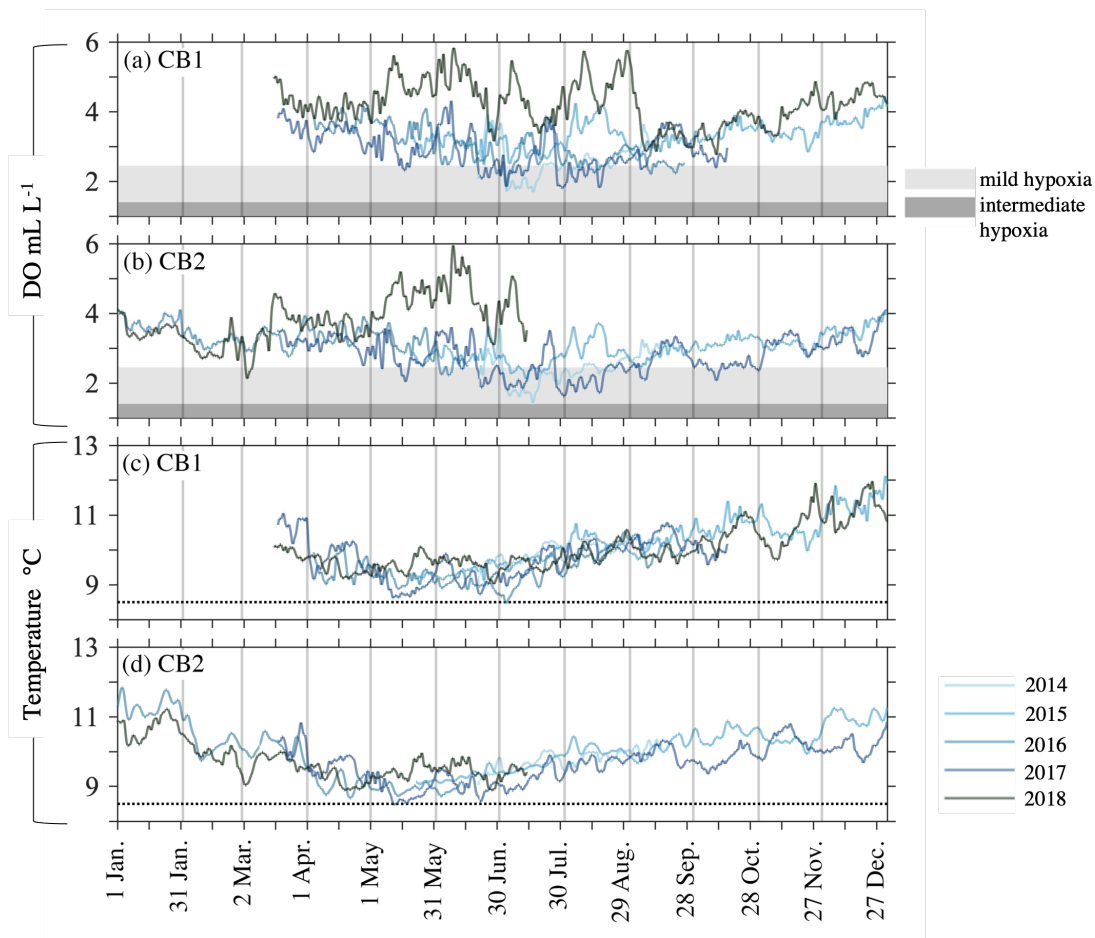


Figure 3.3: Time-series of near-bottom DO and temperature at Cordell Bank. Temperature and DO data from CB1 (a & c: ~ 80 m) and CB2 (b & d: ~ 100 m) across deployments (2014 - 2018) are shown. Mild hypoxia is shaded light grey; intermediate hypoxia shaded dark grey. A horizontal line marks 8.5°C water in c & d. Data presented are all low-pass filtered with a cutoff period of 33 hours (see section 3.2.1).

nitzschia) was present across the CCS in the spring of 2015 (McCabe et al. 2016; Ryan et al. 2017). In the GlobColour product, this event is present in the April/May 2015 data; with a strong presence south of 38°N, but weaker presence north of 38°N (Figure 3.4).

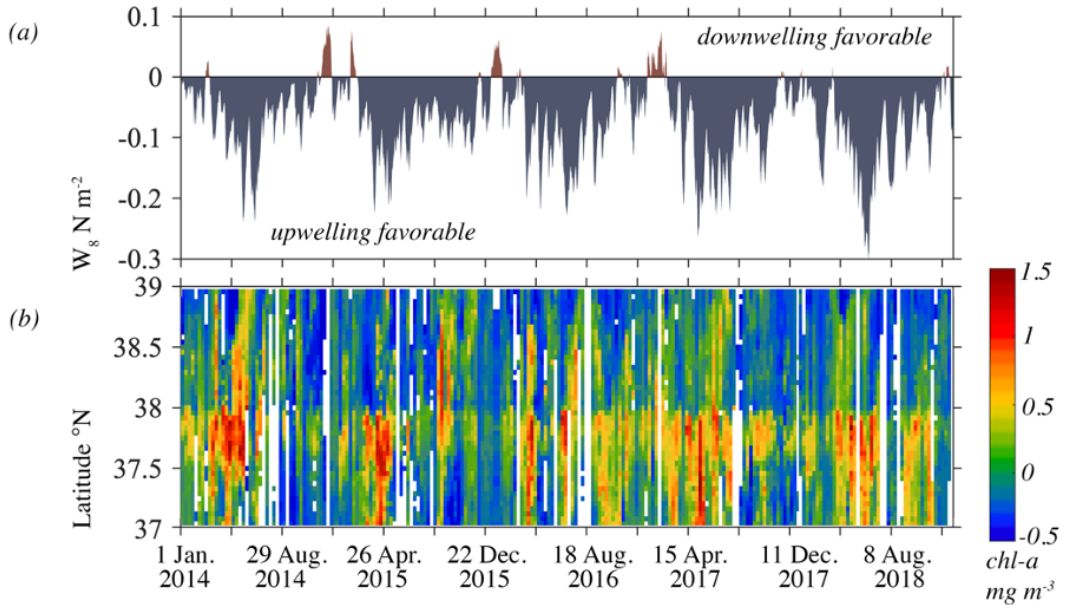


Figure 3.4: Winds and satellite chlorophyll concentration. This figure presents the 8-day upwelling index, W_8 , for alongshore wind stress calculated from winds at N13 (a). Negative values (blue W_8) are upwelling favorable winds while positive values (red W_8) are downwelling favorable. The natural log of the median chlorophyll-a (chl-a) concentration are shown (b). Chl-a values shown represent median values calculated for each 4km section of shelf between 37°N and 39°N and to a distance of 100 km offshore from the coastline. If coverage was < 60% a median value is not presented.

Characteristic to this region, we observe strong, equatorward (negative W_8) wind forcing during the upwelling season during our study years, with the strongest winds present April through June (Figure 3.4a). Strong upwelling favorable winds are often interrupted by brief periods of decelerating winds, referred to as "relaxation"

events (see Beardsley et al. 1987; Dorman and Winant 1995; Pringle and Dever 2009). Relaxation events are common throughout the upwelling season and identified by periods of time when wind velocity drop below its mean value after being strongly upwelling favorable (see also Fewings et al. 2016 and Melton et al. 2009). Towards the end of each upwelling season, a marked decrease in winds occurs at N13 (see decline of W_8 towards zero during the fall; Figure 3.4a). Weaker winds typically continue through the relaxation season (\sim July - August/September). However, 2018 is different from the other deployments years (2014 - 2017), as significant upwelling events are also present (outside the core upwelling season) in August, September and November. This is noteworthy because these events occur during what is typically considered the relaxation season, and although the "late" 2018 upwelling events are weaker than in the core upwelling season (May-June 2018) the strong late summer/fall upwelling favorable events are (1) not present at this time of year in the other deployment years; (2) the peak upwelling in the core upwelling season is stronger in 2018; and (3) reduced winds in the relaxation season typically coincide with a drop in DO levels (and conversely strong, persistent "late" upwelling events in 2018 associate with elevated DO levels at both moorings (Figure 3.3). Finally, based off N13 winds, the spring transition in 2018 occurs earlier than other years, which is followed by a brief hiatus in upwelling winds (see \sim March 2018, Figure 3.4a).

3.4 Discussion

Seasonal patterns in DO levels and temperature are present at the Cordell Bank moorings (Figures 3.2 & 3.3). While lower DO concentrations were observed at the deeper CB2 site (100 m) than at CB1 (80 m), similar seasonal patterns in water temperature and DO are present over the 5-year record. Overall, with the onset of upwelling, near-bottom water becomes cooler and saltier, and DO levels decrease. Although the coolest water occurs early in the upwelling season, the minimum in DO levels occur later, towards the end of the upwelling season and often during the relaxation season. Deviations from the seasonal pattern were observed: (1) during July 2014 when intermediate hypoxia was observed; and (2) during 2018 when elevated DO levels were present from May through August (at CB1; and mid-June/the end of the CB2 2018 deployment). To a lesser extent, but similar to the two aforementioned deviations, during (1) July 2017 DO levels approached intermediate hypoxia, but did not drop below 1.4 mL L^{-1} ; and (2) higher DO levels (when compared to other years) were observed (for a shorter period of time) in August 2015.

To understand the patterns in DO and water type it is important to think about seasonality in regional upwelling. In the central CCS three seasons are recognized. Work by Garcia-Reyes and Largier (2012) describe three seasons using a 29-year record of buoy wind stress: an upwelling season (April - June), a relaxation season (July - September), and a storm season (December - February). Of course variability in winds and the transition in and out of these seasons change across years, but on average,

these seasons are present and influence shelf water properties. The spring transition marks an increase in equatorward wind stress and persistence. Soon after the spring transition, winds strengthen and strong, persistent upwelling-favorable conditions are present (typically from April - June). The coldest shelf water is present during the upwelling season. Relaxation events are common throughout the upwelling season and identified by periods of time when wind velocity drop below its mean value after being strongly upwelling favorable (see also Fewings et al. 2016 and Melton et al. 2009). The start of the relaxation season is marked by a persistent decrease in mean wind stress, when wind strength rapidly declines (typically around July). The storm season represents a transition to weak mean winds. However, from November to March, winds are often strong but can be equatorward or poleward. Therefore, the storm season is typically characterized by weak *mean* winds with high variability (García-Reyes and Largier 2010; 2012). Similar differences in seasonal winds have been described for other areas of the CCS and other upwelling systems (Strub et al. 1987; Bakun and Nelson 1991; Largier et al. 1993; Dorman and Winant 1995; Chavez and Messié 2009). We refer to the period with the strongest, most persistent upwelling favorable winds as the "core" of the upwelling season; and strong, persistent upwelling events which occur outside the typical upwelling season are considered "late" events and prior to the onset of typical upwelling "early" events. The seasonal cycle in upwelling is reflected in the seasonal cycle of temperature at Cordell Bank (Figure 3.3c & d): overall after the onset of upwelling, near-bottom water becomes cooler and saltier (salinity not shown), and DO levels *typically* decline (with the exception of 2018). The coldest temperatures are

observed between April and June (Figure 3.2 & 3.3). However, the lowest DO levels lag the minimum temperature. The lowest DO occurs in July/August. This mismatch points to the importance of local drawdown. We hypothesize this drawdown to be regulated by winds (driving changes in stratification and mixing), regional productivity (driving changes in respiration signal), and feedbacks between the two (e.g., winds controlling relaxation events which facilitate blooms [Largier et al. 2006] and winds controlling cross-shelf export of POC [e.g., Botsford et al. 2006; Yokomizo et al. 2010; Stone et al. 2021]).

Strong winds lead to mixing which can alleviate low DO (and hypoxia if present). Strong winds can also lead to upwelling water from deeper depths in the water column. Upwelling nutrient rich waters, helps maintain productivity. The distribution of POC across the shelf is complex, but overall it is thought that very strong, persistent winds export POC to the outershelf (Botsford et al. 2006, Yokomizo et al. 2010 and Stone et al. 2020), and the rich productivity (primary and higher trophic levels) at Cordell Bank are supported by the export of surface productivity in the upwelling jet that forms off Point Reyes (Largier et al. 2006). The relationship is complex, but we can start to unpack its complexities by (1) examining the differences in wind forcing across each year; (2) exploring an estimate for surface boundary layer thickness; (3) estimating regional biomass presence to help infer a relative estimate of whether we can expect a higher/lower respiration signal. In section 3.4.1, we discuss productivity estimates. In section 3.4.2, we unpack the surface boundary layer depth seasonality. In section 3.4.3, we discuss the interplay of wind-driven mixing, surface productivity

and DO levels; and discuss the similarity of seasonal trends in temperature despite the unique ocean conditions present during each deployment year. Finally, in section 3.4.4, we discuss water mass presence observed across deployments with salinity. Additional work to further assess the impact of timing of wind events and productivity is important to understand DO and carbonate chemistry off northern California (and across the CCS), and help make predictions for future climate conditions.

3.4.1 Regional productivity and DO levels

High rates of productivity characteristic of upwelling systems, may operate at the expense of (1) decreasing aragonite and calcite saturation states and decreasing dissolved oxygen (DO) concentrations because the water that is upwelled to the continental shelf also has reduced DO levels, lower pH, and higher concentrations of dissolved inorganic carbon (DIC); and (2) high productivity maintains a high standing stock of particulate organic carbon (POC) (e.g., Hales et al. 2006), which builds a respiration signal in the water column and at the sediment/water interface and results in DO level declines (Diaz and Rosenberg 2008; Rabalais et al. 2010). These relationships are two mechanisms that makes EBUS, including the CCS, prone to oxygen stress (hypoxia) and acidification, which threaten both benthic and pelagic marine life (e.g., Feely et al. 2008; 2018; Doney et al. 2009; Gruber et al. 2012; Turi et al. 2014; Breitburg et al. 2015; Chan et al. 2017). Recent work by Botsford et al. (2006), Yokomizo et al. (2010) and Stone et al. (2020) also describe the impact of strong winds on cross-shelf export of biomass: intermediate wind speeds yield highest shelf productivity, while very strong

winds export productivity seaward and off the shelf. Based on these works it is likely that a coupling of strong winds and high productivity (Figure 3.4) result in potential for high volumes of POC to be present at Cordell Bank. The relationship is complex as the chlorophyll mass also supports higher trophic levels and the cross-shelf carbon export at depth is also unclear. Prior work has also shown that phytoplankton populations in the Cordell Bank region link with upwelling of nutrient-rich waters at Point Arena which are transported southward towards Point Reyes and exported offshore in the upwelling jet that forms off Point Reyes (e.g., Largier et al. 2006; Figure 3.1). During relaxation events, Cordell Bank may also be impacted by productivity (and POC loading) from the south, especially during major outflow events from San Francisco Bay. While productivity may take time to build a respiration signal over the outer shelf/slope, which may point to why the lowest DO levels are observed at CB in \sim July/August and lag the coldest water, it is also likely that the impact of the downward flux of POC on DO levels is strongest when vertical mixing is weakest, i.e., during times when stratification is strong and/or a more shallow surface boundary layer is present (see section 3.4.2).

Additional statistical analyses to explore the links between DO (especially intermediate hypoxia in 2014), winds and productivity need to be completed. However, we hypothesize the increased satellite chlorophyll observed in 2014 (both north and south of Cordell Bank 38° N) likely contributed to the reduced DO levels. A similar explanation may be present for the 2017 data, when low DO were observed. Additionally, because 2017 was a large water year (CDEC 2017), impacts to Cordell Bank may also be explained by major outflow events from San Francisco Bay and/or the Russian River

(Figure 3.1). Overall, local/regional drawdown of DO can be expected to vary seasonally and interannually, in concert with the strength of surface productivity - accounting for fluctuations in DO levels as well as in the relation between DO and water type, as observed.

3.4.2 Winds and DO levels

To better understand the variability in DO at Cordell Bank, we estimated the surface boundary layer depth based off N13 winds for the deployment period (see section 3.2.3). Following Lentz and Fewings (2012), when the water depth $h < 2\delta_{Et}$, the surface boundary layer approximates the boundary layer thickness ($\delta_s \propto \delta_{Et}$). As the water depth increases (or δ_{Et} decreases), the distance between the surface and bottom boundary layer grows, and an interior region (either forms) or becomes thicker between the surface and bottom boundary layer. This interior region has low turbulent stresses. Here at Cordell Bank, using an Ekman layer scale to estimate the surface boundary layer, it is likely that as the surface boundary layer becomes more shallow (during weaker winds), the depth of the interior layer increases. The net result of reduced mixing through the water column likely points to a reduction in near-bottom DO levels: When there is less mixing, it is likely for DO levels to decline due to a reduced connection with the surface.

With the data we have available, we calculated the Ekman layer scale using wind stress (τ) from N13. A seasonal cycle is present in surface boundary layer thickness and the variability present each month is large (Figure 3.5 & 3.6). Overall, the surface

boundary layer deepens from January through May/June (illustrated by increasing median values Figure 3.6; across all years from $\sim 28\text{m}$ to $\sim 37\text{m}$ Figure 3.5). The deepest surface boundary layer generally occurs in June (at $\sim 49\text{m}$; Figure 3.5), but we can see that this varies across years (e.g., 2015 peaks in April). Then as the relaxation season is approached (typically around July), the wind strength drops at N13 and generally remains low until the transition to storm conditions (\sim September - November). A sharp decline is observed for July ($\sim 29\text{ m}$), and throughout the relaxation season median values remain low ($\sim 21 - 28\text{ m}$), increasing again in the storm season (i.e., November and December $\sim 21 - 28\text{ m}$). During times when the surface boundary layer is thick and winds are strong (e.g., June) water temperatures are cold but DO levels are not at the seasonal minimum. It is after winds relax and the surface boundary layer becomes more shallow (e.g., July/August). Late season upwelling events were present in 2018, but the mean surface boundary layer depth did drop between June to July (like other years). The variability of winds and surface boundary layer are likely just as important as the mean winds present. Additional work to identify meaningful time-scales of decline at Cordell Bank are necessary to more fully understand how wind conditions relate to DO levels at Cordell Bank.

This Ekman layer scaling does not include the effects of stratification. Future work to incorporate stratification (similar to Dever et al. 2006) would be useful. We expect stratification to be strongest over the outer shelf during the relaxation season (or during presence of surface warming associated with the presence of Marine Heat Waves [MHWs]), which would reduce the depth of surface-driven mixing, but during the

months with strongest winds stratification is weak (Dever et al. 2006). Conversely, when significant upwelling events occur during the relaxation season (e.g., August, September and November 2018, Figure 3.4a), increased mixing is likely present (which co-occurs with elevated DO levels at both moorings (see 2018 data; Figure 3.3). We hypothesize "late" 2018 upwelling events contribute to elevated DO levels present from May through August (at CB1; and mid-June/the end of the CB2 2018 deployment).

3.4.3 Synthesis of winds, productivity and DO

This interplay of wind-driven mixing and surface productivity may also explain interannual differences. For instance, two stronger wind years (2017 and 2018) likely have weaker chlorophyll peaks, but longer chlorophyll blooms, because of vertical mixing and advection. DO at Cordell Bank was also higher in 2018 than in other years, which also featured the strongest upwelling-favorable winds across the 5 deployment years. This interplay (between winds, productivity, and linking to DO) is also important in explaining regional differences through comparison of the northern California shelf (which experiences strongest winds; Dorman and Winant 1995) with regions with weaker winds and regions with lower surface productivity (e.g., central California south of Monterey Bay or northern California north of Cape Mendocino). While surface productivity can be high during peak upwelling months, the role of wind in driving vertical mixing freshens low DO levels (and may alleviate hypoxia). However, as winds weaken during the summer, it is likely that the downward mixing of DO decreases and a seasonal minimum in near-bottom DO is observed in ~July, when surface productivity is

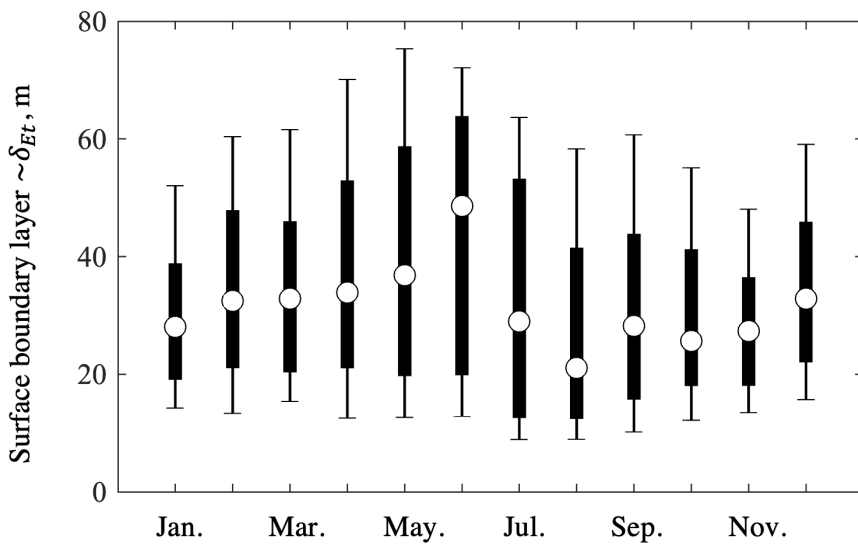


Figure 3.5: Surface boundary layer depth summary statistics estimated from hourly N13 wind data using the Ekman layer scale, $\delta_{Et} \propto \delta_s$. Summary statistics represent the 10th, 90th, 75th, 25th and 50th percentiles grouped by month including data during the period 2014 - 2018.

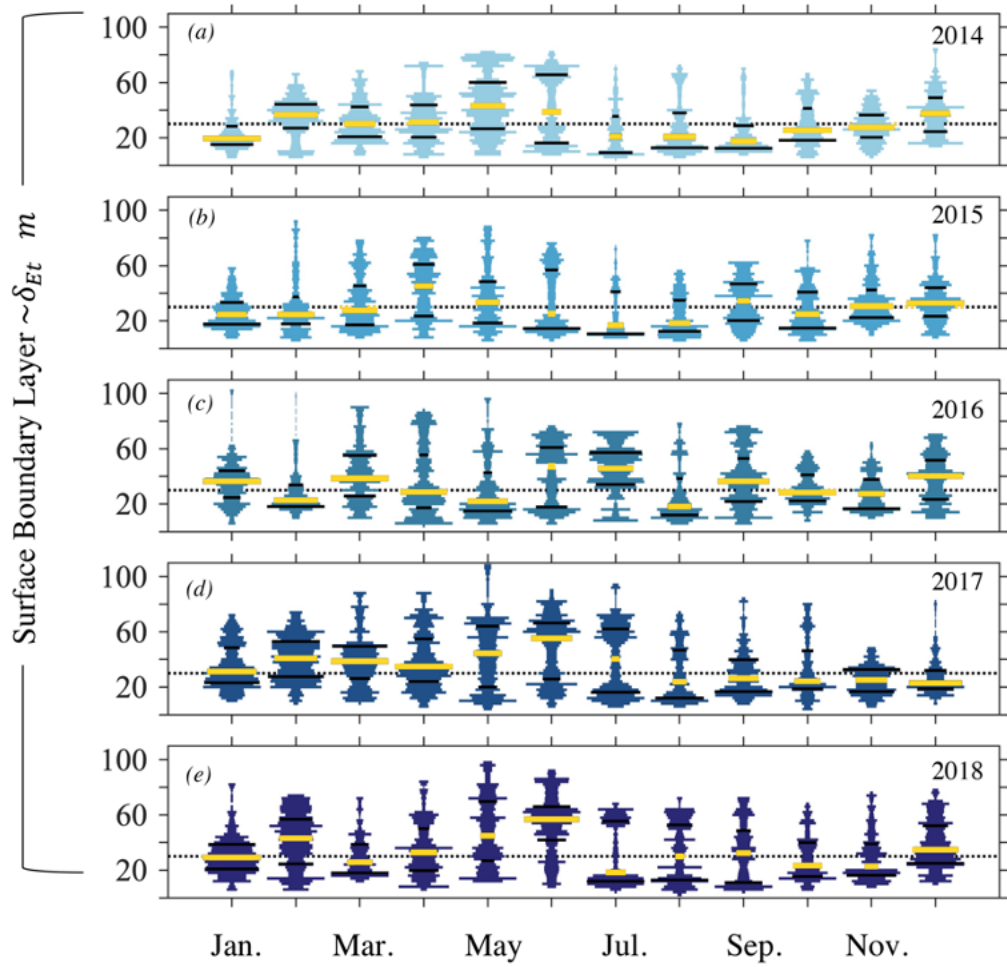


Figure 3.6: Surface boundary layer depth - monthly This figure shows summary statistics for the surface boundary layer depth, estimated from hourly N13 winds using the Ekman layer scale, $\delta_{Et} \propto \delta_s$. Summary statistics represent the 25th & 75th percentiles (thin black lines) and 50th percentile (thicker yellow line). Data are grouped by month and year (2014 - 2019). Median values are shaded yellow. The median Ekman layer scale is $\sim 30\text{m}$ (across all months and years), which is provided for reference as a black dashed line in each subplot.

typically still high. It is likely that wind mixing, a developed respiration signal, and variability source water presence work together to shape the DO levels at Cordell Bank. We are still working to separate these signals.

Changes in wind forcing (and mixing) may result in an accumulation of productivity in the interior region (just below the surface boundary layer), but more work and incorporation of CTD+DO+Fluorescence data would be required to further examine that question. Use of Observational data sets combined with idealized numerical models may be able to better approximate the evolution of mixing during different wind conditions. These resources could also be used to approximate the depth and evolution of the bottom boundary layer, which is not known for Cordell Bank during these deployment years.

For this analysis, we selected an 8-day chlorophyll concentration value because it represents an appropriate response time for an upwelling event (3 - 10 days) (Wilkerson et al. 2006). However, using daily chlorophyll values in combination with hydrographic cruise data (conductivity, temperature, depth (CTD) + fluorescence and DO) through the water column, may help address this question. Estimates from Largier et al. (2006) indicate a ~ 3.5 day lag from Point Arena to Cordell Bank. Although the 8-day data set we explored is helpful to understand interannual differences and regional patterns (Figure 3.4), using daily chlorophyll data may help resolve DO variability at Cordell Bank.

The similarity of seasonal patterns across years (2014 - 2018) is interesting, especially given the unique set of oceanographic conditions the CCS experienced from

2014 – 2019. From 2014 – 2016, the northeast Pacific experienced a high-temperature anomaly, which has been characterized as the largest Marine Heat Wave (MHW) on record (DiLorenzo & Mantua 2016) and extended to the central and southern CCS (Gentemann et al. 2017; Zaba and Rudnick 2016). A strong El Niño event also developed in 2015, with a poleward expansion of warm water (DiLorenzo & Mantua 2016; Jacox et al. 2016). Then, just after these mooring deployments, a second MHW formed in the north Pacific in 2019, which has been characterized as the second largest MHW on record by the end of 2020 (Weber et al. 2021). At the same time, a salinity anomaly also formed in the central North Pacific in 2015, advected to the source waters of the California Current, and by 2017 a high salinity anomaly was observed in water offshore California (Thompson et al. 2018 & 2019; Ren and Rudnick 2021) and in shelf waters off Washington by 2016 (as discussed in Chapter 4). There is not enough mooring data available at Cordell Bank to make a climatology for these data to comment on whether or not here are anomalous years with reference to a baseline (or climatology), especially since salinity data is only available for 2016 - 2018 (the time when anomalous salinities were observed in the CCS). To identify when MHW conditions impacted surface conditions in our study region, we use thresholds developed for N13 by Sanford et al. (2009) (see also Chapter 2; section 2.2.5). If we employ these thresholds and look at 2015 mooring data (Figure 3.7), it is clear that DO levels remain relatively high (generally above the threshold for mild hypoxia) (Figure 3.7c) and the seasonal cycle in bottom temperature track well with other deployment years (Figure 3.3). Even during times when strong surface heating is present (see shading Figure 3.7b), reduced DO

levels are not observed, and in August 2015 DO values were higher than 2016 and 2017 observations (Figure 3.3a & b). Overall, bottom DO levels in 2015 and *bottom* temperature seem to be consistent with other years. It is likely that MHW conditions did not penetrate to depths of 80 to 100m (CB1/CB2 bottom sensor depths), but a better understanding of why strong stratification did not result in lower DO is necessary. Given the following observations: (1) MHW presence is stronger during periods of low (or relaxing winds); (2) MHW conditions are not present at N13 during the core of the 2015 upwelling season (April - June); and (3) the seasonal variability of bottom temperature and DO at Cordell Bank appears to relate to wind conditions; a reasonable hypothesis includes that although upwelling events occurred during 2015 MHW conditions, the winds in August/September and October 2015 were not strong enough to overcome the increased stratification present. This would have resulted in surface cooling and a drop in bottom DO levels. It is possible that due to the stratification presence, upwelled water originated from shallower depths and/or the depth of the California Undercurrent may have been deeper. While time-series observations for this region of the CCS are relatively scarce, and although coping with a lack of subsurface data is not unique to our study, additional future work to better understand where these observations fit with more long-term observational platforms (e.g., gliders or hydrographic survey data) are necessary; especially given the unique set of conditions present in the CCS during 2014 - 2019. There is also active research underway to better understand the depth of MHW impacts (e.g., Scannell et al. 2020; personal conversations with A. Leising and S. Bograd; see also CCS MHW Tracker, NOAA 2022).

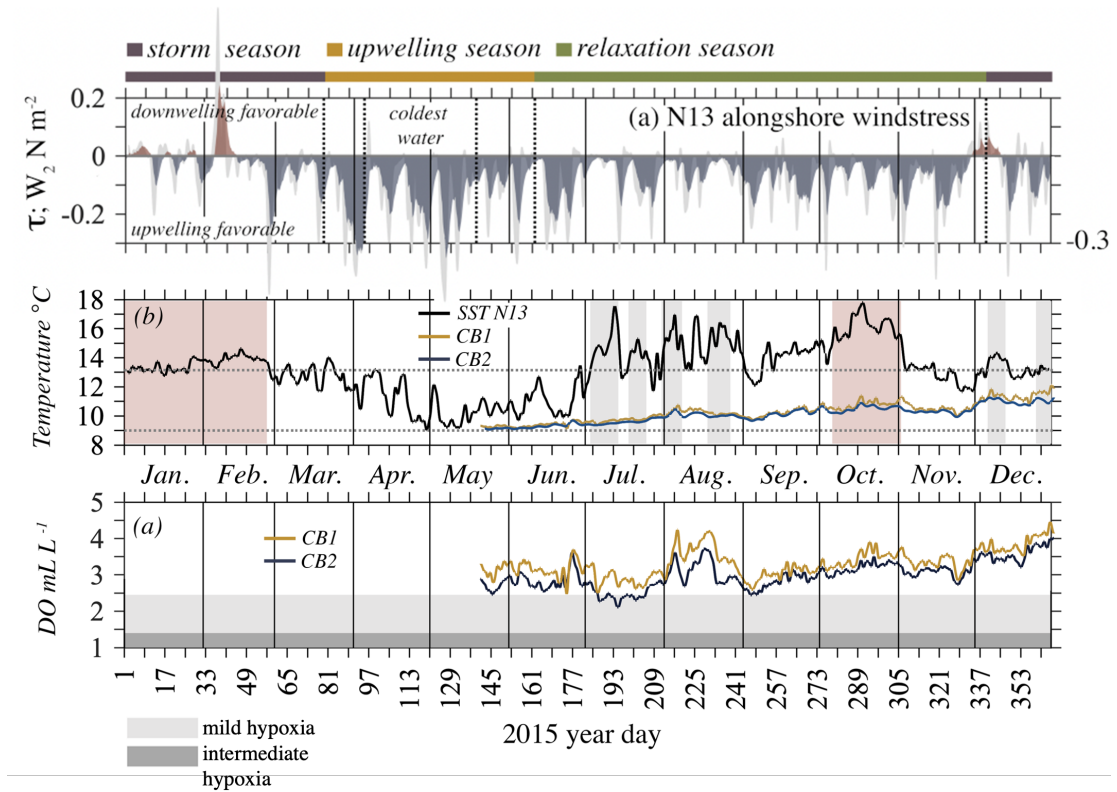


Figure 3.7: 2015 alongshore wind stress, SST and CB mooring bottom temperature time-series. This figure presents (a) low-pass filtered alongshore wind stress at N13 (grey) and W_2 (red, downwelling favorable; blue upwelling favorable). Approximate seasonal transitions shown above subplot (a): the storm season (purple bar), upwelling season (yellow bar); and relaxation season (green bar). (b) SST at N13 (black line) shown with MHW presence flagged following Sanford et al. (2019). Shading, either grey or red, marks periods where the 2015 temperature at N13 exceeded the 90th percentile based on a 30-year record at N13 (1981 – 2011) for ≥ 5 days. Red shading represents one of 10 most intense events since 1981. For reference, the mean SST for 2015 is shown by a dashed horizontal line (13.15°C) and 9°C is also shown. (c) time-series of bottom DO for each mooring site are shown: CB1 (gold) and CB2 (blue). Hypoxia thresholds are shaded (c) light grey (mild) and dark grey (intermediate). Vertical black lines mark the first of each month in all subplots (a-c). Temperature and τ and are low-pass filtered. Date tick marks are spaced at 8-day increments.

3.4.4 Source Water Variability

A relationship between season and DO as well as DO and water type are present (Figure 3.8): higher spiciness co-occurs with lower DO concentrations, and DO

concentrations are lowest later in the upwelling season and during the relaxation season.

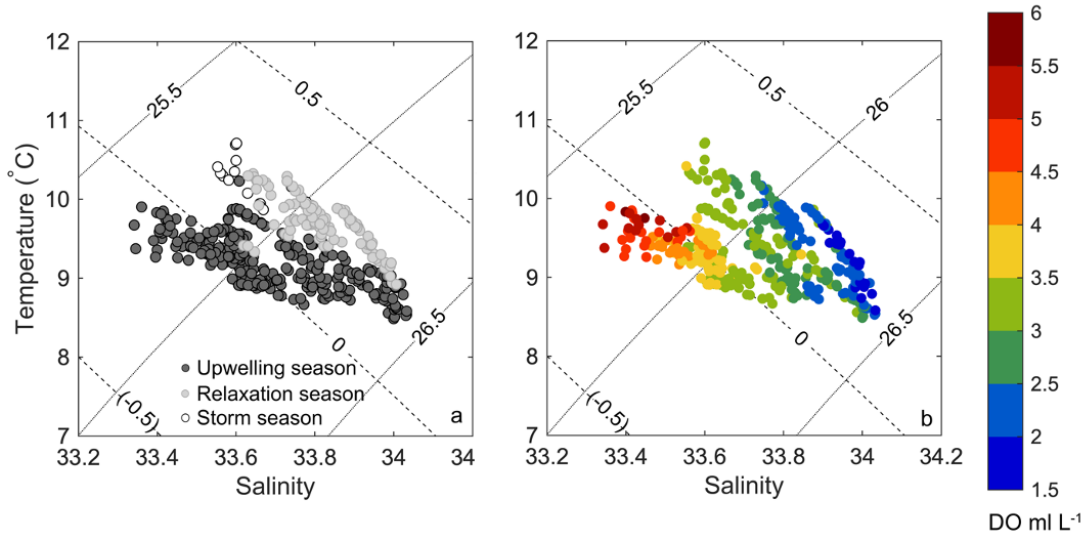


Figure 3.8: T-S diagram showing CB2 mooring data ($100m$) collected during 2016 – 2018. (a) Seasons are colored dark grey "Upwelling season"; light grey "relaxation season"; and white "storm season" in accordance with thresholds described in section 2.3. DO concentration are provided (b) in ml L^{-1} . Black contours are constant potential density and gray contours are constant spiciness. Potential salinity is presented here.

Deep waters upwelled on to the shelf predominantly include two end-member source water masses: Pacific Subarctic Upper Water (PSUW) and Pacific Equatorial Water (PEW) (Hickey 1979). But we are learning that Eastern North Pacific Central Water (ENPCW) also contributes to salinity anomalies in the CCS (e.g., Ren and Rudnick 2021) and oceanic change in interior water may drive regional variability in the CCS (e.g. Bograd et al. 2019; Monterio et al. 2011). The sluggish surface California Current transports PSUW equatorward, while the California Undercurrent transports PEW poleward. The advection of low-oxygen PEW water by the California Undercurrent has often been pointed to as a cause of decreasing coastal DO which co-occurs with

an increase in spiciness (e.g. Bograd et al. 2008; Pierce et al. 2012; Meinvielle and Johnson 2013), and changes in relative proportion of PEW has pointed to change in community composition in the CCS (McClatchie et al. 2010; Schroeder et al. 2019). However, if ENPCW were present in the surface California Current from 2016 - 2019 (see Ren and Rudnick 2021), then it becomes difficult to solely accredit an increase in spiciness to an increase in amount of PEW present across the slope; As an increase in spiciness can *also* be from an increase in ENPCW present. Both water masses, ENPCW and PEW, are characterized by high salinity, high temperature and low DO levels (Lynn and Simpson 1987), therefore increased presence of either would correspond to an increase in spiciness and lower DO levels. One key difference is that ENPCW is typically low in nutrients (Lynn and Simpson 1987; Talley et al. 2011), which may result in lower productivity, and introduction of water with different nutrient properties may have supported different plankton communities (Bernal and McGowan 1981; Chelton 1981; McClatchie 2014; Bograd et al. 2019; Ren and Rudnick 2021).

Applying an end-member mixing analysis here, based on upwelling of the two commonly assumed source waters alone (PSUW and PEW), the expected DO is higher than the observed. Specifically, if we take end member data for April-May data from 2002 to 2016 (following Schroeder et al. 2018), DO values on the 26.0 potential density isopycnal are approximately 6.4 mL^{-1} at 50N (PSUW) and 1.3 mL^{-1} at 25N (PEW). These values yield an expected DO at Cordell Bank of $4.1 - 4.6 \text{ mL}^{-1}$ based on observed water type in relation to the two known end-member source water masses, but *observed* DO levels are much lower ($\sim 3.9 \text{ mL}^{-1}$ stdev 0.7 mL^{-1}). Although this end-member

mixing analysis can work well at depths greater than 100 m and when there are only 2 source water masses present, there are several potential reasons this might breakdown at our CB mooring sites. We hypothesize that this discrepancy may be accounted by: 1) local modification of the DO levels (e.g., respiration signal and links to productivity); 2) variability in end-member DO content; 3) upwelling of water from deeper in the water column owing to the effect of the adjacent canyon (Bodega Canyon); (4) presence of more than two source water masses (e.g., PSUW, PEW *and* ENPCW presence as described in Chapter 3 and hypothesized to be present in the CCS from 2017 - 2019 [Ren and Rudnick 2021]); and/or (5) seasonality of upwelling resulting in modification of water present at \sim 100 m depth. Overall, the data from Cordell Bank suggest there may be a different water mass presence during the upwelling season (Figure 3.8), however further work is needed to understand the source of this water mass. Our observations suggest that an interplay of wind-driven mixing and surface productivity modulate the local DO levels at Cordell Bank, i.e., that the signal observed is unlikely to be from upwelling source waters alone, especially given the consistent seasonal temperature cycle but a more variable DO seasonal cycle.

3.5 Conclusions

From 2014 to 2018 we monitored DO concentrations over a submarine bank located at the shelf break off northern California. We observed seasonal variability. The similarity of seasonal patterns across years (2014 - 2018), especially in temperature,

is interesting given the unique set of oceanographic conditions the CCS experienced from 2014 – 2019. Overall, with the onset of upwelling, near-bottom water becomes cooler and saltier, and DO levels decrease. Although the coolest water occurs early in the upwelling season, the minimum in DO levels occur later, towards the end of the upwelling season and often during the relaxation season. Deviations from the seasonal trend observed are likely attributed to a combination of physical and biogeochemical processes working together. Specifically, we hypothesize that the interplay of wind-driven mixing and surface productivity may help explain interannual differences, but additional work is needed to separate these signals. At Cordell Bank, DO concentrations were often below the threshold of mild hypoxia (2.45 ml/L), but only one instance of intermediate hypoxia was observed (1.4 to 2.45 ml/L) during the relaxation season (July 2017). A step towards better understanding drivers of DO variability (and multi-stressor interactions) includes analysis of subsurface observations to identify relationships and trends in shelf waters. Continued monitoring at Cordell Bank, and incorporation of this mooring data set with long term time-series, may help make management decisions and/or predictions for future climate conditions. Finally, observed DO is also lower than expected using two end-member source waters (PEW and PSUW) thus pointing to the likely importance of local drawdown (and potentially presence of more than two source water masses).

Chapter 4

Interannual variability in shelf hypoxia off the Washington coast

4.1 Introduction

Eastern Boundary Upwelling Systems (EBUS) are among the world's most productive ocean ecosystems (Kämpf and Chapman 2016), which provide wide benefit to society and directly support coastal communities (Garcia-Reyes et al. 2015; Levin and Le Bris 2015; Bindoff et al. 2017). Across EBUS, wind-driven coastal upwelling ("upwelling") supplies the continental shelf with deeper, nutrient-rich water (Smith, 1981; Hickey 1976; Huyer 1983) that supports high primary productivity and fisheries (e.g., Ryther 1969; Pauly and Christensen 1995). However, high rates of productivity in the coastal zone may operate at the expense of (1) decreasing aragonite and calcite saturation states and decreasing dissolved oxygen (DO) concentrations because the wa-

ter that is upwelled to the continental shelf also has reduced DO levels, lower pH, and higher concentrations of dissolved inorganic carbon (DIC); and (2) high productivity maintains a high standing stock of particulate organic carbon (POC) (e.g., Hales et al. 2006), which builds a respiration signal in the water column and at the sediment/water interface and results in DO level declines (Diaz and Rosenberg 2008; Rabalais et al. 2010). These relationships are two mechanisms that makes EBUS, including the California Current System (CCS), prone to oxygen stress (hypoxia) and acidification, which threaten both benthic and pelagic marine life (e.g., Gruber et al. 2012; Turi et al. 2014; Feely et al. 2008; 2016; Chan et al. 2017). Although EBUS total area is small when compared to other pelagic ecosystems, a growing body of literature demonstrate that climate impacts on EBUS will have disproportionately large consequences for human society, as summarized the Fifth Assessment Report (AR5) of the United Nations (UN) Intergovernmental Panel on Climate Change (IPCC) (Chapter 5, AR5 Bindoff et al. 2019). A step towards better understanding drivers of multiple stressor interactions includes analysis of subsurface observations to identify relationships and trends in shelf waters. In this work we focus on the physical dynamics which influence shelf DO in the northern CCS (off Washington, Figure 4.1) in attempt to better understand the physical dynamics that influenced the extreme low DO observed in the summers of 2017 - 2019. Understanding the conditions that contributed to anomalously low dissolved oxygen (DO) observed on the Washington shelf during 2017-2019 is critical to understand low DO drivers and help make predictions for future climate conditions. After describing the regional context in section 4.1.1, we then describe the data (section 4.2). In sections

4.3 and 4.4, mooring data (2011 - 2020) are used to describe the timing and severity of hypoxia off Washington. River and winds data (1991 - 2020) are also used to better understand the coastal environment and drivers of low DO.

4.1.1 The California Current System

The CCS is an EBUS, located in the North Pacific that extends from $\sim 50^\circ\text{N}$ (where the east-flowing North Pacific Current approaches North America) to $\sim 15^\circ\text{N}$ - 25°N (off Baja California, Mexico). With regional divides around Cape Mendocino and Point Conception, the CCS contains to three main regions: the northern, central and southern CCS (Hickey 1979; Checkley and Barth 2009) (see Figure 1.1). Wind forcing over the CCS varies from moderately strong, seasonally varying in the northern CCS, to persistently equatorward in the central and southern portions (Huyer 1983). However, the strongest upwelling favorable winds occur in the central CCS off Bodega Head (in the vicinity of N13; Figure 2.1) and another in region south of Point Sur (García-Reyes 2010; 2012) (Figure 1.1). North of Cape Mendocino winds are generally northward and downwelling favorable in the winter, while south of Cape Mendocino alongshore winds generally equatorward and upwelling favorable (Huyer 1983). Across the CCS, during the spring and summer, prevailing winds upwelling-favorable on which weather-band fluctuations are superimposed (see review by Fewings et al. 2016). Off Washington, upwelling winds typically occur \sim half to two-thirds of the season with downwelling conditions present for the remainder (Hickey and Banas 2008). The efficiency and depth from which shelf water is derived during upwelling is dependent on

the magnitude/persistence of upwelling winds (e.g. Hickey et al. 2006) and the local cross-shelf wind profile (Jacox and Edwards 2012), as well as other physical characteristics like local stratification, bottom slope, and shelf width (Allen et al. 1995; Lentz and Champan 2004; Chapman and Lentz 2005; Estrade et al. 2008) and coastline shape (Barth et al. 2000; Pickett and Paduan 2003). These factors combine to differentiate regions of the CCS (see review by Checkley and Barth 2009), and each are strongly influenced by remote and local physical forcing (e.g., Jacox et al. 2015; Bograd et al. 2015). Finally, while upwelling favorable winds are much stronger ($\sim 8\times$) off California (in the central CCS) than off Washington (in the northern CCS), the degree of freshwater input (by rivers, estuaries and associated energetic tidal flows) is significantly higher in the northern CCS (Hickey 1998; Hickey and Banas 2008).

The chemistry and character (T-S) of water brought to the shelf during upwelling is dependent on the source water origin, which is an active area of research (both understanding what water is present for upwelling and how the biogeochemistry of water masses are changing). The CCS represents a union of different water masses that originate in the tropical, subtropical, and subarctic regions of the eastern Pacific Ocean; each defined by temperature, salinity, DO and nutrients at the time of entry to the CCS (Table 1.1; Lynn and Simpson 1987; Talley et al. 2011). Deep waters upwelled on to the shelf predominantly include two end-member source water masses: Pacific Subarctic Upper Water (PSUW) and Pacific Equatorial Water (PEW) (Hickey 1979). Although, we are also learning that presence of Eastern North Pacific Central Water (ENPCW) can contribute to biogeochemical variability (Bograd et al. 2019) and can

result in salinity anomalies (Ren and Rudnick 2021) in the CCS. The sluggish surface California Current typically transports PSUW equatorward, while the California Undercurrent transports PEW poleward (Hickey 1979; 1998) (Figure 1.1). The percentage of PEW in upwelled waters varies with season and with latitude (decreasing poleward) (Thomson and Krassovski 2010). As each upwelling season progresses, development of the California Undercurrent occurs which plays an important role in providing nutrients to (or removing nutrient-depleted waters from) the shelf (Hickey and Banas 2008). Further, the advection of low-oxygen, PEW by the California Undercurrent has often been shown to cause a decline in coastal DO levels (e.g. Bograd et al. 2008; Pierce et al. 2012; Meinvielle and Johnson 2013), and the relative proportion of PEW present has been shown to impact community composition in the CCS (e.g., fish community composition as shown in McClatchie et al. 2010; Schroeder et al. 2019).

The coastal waters of Washington and southern British Columbia have the highest primary productivity in the CCS, but this high productivity is not co-located with the highest magnitude of upwelling-favorable alongshore winds (Ware and Thomson 2005). This mismatch has been addressed by Hickey and Banas (2008), who describe additional mechanisms that facilitate the region's high productivity beyond the traditional focus of the coastal wind field. First, the PNW shelf is wider than the California shelf (where peak winds occur), which promotes retention of upwelled nutrients (Strub et al. 1991). Second, energy from upwelling off northern California, in the form of coastal trapped waves contributes to upwelling in the northern CCS (Connolly and Hickey 2014). Third, the presence of shelf-break canyons are common across the CCS

with a high density of canyons present off Washington (Hickey 1995). Canyon presence facilitates enhanced upwelling and allows water from deeper depths to reach the shelf (Allen and Hickey 2010; Connolly and Hickey 2014), which contribute high rates of nutrients to the shelf (Hickey and Banas 2008; Crawford and Dewey 1989). Plus, canyons also experience intense mixing (Lueck and Osborn 1985; Kunze et al. 2002; Wain et al 2013; Zhao et al. 2012), which can impact source depth and modify water mass properties transiting the canyon sill (Alford and MacCready 2014). Fourth, freshwater-driven mechanisms play an important and complex role in coastal productivity which includes but is not limited to: modifying nutrient distributions across the shelf, shifting primary productivity offshore and/or deeper in the water column, and modifying retention time, estuarine exchange, and regional circulation in the cross- and along-shelf direction (Lohan and Bruland 2006; Hickey and Banas 2008; Banas et al. 2009; MacCready et al. 2009; Hickey et al. 2009; Kudela et al. 2010; Giddings et al. 2014; Davis et al. 2015).

Analysis of ocean observations from the 1980s to 2000s point to a significant decline in DO across the CCS: off Oregon and Washington (Grantham et al. 2004; Chan et al. 2004;2008; Pierce et al. 2012), in the Southern California Bight (Bograd et al. 2008; 2015), and off Monterey Bay (central California; Ren et al. 2018). Plus deoxygenation trends have been observed in the North Pacific (Emerson et al. 2001; 2004; Ono et al. 2001; Watanabe et al. 2001; Whitney et al. 2007; Mecking et al. 2008) and oxygen minimum zone expansion has been observed in the tropical eastern Pacific (Stramma et al. 2008; Moffitt et al. 2015; Schmidtko et al. 2017). These large-scale trends in offshore DO content intensify hypoxic events, especially over the continental

shelf (e.g., Grantham et al. 2004; Bograd et al. 2008; Chan et al. 2008; Booth et al. 2012; 2014; Levin and Breitburg 2015). An important question is whether nearshore hypoxic events are worsening over time. Before long-term impacts can be adequately predicted, it is necessary to better understand physical processes that contribute to low DO events. To accomplish this, subsurface observations are required across each region of the CCS.

During the upwelling season (\sim May - October) (Huyer et al. 1979; Landry et al 1989) a characteristic seasonal DO decline occurs in Pacific Northwest (PNW) shelf water, often with DO levels reaching $\leq 1.4 \text{ ml } L^{-1}$ ($\leq 2 \text{ mg } L^{-1}$; "intermediate hypoxia") (Chan et al. 2008; Connolly et al. 2010; Crawford and Peña 2013; Adams et al. 2013; Peterson et al. 2013). Historically lower DO levels are observed off Washington compared to Oregon (see Connolly et al. 2010; Siedlecki et al. 2015). While the ecosystem impacts of hypoxia vary depending on the magnitude and duration of hypoxia, the types of organisms present, and the typical seasonal cycle experienced in that region (Diaz and Rosenberg 1995; Levin et al. 2009), often mortality begins when DO levels drop below $1 \text{ ml } L^{-1}$ with mass mortality at levels $< 0.5 \text{ ml } L^{-1}$ (Diaz and Rosenberg 1995). Further, severe hypoxia ($< 0.5 \text{ ml } L^{-1}$; see section 1.2.4) has been linked to mass mortality events of invertebrates and fish off the Oregon coast (Grantham et al. 2004; Chan et al. 2008).

In the summer, on the Washington shelf, advection and respiration typically create a shelf environment that is $\leq 1.4 \text{ ml } L^{-1}$ ($\leq 2 \text{ mg } L^{-1}$; "intermediate hypoxia") but not anoxic (zero oxygen) (Chan et al. 2008; Connolly et al. 2010; Crawford and

Peña 2013; Adams et al. 2013; Peterson et al. 2013). However, in 2017, anomalous subsurface DO levels on the Washington (and Oregon) shelf were observed: The data we present here shows anoxia was detected at several locations with low DO levels reported each summer from 2017 - 2019. To the south, on the Oregon shelf, a level of $0.29 \text{ ml } L^{-1}$ was also recorded, which was the lowest measurement observed in the 12-year time-series (Thompson et al. 2018). These anomalously low DO levels, combined with reduced fish catch¹, motivated this study, to better understand what conditions facilitated anomalously low DO observed on the Washington shelf during 2017-2019.

4.2 Data and methods

4.2.1 Oceanographic data

4.2.1.1 Moored sensors

Moored sensors are deployed on the Washington shelf as part of routine monitoring activities within the Olympic Coast National Marine Sanctuary (OCNMS; Figure 4.1). Moored sensors were first deployed in 2000 and 10 lightweight, coastal moorings are currently maintained from Cape Elizabeth (“CE”; $47^{\circ} 21.2'N$) to Makah Bay (“MB”; $48^{\circ} 19.5'N$) at depths ranging from $\sim 42\text{m}$ to $\sim 15\text{m}$. Moorings are generally deployed in the spring, recovered in the late summer/early fall, and serviced several times over the summer. In this analysis, we focused on sites that had moored DO sensors during years 2011 – 2020. This includes 6 moorings: 5 mid-shelf moorings (MB042, TH042,

¹In 2017, catch per unit effort (CPUE, number per km trawled) of both yearling Chinook and coho salmon were the lowest of the 20-year time-series (1998 - 2017) (Thompson et al. 2018)

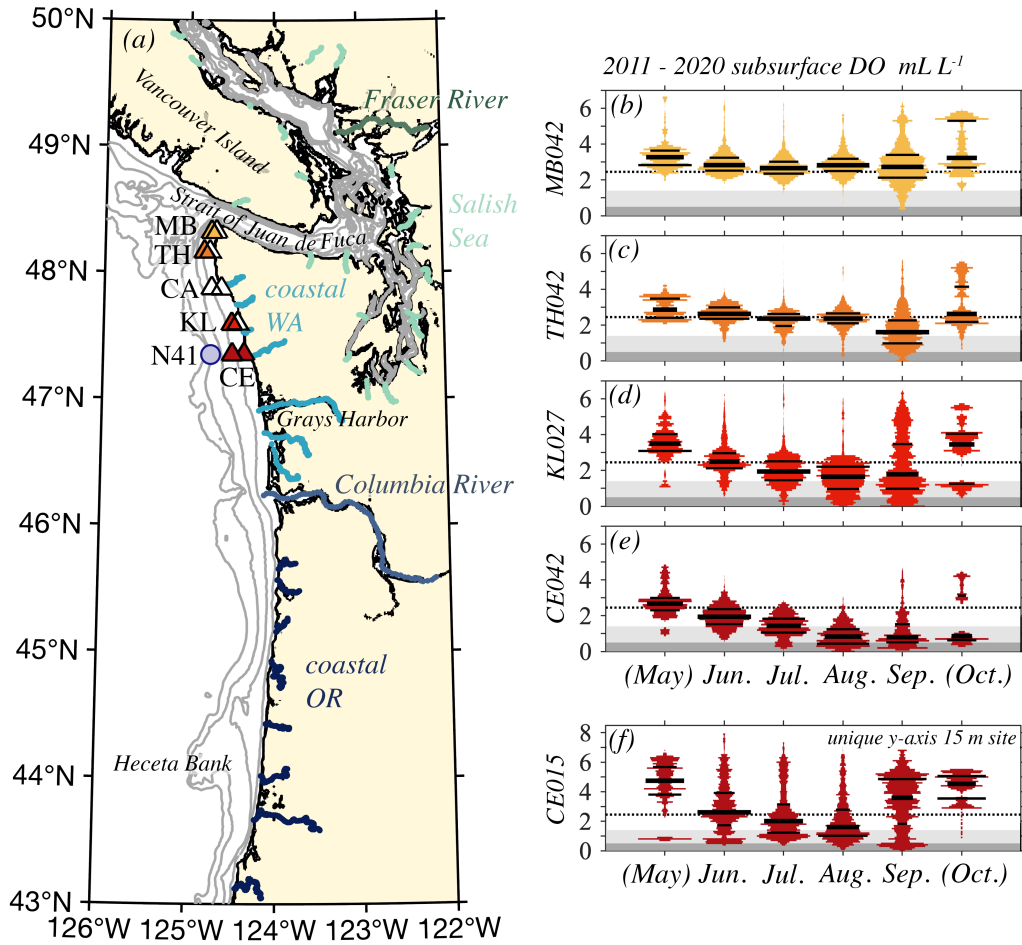


Figure 4.1: Site map and summary of subsurface DO at OCNMS from 2011 – 2020), showing 10 OCNMS mooring locations (a). This study used moorings with available DO data (filled triangles); CA042 was excluded due to a gap in DO data from 2016 – 2018. Wind buoy NDBC46041 (N41) marked with a blue/purple circle. Contours shown: 40, 80, 130, 200 m. In this work, Salish Sea rivers (light green) include: the Duckabush, Skokomish, Deschutes, Nisqually, Puyallup, Duwamish, Cedar, Snohomish, Stillaguamish, Skagit, SanJuan, Elwha, Dungeness, Clowhom, Squamish, Tsolum, Oyster, Englishman, Cowichan, Nanaimo, Nooksack rivers and the Fraser River (dark green). Coastal Washington (light blue) include: the Calawah, Hoh, Queets, Quinault, Chehalis, Willapa, Naselle rivers. The Columbia River (mid blue) is in a group alone. Coastal Oregon (dark blue) include: the Nehalem, Wilson, Nestucca, Siletz, Alsea, Siuslaw, Umpqua and Coquille rivers. (b-e): Mirrored histograms of observed DO for years 2011 – 2020 binned by month are presented for mooring locations from north to south: The northern-most site MB042 (b) to southern-most sites CE042/CE015 (e and f). There is less data coverage across years for (May) and (October), indicated by parentheses see Figure 4.2. Approximate DO data coverage for each site is provided in Figure 4.2. Bin widths for each mirrored histogram are 0.1 mL L^{-1} between 0 and 8 mL L^{-1} . The 25th/50th/75th percentiles are marked with black lines. Mild hypoxia is marked with a dashed black line; intermediate hypoxia is shaded light grey; severe hypoxia shaded dark grey. Anoxic/suboxic thresholds are not distinguished. Sites CE042, TH042, MB042 are all at the same approximate depth (42m), while KL027 is 27m and CE015 15m.

CA042, KL027 and CE042) and 1 inner shelf mooring (CE015; see Figure 4.1). The mooring depth is listed with its site id, e.g., CE042 is placed at 42m; KL027 at ~27m; and CE015 is placed at ~15m. While acknowledging that the width and location of the inner shelf is dynamic, and depend on wind and wave forcing and density stratification (see review by Lentz and Fewings 2012; Garvine 2004), in this paper we refer to moorings as either inner shelf (CE015) or mid-shelf (MB042, TH042, CA042, KL027 and CE042).

Coverage of 2011 – 2020 DO data used in our analysis is shown in Figure 4.2. At all mooring sites (MB042, TH042, CA042, KL027, CE042 and CE015), bottom temperature, conductivity, and DO are collected at 1m above bottom; most often pressure sensors are included at the mid-shelf sites. These data are collected using a Sea-Bird Electronics (SBE) 16+ SEACAT with pumped Sea-Bird 43 DO (“CTPO”) or SBE 37 SMP-IDO MicroCAT with DO (“CTO”). At the mid-shelf sites, temperature and conductivity are also collected near surface, at 4m below mean lower low water, using a SBE 37 SM MicroCAT (“CT”). Onset HOBO TidbiT temperature loggers (“T”) also span the mooring line from 1m below the surface to bottom. These sensors provide a rough estimate of thermal stratification, as their accuracy is $\pm 0.2^{\circ}C$. Instruments all collected data at 10-minute intervals. Site CA042 was excluded from most of our analysis in this study due to a DO data gap between 2016 - 2018.

Density and other seawater properties were calculated using the Thermodynamic Equation of Seawater 2010 standard, using the Gibbs-SeaWater Oceanographic Toolbox (McDougall et al. 2012). To that end, unless otherwise specified, salin-

ity reported in this manuscript is Absolute Salinity ($g\ kg^{-1}$). Sigma-density values, $\sigma_\theta = \rho(S, T, P) - 1000$ and spiciness, π , presented were calculated using Absolute Salinity, conservative temperature, and pressure.

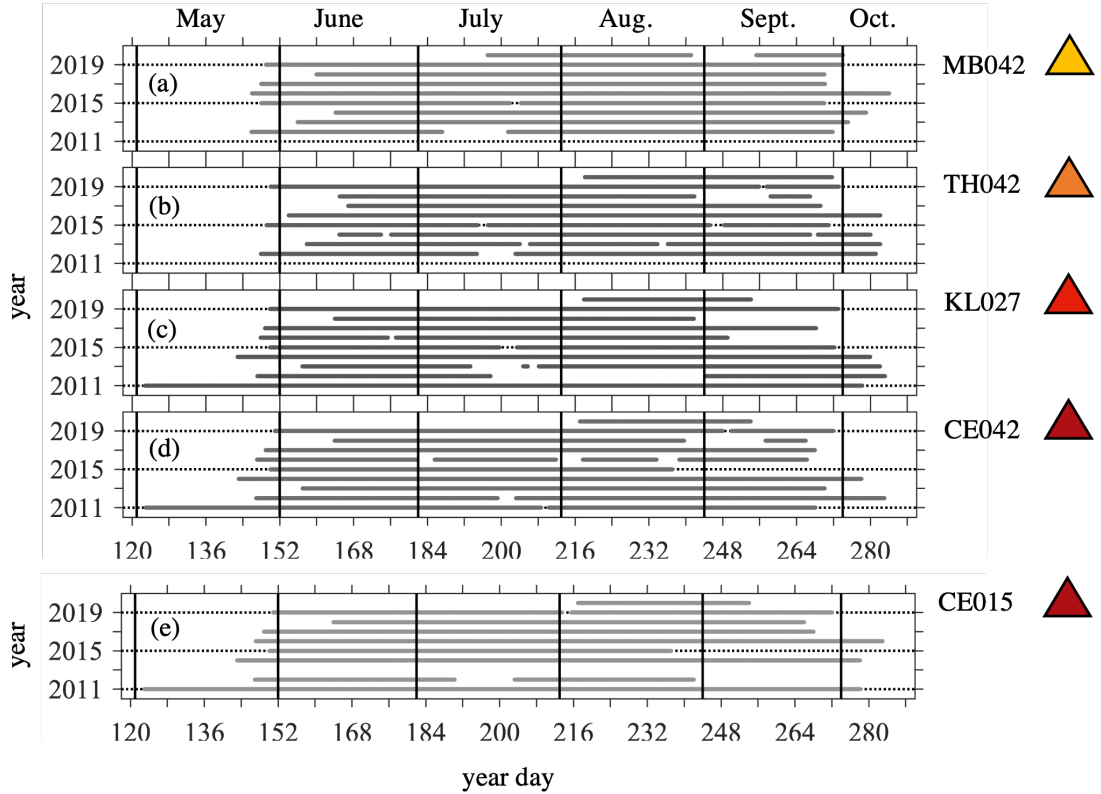


Figure 4.2: OCNMS coastal mooring coverage of DO data from 2001 - 2020 Black vertical and horizontal lines are shown to help visualize the first of each month (vertical lines) and different mooring years (horizontal at 2011; -15 and -19). CA042 is excluded because of DO data gap from 2016 - 2018. Approximate coverage for CA042 can be seen in Figure 4.5c.

4.2.1.2 Hypoxia thresholds

In this analysis we employ classification thresholds of hypoxia to visualize the spatial and interannual expression of hypoxia, which we define as “mild hypoxia”

between 1.4 - 2.45 $ml L^{-1}$; “intermediate hypoxia” $\leq 1.4 ml L^{-1}$; “severe hypoxia” $\leq 0.5 ml L^{-1}$; and “suboxia” $\leq 0.2 ml L^{-1}$. Anoxia refers to zero oxygen. A summary of these thresholds are provided in subsection 1.2.4, with alternate units (Table 1.2).

4.2.1.3 Baseline

We developed a baseline to explore potential changes in water mass properties observed in our mooring record between 2016 - 2019. We selected years 2007 – 2013 to create a baseline because (1) our mooring record with DO at CE042 only begins in 2007; (2) this baseline excludes 2014 – 2019, which represent years when the CCS experienced a unique set of oceanographic conditions; and (3) this baseline was also used by Ren and Rudnick (2021) to identify a salinity anomaly in the California Current, offshore waters (Thompson et al. 2018; Ren and Rudnick 2021). To create a baseline, we calculated summary statistics for a subset of mooring data (temperature, salinity, spice, σ_θ and DO) collected at site CE042 during years 2007 - 2013. To test for differences between years at CE042, we used a Kruskal-Wallis test with Dunn-Sidak post hoc testing. This allowed us to determine which variables – across years – had a significantly different mean rank when compared to the baseline.

4.2.2 River data

Daily discharge data for the Columbia River at Port Westward (14246900) and the Fraser River at Hope (08MF005) were obtained from the U.S. Geological Survey (USGS) and the Water Survey of Canada (WSC). Unless otherwise specified, when

referring to data from the Columbia and Fraser rivers, we are referring to data from these gauges. When comparing individual years (e.g., high flow events of 2011 and 2017), we also present discharge data for 34 additional rivers that empty to the Salish Sea, coastal Oregon, and coastal Washington. The river locations, names and groupings are shown on Figure 2.1.

4.2.2.1 Streamflow-condition classifications

We created streamflow-condition classifications for the Fraser and Columbia Rivers following the USGS methodology used to create national water conditions (USGS 2021). This required a long-term average discharge record for each month over a 30-year period; here we used a reference period of 1991 – 2020. Comparative data were created for each river using the same methodology: We first calculated standard quartiles using the average monthly discharge for each month of the reference period. The comparative data results (Figure 4.3) were used as streamflow-condition classifiers. A monthly discharge rate was considered in the normal range if between the upper and lower quartile; below normal range if below the lower quartile; and above average if greater than the upper quartile. Note the Columbia River reference period was truncated by 6 months, as discharge data from the Columbia River gauge 14246900 is available from 28 June 1991 and onward. A 10-day gap in data is also present from 1 – 10 January 1997 at the Columbia River gauge.

Annual average flow conditions at both rivers have been connected to both El Niño southern oscillation (ENSO) and the Pacific Decadal Oscillation (PDO) (Redmond

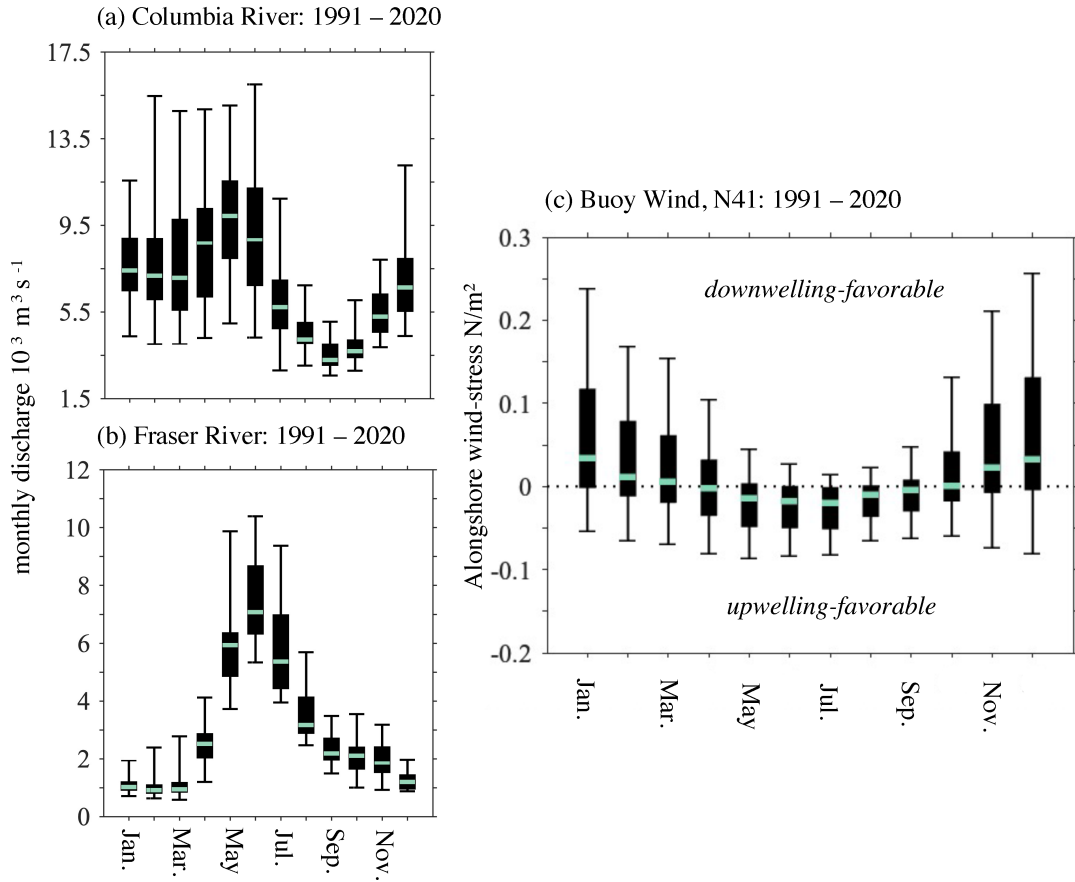


Figure 4.3: Summary statistics of flow for the Columbia and Fraser Rivers and winds at N41. Median values marked with a horizontal sea green line; boxes represent the upper and lower quartiles (25th and 75th percentiles). The 90th and 10th percentiles are shown as whiskers with dashed ends. Summary statistics of flow data (a & b) and N41 winds (c) are shown for each month of the reference period (1991 – 2020). In subplot (c) upwelling-favorable winds are negative; downwelling-favorable positive.

and Koch 1991; Kahya and Dracup 1993, Dracup and Kahya 1994; Gershunov et al. 1999; Bottom et al. 2005; Foreman et al. 2010; Curry and Zwiers 2018), therefore these indices are provided alongside the reference period discharge conditions (Figure 4.4). Strong La Niña winter or cold PDO winters are associated with increased annual Columbia River flows, while warm El Niño winters or warm PDO cycles are associated

with below average flows (Bottom et al. 2005). Gershunov et al. (1999) also show winter conditions that feature a warm PDO with warm El Niño, or cold PDO with cool La Niña conditions amplify impacts; even lower annual flows or much higher annual flows. Although the number of extreme years were limited at the time of their analyses, Bottom et al. (2005) suggest the opposite winter combinations, El Niño/cold PDO or La Niña/warm PDO, show suppressed effects on Columbia River flow. Foreman et al. (2010) show La Niña winters are followed by high summer flows in the Fraser River; and that El Niño conditions tend to have slightly higher flows earlier in the spring because of earlier snow melt and smaller flows through the rest of the summer.

4.2.2.2 Cumulative discharge

When calculating cumulative discharge, we used daily discharge data from the Columbia and Fraser Rivers, and sum across each water year (1 October – 30 September); This allows us to include the winter, pre-conditioning phase to each summer. The term water year is defined as the 12-month period from 1 October through 30 September of the following year, with a designation by the calendar year in which (September) it ends. Thus, the water year ending 30 September 2011 is called the “2011” water year and includes 3 months (October – December) of 2010, and 9 out of 12 months of 2011. For this analysis we present 2011 – 2020 water years and used a reference period (1991 – 2020) to create a median cumulative discharge for comparison.

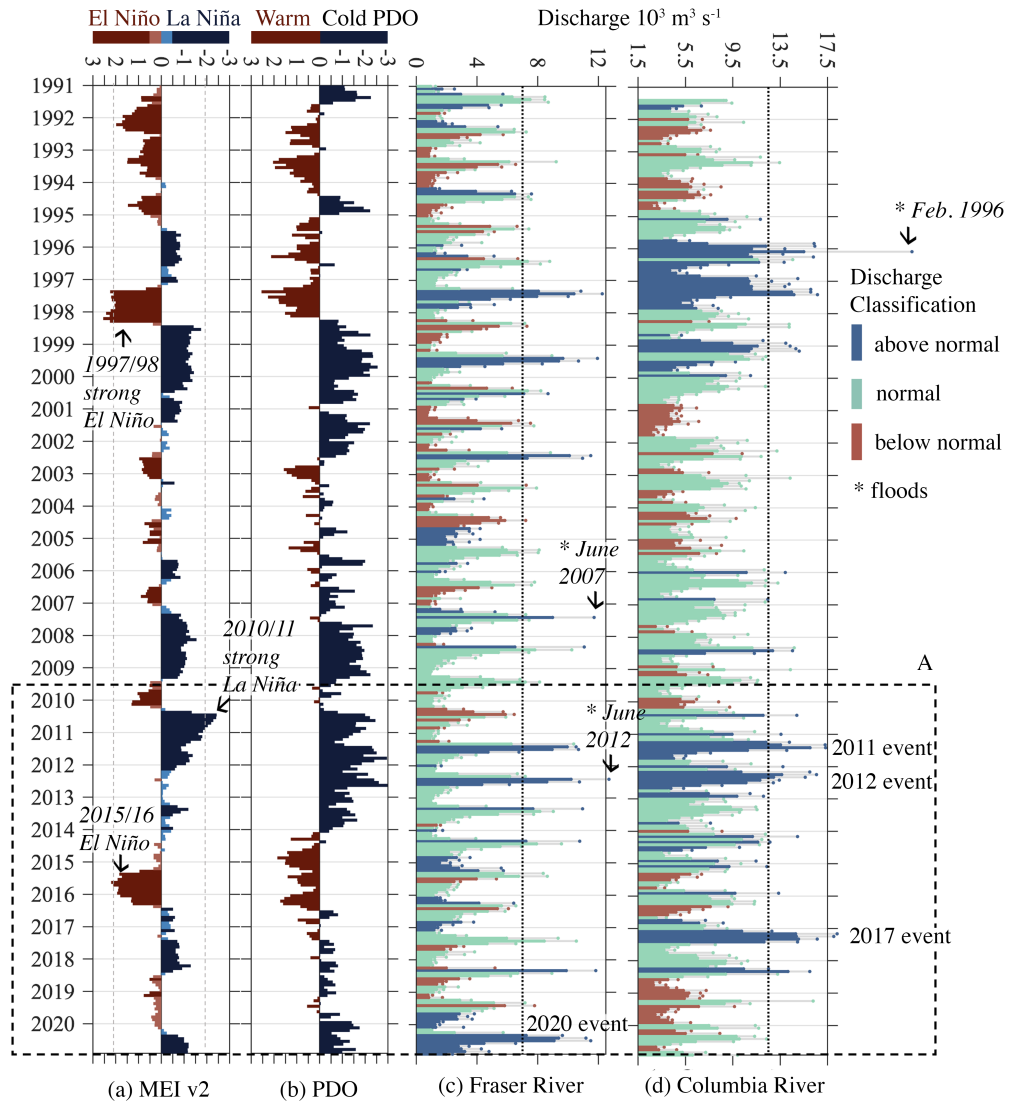


Figure 4.4: 30-year summary of discharge at the Columbia and Fraser Rivers. Multivariate ENSO index (MEI) v2 (a) shown together with PDO cycle (b) and river discharge (c & d). (a) Light pink and light blue shading represent neutral conditions ($-0.5 < \text{MEI v2} < 0.5$). Mean monthly and peak monthly discharge are each shown for the Fraser (c) and Columbia (d). Both stem and marker are colored for mean monthly discharge, while the stem is grey and marker colored for each peak monthly discharge. Below normal flow conditions are less than the lower quartile (red); above normal if greater than the upper quartile (blue), and within normal range if between the upper and lower quartiles (sea green). High flow events of interest discussed in text are labeled. Quartiles for each river are presented in Figure 4.3. A closer look of 2011 – 2020 (dashed box A) shown in Figure 4.8.

4.2.3 Atmospheric data

4.2.3.1 Buoy Winds

We used two types of wind data. The first type is from the National Data Buoy Center (NDBC) meteorological monitoring buoy located off Cape Elizabeth, Washington (46041; N41; Figure 4.1), which are available at: ndbc.noaa.gov. A 30-year record of wind (1991 – 2020) was selected to match the temporal coverage of river discharge data analyzed for the Columbia and Fraser Rivers as discussed in section 4.2.2.1. We used a flat line test to flag values if the reported speed and direction continuously repeated the same value for 12 hours or longer. Small gaps in the buoy record were gap filled using linear interpolation; gaps larger than 3 hours were filled using hourly estimates of wind data from the ERA5 dataset (described in the following subsection). Summary wind statistics are provided in Figure 4.3).

4.2.3.2 ERA5 reanalysis data for winds

Our second source of wind data is a reanalysis product from the European Centre for Medium-Range Weather Forecasts (ECMWF), which combines model data with observations from across the world. We used ERA5, which is the fifth generation of ECMWF reanalysis for the global climate and weather. Atmospheric reanalysis data are available on a regular 0.25 degree grid and are available at, cds.climate.copernicus.eu. We extracted the 10m u and v wind components from the ERA5 reanalysis point closest to the N41 buoy location from 1991-2020. For the 30-year record we analyzed, the

correlation coefficient between the N41 buoy and ERA5 extracted wind data sets is 0.9 and 0.93 for the 10m u- and v- components, respectively, supporting the use of this reanalysis product to fill gaps in the buoy data. Gap-filling occurred for 20% of the record, with the longest stretch from \sim 30 June 1997 - 13 June 1998.

4.2.3.3 Wind stress and time history

We used hourly wind speed and direction data from 1991 – 2020 and calculated equivalent 10m wind velocity and wind stress (Edson et al. 2013). Wind data were rotated into a local coordinate system based on the principal axes of wind variability and are referred to as alongshore (positive poleward; downwelling-favorable) and cross-shore (positive onshore) winds, where only the former is used in this manuscript. Both hourly wind and wind stress were low-pass filtered, using the PL33 filter described by Rosenfeld (1983) with a 33 hour cutoff period, to remove higher frequency signals.

To account for the cumulative effect of wind, we used an upwelling index based on an 8-day weighted mean of instantaneous (hourly, not-filtered) wind stress in the alongshore direction. This upwelling index is based on work described in Austin and Barth (2002) and is applied as a filter following Giddings et al. (2014) to retain the units of wind stress (τ):

$$W_k = \frac{1}{k} \int_0^t \tau e^{(t'-t)/k} dt'$$

where k is a filter time scale, 8 days here as found to be a regionally important event time scale (Austin and Barth, 2002), and t is time.

4.3 Observations

4.3.1 OCNMS hypoxia observations across 2011 - 2020

A summary of subsurface DO observations at the OCNMS coastal moorings from 2011 – 2020 is presented in Figures 4.1 and 4.5. Observations of interannual hypoxia at CA042 are shown in Figure 4.5, but the site is excluded from other analysis due to a data gap from 2016 - 2018.

Each year we observe low DO concentrations in the summer/fall across all sites, with the most extreme hypoxia in August and September (Figures 4.1). DO levels across the mid-shelf exhibit a seasonal decline from May through August, sometimes into September, with southern-most sites exhibiting a steeper decline (thus experiencing lower DO values earlier in the season), while the northern-most sites stay relatively high in DO until around August/September and then experience DO declines below mild hypoxia later in the season (Figure 4.1). We typically observe formation of the worst hypoxic conditions (in August) at the southern sites (CE015/CE042/KL027), and later in the season (early September) at the northern sites (TH042/MB042). September and October have greater spread due to re-oxygenation occurring in those months, which associates with a switch to downwelling favorable winds (the fall transition; Figure 4.1). The bimodal distribution in DO observed in October is due to the timing of the fall transition, and it is also due to reduced deployment coverage in October (Figure 4.2). After 2016, DO data is not available for most days (if any) in October. For instance, the October data shown in Figure 4.1 from site CE042 only represents two deployments

(2012 and 2014). The switch to downwelling favorable winds began earlier in 2014 and associate with the group of DO data above the threshold for mild hypoxia in Figure 4.1, while the 2012 DO levels were lower (and group around intermediate to severe hypoxia).

Across years 2011 to 2020, strong interannual variability of hypoxic conditions are present in DO levels, with more persistent and intense hypoxia in years 2016 – 2019 and overall higher DO levels in 2015 (Figure 4.5). At the shallow mooring, the lowest DO levels (below or at the threshold for severe hypoxia) are present for ~ 3.7 days total across the 2011 deployment; (~ 7 -8 hours total across the 2016 deployment; and ~ 3.4 days total across the 2017 deployment. At the deeper sites (CE042, KL027, CA042), where 2011 DO data is available, DO levels are comparatively better than other years. The lowest DO at MB042 is present in 2018, where severe hypoxia is present for ~ 1.7 days total in September. Across all deployments, minimum DO levels are observed in 2017 at sites TH042, KL027 and CE042 with anoxia (zero oxygen) present: first at CE042 (and for ~ 5.5 days total across the 2017 deployment) in early August; then at KL027 (for ~ 3.7 days total) in late August/early September; and at TH042 (for ~ 1.2 days total) in mid-September (Figure 4.5*). Although very low DO levels are present in the 2016 - 2019 data, a rebound from more extreme hypoxic conditions appears in the 2020 deployments with an overall increase in DO levels across all sites. In 2020, suboxia was only observed for ~ 3.4 days total across the 2020 deployment. Across years 2011 - 2020, 2017 is the worst in terms DO levels but we can not confirm or challenge whether a monotonic decrease in shelf DO is present without a longer DO time-series.

Although hypoxia is a common feature in the PNW with diminished DO ex-

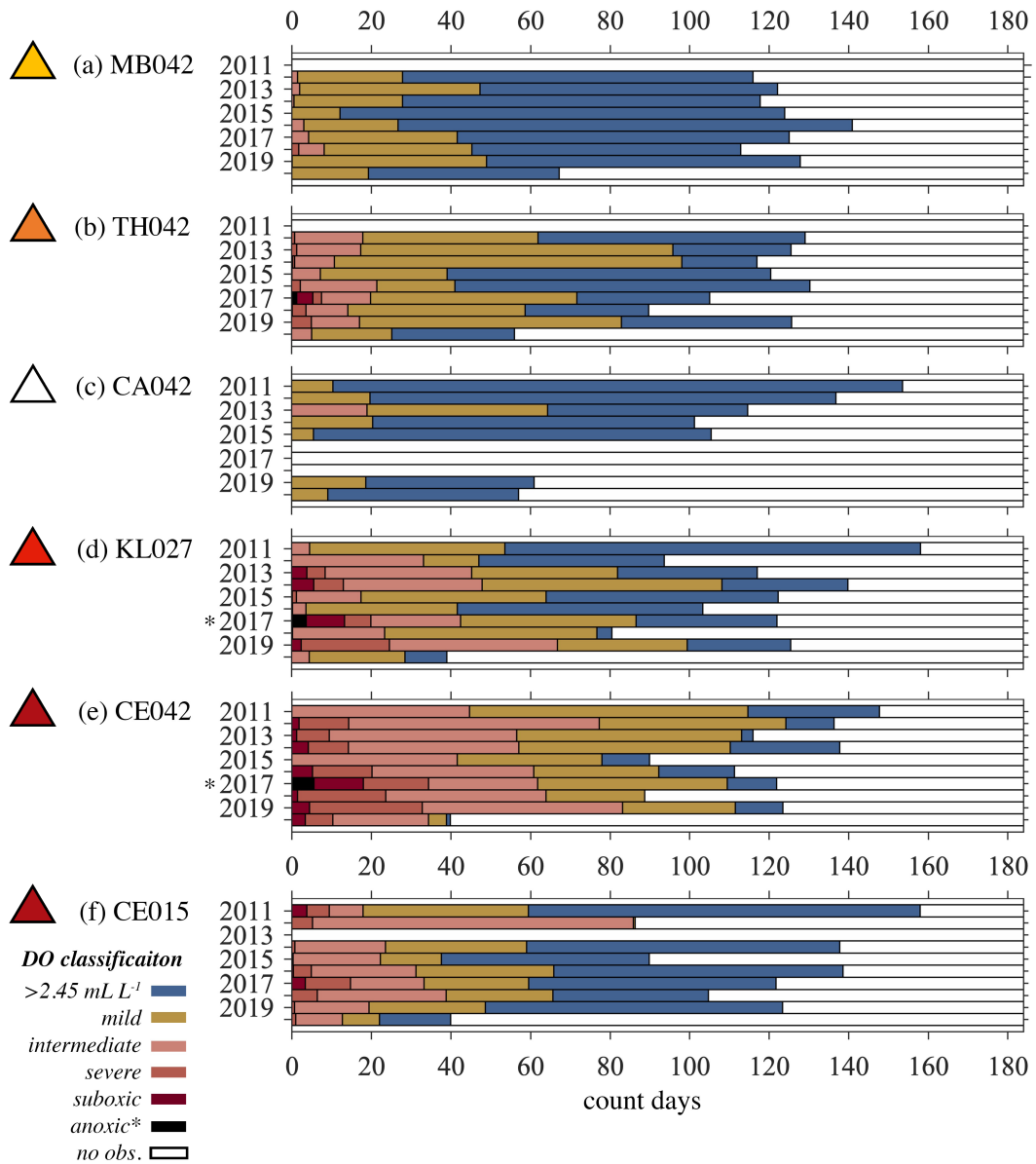


Figure 4.5: Interannual hypoxia at OCNMS coastal moorings showing binned subsurface DO levels for 2011 – 2020. Data are classified by observed DO level: (blue) DO > 2.45 ml L⁻¹; "mild hypoxia" DO 1.4 – 2.45 ml L⁻¹; "intermediate hypoxia" DO 0.5 - 1.4 ml L⁻¹; "severe hypoxia" DO 0.2 – 0.5 ml L⁻¹; "suboxic" DO ≤ 0.2 ml L⁻¹ with "anoxia" zero DO. Each bar represents the number of days between 1 May to 31 October for each deployment year (180 days; 2011 – 2020). White space indicates no observations. Colored triangles next to each subplot title relate to their color designation on Figure 4.1. CA042 does not have DO data for 2016 – 2018. Anoxia observed in 2017* at KL027 and CE042.

pected each summer (e.g., Chan et al. 2008; Connolly et al. 2010; Peterson et al. 2012; Adams et al. 2013), the severity of hypoxia observed in the 2017 - 2019 deployments is striking. The worst DO is observed at the southern sites, with a median *monthly* DO for each August at CE042(KL027) of 0.16 ml L^{-1} (0.90 ml L^{-1}) in 2017; 0.35 ml L^{-1} (1.11 ml L^{-1}) in 2018; and 0.58 ml L^{-1} (0.62 ml L^{-1}) in 2019. As discussed, development of hypoxia at the northern-most sites generally lag the southern-most sites. At sites MB042 and TH042, August DO levels are relatively higher and diminished DO generally present in September (Figure 2.1). For example, we observe a median monthly DO for each August(September) at TH042 during 2017 - 2019 of $2.3(0.88) \text{ ml L}^{-1}$ in 2017; $2.26(0.85) \text{ ml L}^{-1}$ in 2018; and $2.19(1.53) \text{ ml L}^{-1}$ in 2019. DO levels at TH042 also drop to suboxia in 2018 and 2019, and even anoxia in 2017. While DO levels at MB042 are generally just at (or below) the threshold for mild hypoxia with only intermittent observations of intermediate hypoxia, with only one instance of severe hypoxia for <2days total across the deployment in September 2018 (as mentioned above).

4.3.2 Anomalous hypoxia in 2017: winds, rivers and mooring data

Within the decade of mooring data we explored (2011 - 2020), 2017 represents the worst conditions in terms of shelf DO levels. To illustrate the progression and timing across the shelf, we provide all mooring data for sites MB042, TH042, KL027 and CE042 alongside winds at N41 and river flow data (Figure 4.7). Note grouping of rivers is provided in Figure 2.1, and the Fraser River flow included within the Salish Sea. Captured within the 2017 mooring record is the drop from oxygenated subsurface

waters ($> 2.45 \text{ ml } L^{-1}$) to anoxia (zero oxygen) in August/September 2017 (Figure 4.7 g & h).

Early in the 2017 deployment, in late May and through June, variable winds are present at N41 and high river flow is observed (Figure 4.7a&b). Columbia River flow peaks in March at $\sim 18,200 \text{ m}^3 \text{ s}^{-1}$ (not shown), but above average discharge is present from February - June 2017 (Figures 4.4 & 4.8). Outflow from the Fraser River (and Salish Sea) peaks near the transition from May to June, and peaks in coastal river flow off Washington and Oregon are present in mid-May and mid-June (Figures 4.7c). We index stratification using the buoyancy frequency, $N^2 = (-g/\rho_0)(\Delta\rho/\Delta z)$, which is stronger at beginning of each mooring deployment; strongest at the more shallow mooring site, KL027; and overall stronger in the north, at MB042/TH042, than in the south, at CE042 (Figure 4.7c-f). Events where surface waters are mixed to bottom (or near bottom) relates to relatively high subsurface DO (e.g., June 2017 events where the 9.5°C water reaches near-bottom depths; Figure 4.7 c-h). Mixing at the mooring site and/or advection of water masses to the mooring which previously experienced exchange with surface waters - at a different location on the shelf - maintain DO levels above (and just at) mild hypoxia in May and June 2017 (Figure 4.7g & h).

On ~ 18 June 2017 downwelling winds subside, and a switch to upwelling favorable conditions are present (negative W_8 ; Figure 4.7a). With this change in wind condition, cooler water and a reduction in DO is present at each site. The coldest water (7.5°C) appears at MB042 in early July and at CE042 in late August (Figure 4.7c* & f*) but only for a short period of time, and only at those two mooring sites. From late-June

through ~ 20 July, low-pass filtered data remains around the threshold for mild hypoxia at each mid-shelf location (Figure 4.7g-h). After ~ 20 July, the southern-most mooring DO levels decline to severe hypoxia (and eventually anoxic conditions in August), while the northern-most moorings DO levels remain around the threshold for mild hypoxia through the end of August 2017. One exception occurred at TH042, when DO levels declined in mid-August (see Figure 4.7g**).

Declines in DO to intermediate (and eventually anoxia) at the southern-most sites associate with relaxation events at N41, warming of surface waters, and slight increases in N^2 . For illustration of this phenomena, we can see in Figure 4.7a & h (see brown shading) that relaxation of winds at N41 starting after ~ 11 -12 July are followed by decreasing DO levels at the southern-most sites (Figure 4.7h). A strong DO decline is not observed in the northern-most sites, but the layer of warm water present at the southern-most sites is comparatively thicker during these events (4.7c & d). A strong upwelling event alleviates subsurface hypoxia briefly (see area between brown shading Figure 4.7a & h), but during a second relaxation event at N41, starting after ~ 1 August DO levels at both CE042 and KL027 decline. In early August 2017, the drop in DO levels is more rapid at CE042, and declines to severe hypoxia, suboxia and finally anoxia each occur earlier at CE042 than at KL027. By ~ 5 August 2017, anoxia is present at CE042, and KL027 follows on ~ 31 August. Winds at N41 remain weakly upwelling favorable for the remainder of August and into September (evident by a low W_8), and DO levels remain every low (between severe and anoxic conditions) at CE042 (through the end of the deployment) and at KL027 (until ~ 16 September). A rebound in DO is

observed at KL027, when light downwelling winds arrive and surface waters are mixed downward and subsurface DO rises, but DO levels decline afterwards back to severe hypoxia on \sim 23 September (Figure 4.7e). Although 9.5°C water is also mixed down at CE042 (during this September event), the event is not strong enough to raise subsurface DO levels at CE042 out of severe hypoxia. Instead a slight increase in subsurface DO at CE042 brings bottom water out of suboxia and to severe hypoxia (Figure 4.7e). It is likely that subsurface chemistry at this mooring location was complicated by the prolonged suboxic to anoxic events present, which can create a strong chemical oxygen demand (COD). However, we do not have data available to quantify COD at CE042.

The evolution of hypoxia in 2017 is different at the northern-most sites (MB042 and TH042) (Figure 4.7). DO remains at or above the threshold for mild hypoxia through \sim August (at MB042/TH042), with only a slight decline to intermediate hypoxia in mid-August (at TH042) which associates with relaxation conditions at N41 (Figure 4.7g**). The DO decline to intermediate hypoxia at the northern-most sites lags the southern-most sites and occurs in early to mid-September. In September 2017, intermediate hypoxia occurs at MB042 (for \sim 4 days) and DO levels at TH042 decline to anoxic conditions (Figure 4.7g) during a period of low W_8 winds at N41 (Figure 4.7a). At TH042 suboxia(anoxia) is present in for \sim 4.1days(\sim 1.2) days total during September 2017. A downwelling winds event that alleviates subsurface DO at KL027 (discussed above), also benefits subsurface DO at MB042 (and less so at TH042). While DO at MB042 rebound to levels above mild hypoxia, TH042 DO levels increase but remain hypoxic (see mid-September; Figure 4.7).

In 2017, variability in bottom water type is higher at the northern-most sites (especially MB042), than the southern-most sites (especially CE042). As shown in Figure 4.7c-f), from July to August, bottom water at MB042 is more variable than CE042 (as indicated by temperature; see 8°C contour), and TH042 and KL027 site in-between those two sites in terms of variability. When variability of bottom water type is small (or declines), DO levels tend to also decline. This observation extends to other years, where the variability in salinity relates to the variability in DO as discussed in section 4.4.3.

4.3.3 Columbia and Fraser River discharge

By calculating cumulative discharge across each water year (2011 - 2020) for the Fraser and Columbia Rivers, as we show in Figure 4.6, the top three largest water years in the Columbia River are 2011, 2017 and 2012; while the top three largest water years in the Fraser River are 2020, 2012, and 2011. Above average spring flows are evident in 2017 at the Columbia River (Figure 4.6a), and at the Fraser River in 2015 (above average winter/spring flows) (Figures 4.6 & 4.8).

Winter ENSO and PDO cycle conditions impact discharge rates in the Fraser and Colorado Rivers (see section 4.2.2.1). We observe a few years that follow expected relationships between ENSO/PDO cycles and river discharge: (1) two extreme high flow events in 2011 and 2012, both follow winters with a cold PDO cycle and cold La Niña conditions; and (2) the low flow event in summer 2016, follows a warm PDO with warm El Niño winter conditions (Figure 4.8). However, the extreme high flow Columbia

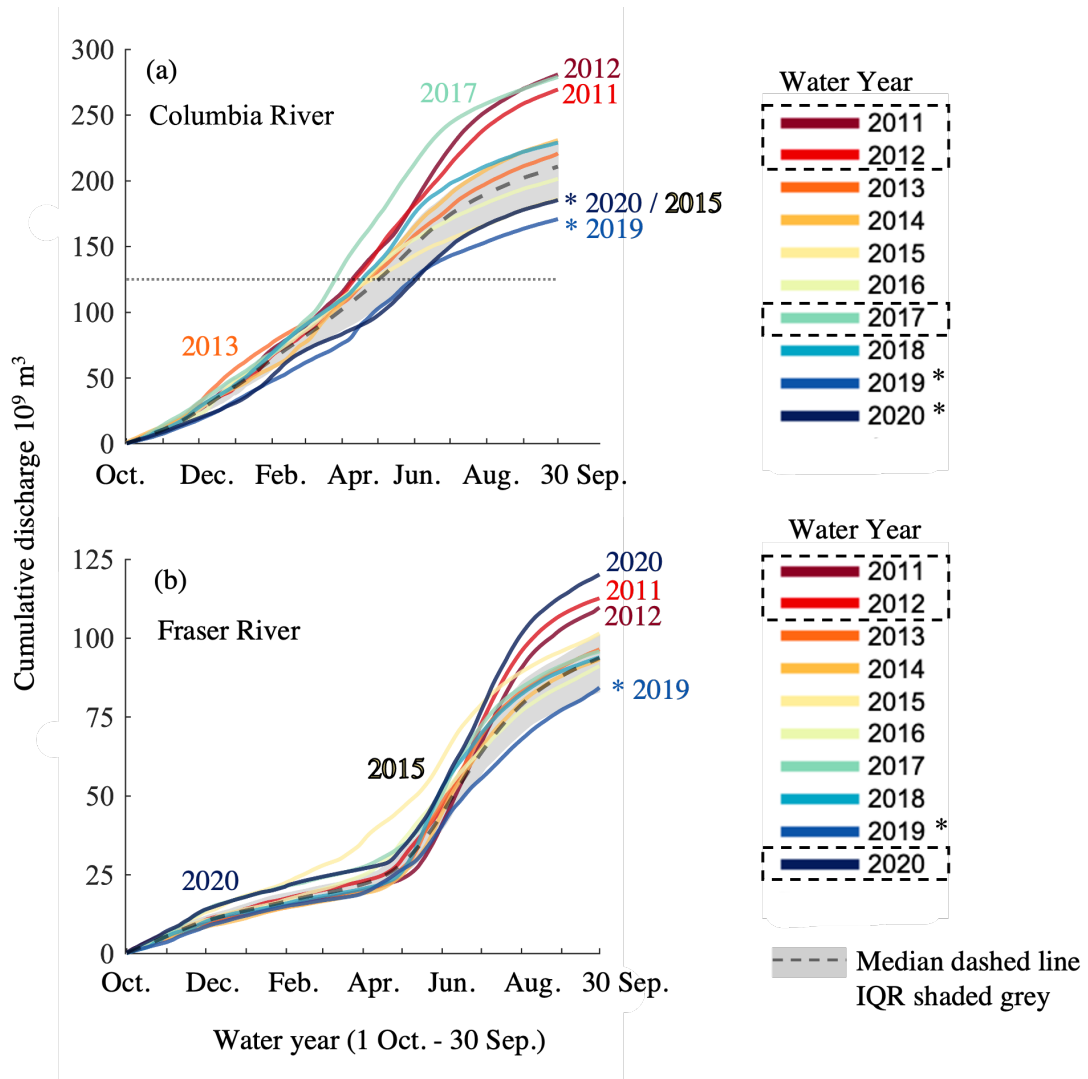


Figure 4.6: Cumulative discharge for the Columbia and Fraser Rivers. Cumulative discharge is shown for each river: Columbia River (a) and Fraser River (b) across 10 water years (2011 - 2020). The three largest values at the end of each year are flagged in each legend with a dashed box and marked on the figure. Water years with below normal cumulative discharge at the end of each water year are marked with an asterisk. The median cumulative discharge for the reference period (1991 - 2020) is shown as a black dashed line in both plots. Note the y-axis are not the same, and a dashed line in subplot (a) marks the max y-axis value of subplot (b). IQR = interquartile range = upper - lower quartile(s) and the IQR for 1991 - 2020 is shaded grey in each subplot.

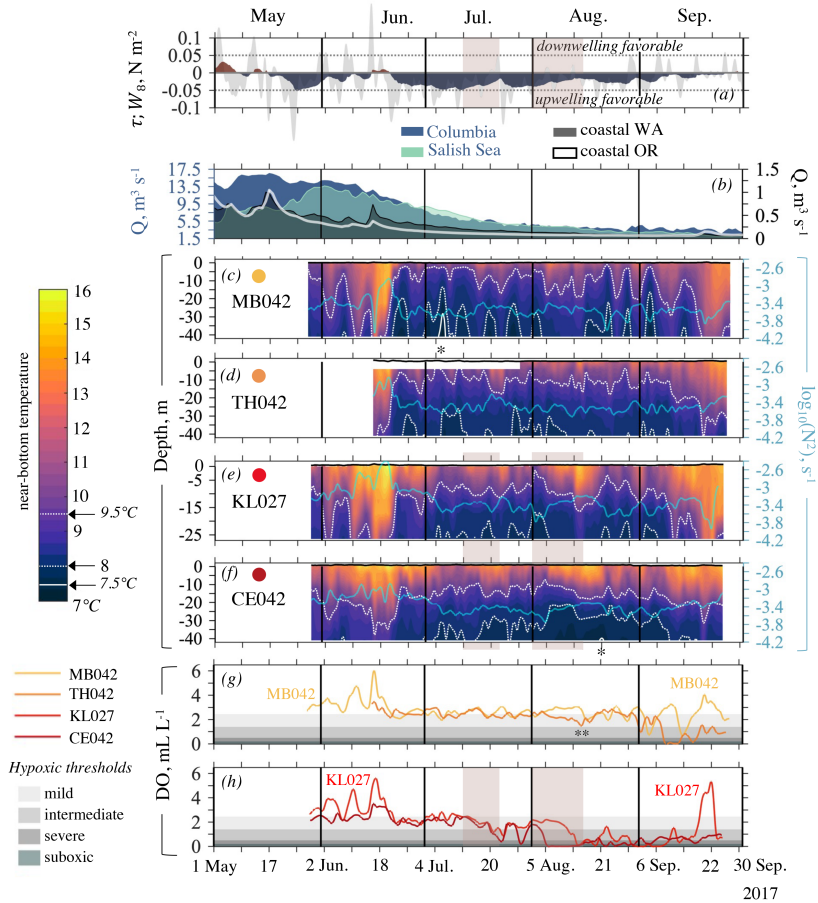


Figure 4.7: 2017 spring/summer: N41 winds, discharge and OCNMS coastal mooring data This figure presents low-pass filtered alongshore wind stress (a) calculated from N41 winds (grey) with the 8-day upwelling index, W_8 , overlain in color. Negative values (blue for W_8) are upwelling favorable winds while positive values (red for W_8) are downwelling favorable. Discharge data for the Columbia River (blue) and rivers that empty to the Salish Sea (including the Fraser River; sea green) are shown (b) on the left y-axis, while coastal rivers off Oregon (white) and Washington (black) are shown on the right y-axis. The river locations, names and groupings are shown on Figure 2.1. Temperature plots created using low-pass filtered temperature sensors moored through the water column are shown for MB042 (c); TH042 (d); KL027 (e); CE042 (f), with depth on the left y-axis. In the same subplots, the buoyancy frequency (N^2 ; blue line) is shown using the right y-axis. Low pass filtered near-bottom DO data are shown for MB042 (yellow) and TH042 (orange) (g); and KL027 (red) and CE042 (dark red) (h). Hypoxia thresholds are shaded grey (mild, intermediate, severe and suboxic; anoxia is zero oxygen). Data shown (except for W_8) were filtered using the PL33 filter described by Rosenfeld (1983) with a 33 hour cutoff period, to remove higher frequency signals.

River event in 2017 has the highest peak flow observed in the period 2011 – 2020, but it follows a weak La Niña and weak PDO index that is in transition from warm to cold.

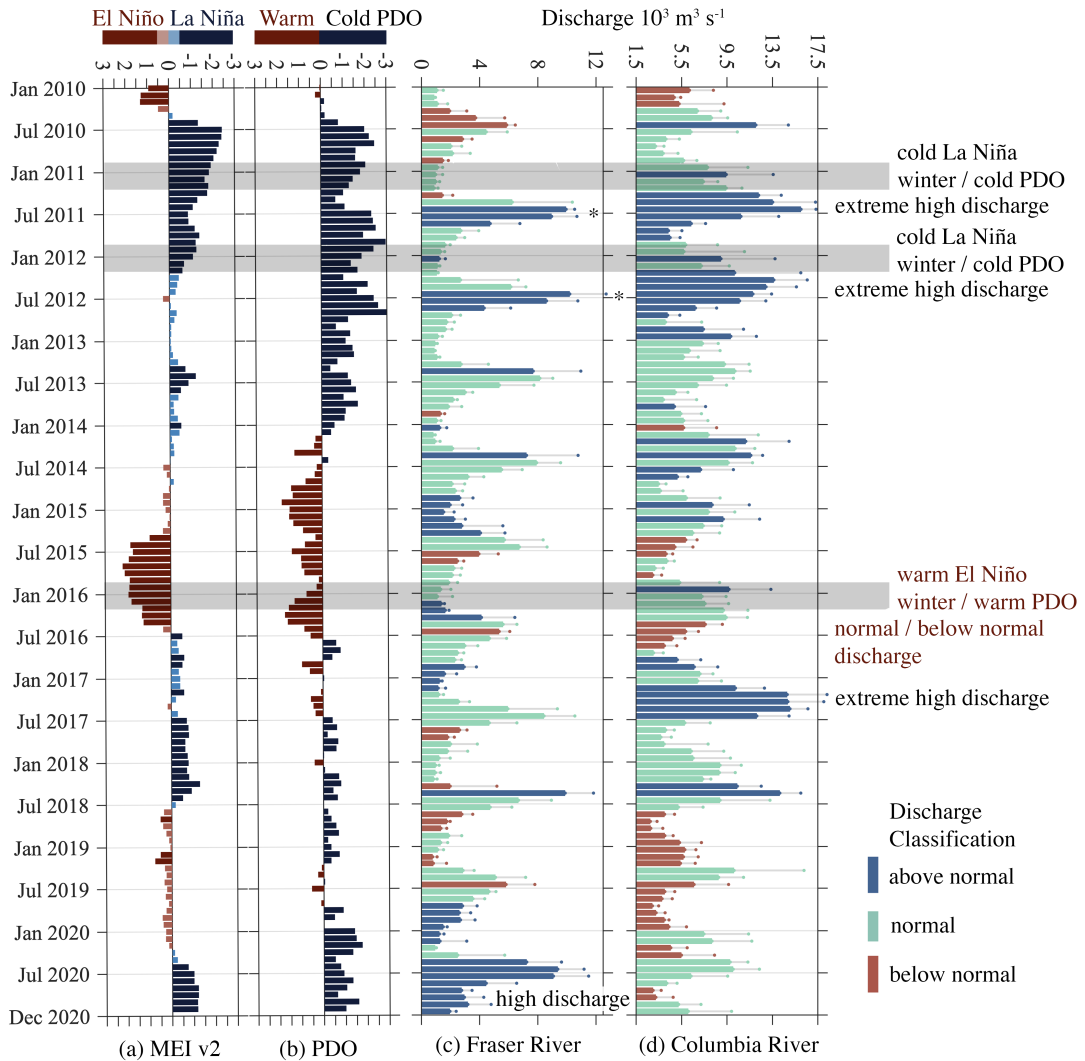


Figure 4.8: Summary of discharge at the Columbia and Fraser Rivers (2011 – 2020). A closer look at years 2011 - 2020 from Figure 4.4 dashed box A.

The extreme 2010/2011 La Niña and extreme discharge event in the Columbia River that took place in mid-May through August 2011 is well documented (see Mazzini

et al. 2015; Johnstone and Mantua 2011; Crouch et al. 2012). With a peak discharge rate of $\sim 17,300 \text{ m}^3 \text{ s}^{-1}$ in June (Figure 8a), the 2011 discharge in the Columbia River is considered extreme, and 82% higher than the baseline average used by Mazzini et al. (2015) (20 years; 1993–2012). To explore years since 2011, we created summary statistics based off discharge at each river from 1991 - 2020 (see section 4.2.2.1. Interestingly, in the years following 2011, we observe high to extreme discharge in 5 years at the Columbia River: year [peak flow/month of peak flow(month of physical spring transition)]; 2011 [$\sim 17,300 \text{ m}^3 \text{ s}^{-1}$ /June(April)]; 2012 [$\sim 16,500 \text{ m}^3 \text{ s}^{-1}$ /April(May)]; 2014 [$\sim 14,900 \text{ m}^3 \text{ s}^{-1}$ /March(May)]; 2017 [$\sim 18,200 \text{ m}^3 \text{ s}^{-1}$ /March(April)]; 2018 [$\sim 15,900 \text{ m}^3 \text{ s}^{-1}$ /May(April)]; 2019 [$\sim 16,200 \text{ m}^3 \text{ s}^{-1}$ /April(April)]. This equates to observing high to extreme peak discharge in approximately half of the years examined, from 2011 – 2020, in the Columbia River (Figure 4.8). The 2017 peak flow also exceeds the 2011 peak at the Columbia River. Further, of these above normal flow events, 3 occur before the physical spring transition and prior to the onset of strong upwelling, in 2012, 2017 and 2018. During 2017, wind conditions are strongly downwelling favorable at N41 in April when the peak flow at the Columbia River occurs. In 2017, discharge rates decline to normal discharge conditions in the summer, and the Fraser River summer discharge are normal to below normal. While the 2011 extreme discharge event at the Columbia River occurred during upwelling conditions at N41, and high discharge conditions extended into the summer. We also observe that the Fraser River discharge is above normal in June/July 2011 but normal in 2017 (Figure 4.8). After 2016, May 2018 was the only month where above normal flows occurred in both the Columbia and Fraser

Rivers (Figure 4.8).

Peak discharge at the Fraser River generally occurs later than the Columbia River (Figures 4.4 & 4.8). On average (across the years 1991 - 2020) the peak flow in the Fraser River occurs in May/June while the Columbia River peaks in May. Peak discharge rates for the Columbia are provided above. During the 2011 - 2020 time span at the Fraser River, peak flows occur in May (2013; 2014; 2018), June(2012; 2016; 2017; 2019), and July(2011; 2020). During the three largest water years (see Figure 4.6), peak flows at the Fraser are: $\sim 10,600 \text{ m}^3 \text{ s}^{-1}$ in 2011; $\sim 11,700 \text{ m}^3 \text{ s}^{-1}$ in 2012; and $\sim 10,200 \text{ m}^3 \text{ s}^{-1}$ in 2020 (Figure 4.8). In 2017, the Fraser peaks at $\sim 10,100 \text{ m}^3 \text{ s}^{-1}$. While the peak flows listed are relatively similar, the spring/summer conditions that follow each peak flow change the shape of the cumulative discharge shown in Figure 4.6b.

4.4 Discussion

4.4.1 Stratification and DO

To explore the north-south gradient in DO across the OCNMS mooring deployments, we calculated and summarized buoyancy frequencies for the mid-shelf moorings, $N^2 = (-g/\rho_0)(\Delta\rho/\Delta z)$, using the top-bottom density difference ($\Delta\rho$) (Figure 4.9). To compare stratification strength and DO across sites, a subset of data is presented which represent times when top-bottom density and bottom DO are available at all sites: CE042, KL027, TH042 and MB042 (Figure 4.9b). Site CA042 was omitted from this analysis because of a data gap from 2016 – 2018; CE015 was omitted because near-

surface density is not available. Overall, we observe stronger stratification and lower DO conditions in the southern sites (CE042; KL027) than the northern sites (TH042; MB042). Noteworthy, stronger (and more variable) stratification strength associated with higher (and more variable) DO concentrations is observed at the shallower southern site, KL027, when compared to the deeper, southern further south site, CE042 (Figure 4.9a).

Although stratification strength plays an important part in achieving hypoxia, the strongest stratification does not always equate to the worst hypoxia. This is illustrated at CE042 and across all mid-shelf sites in Figure 4.7, where early in 2017 the deployment stratification was strong (due to a higher amount of freshwater present across the shelf) but DO levels also remained high. If we explore the relationship between stratification strength (N^2) and DO across all deployments (e.g., at CE042; Figure 4.10), it is clear that across a range of surface salinities higher stratification correlates to lower DO. However, when low surface salinity water is present at the mid-shelf, stratification may be stronger but DO levels remain above the threshold for intermediate hypoxia. Assuming a river index of 31.5 g kg^{-1} (following Davis et al. 2014; Hickey et al. 2009), we can see that presence of river water at CE042 (and other mid-shelf moorings) seldom associates with intermediate hypoxia (Figure 4.10). Rather, the worst hypoxia is present when surface salinity values are high ($> 31.5 \text{ g kg}^{-1}$), and within each salinity range higher stratification associates with lower DO. Note surface salinity here refers to CT data collected ~ 4 m below MLLW (see section 4.2.1.1).

We present three reasonable hypothesis based on our data to explain why

strongest stratification does not always equate to the lowest DO. First, the type (T-S) and chemical character (DO level) of subsurface water present later in the season, when higher salinities are present, likely has a lower starting point DO. Second, later in the season, a stronger respiration signal is likely present in the water column at the sediment/water interface. Therefore, across seasons, as stratification strengthens DO declines, but achieving intermediate (or severe) hypoxia occurs withing waters that started with a lower DO level and/or experienced higher respiration signals. Third, mixing of plume waters may have potential to help alleviate hypoxia on certain sections of the shelf. While stratification is a mechanism that can drive (and maintain) hypoxia, with either (1) high river flows and/or (2) high winds, presence of freshwater may create conditions that can alleviate hypoxia. Enhanced mixing inherent to plume fronts and mixing associated with entrainment, are well known to affect the distribution of sediment, nutrients and pollutants, and momentum and buoyancy. For example, despite high stratification vigorous mixing is present at the Columbia River plume fronts which can disturb the seabed to $\sim 50\text{-}60$ m (Orton and Jay 2005). Even if the Columbia River plume only impacts the bed immediately beneath plume fronts and in the plume near-field (Orton and Jay 2005; Spahn et al. 2009), advection of a water mass that experienced mixing with surface waters on a different section of the shelf still has potential to alleviate hypoxic conditions elsewhere.

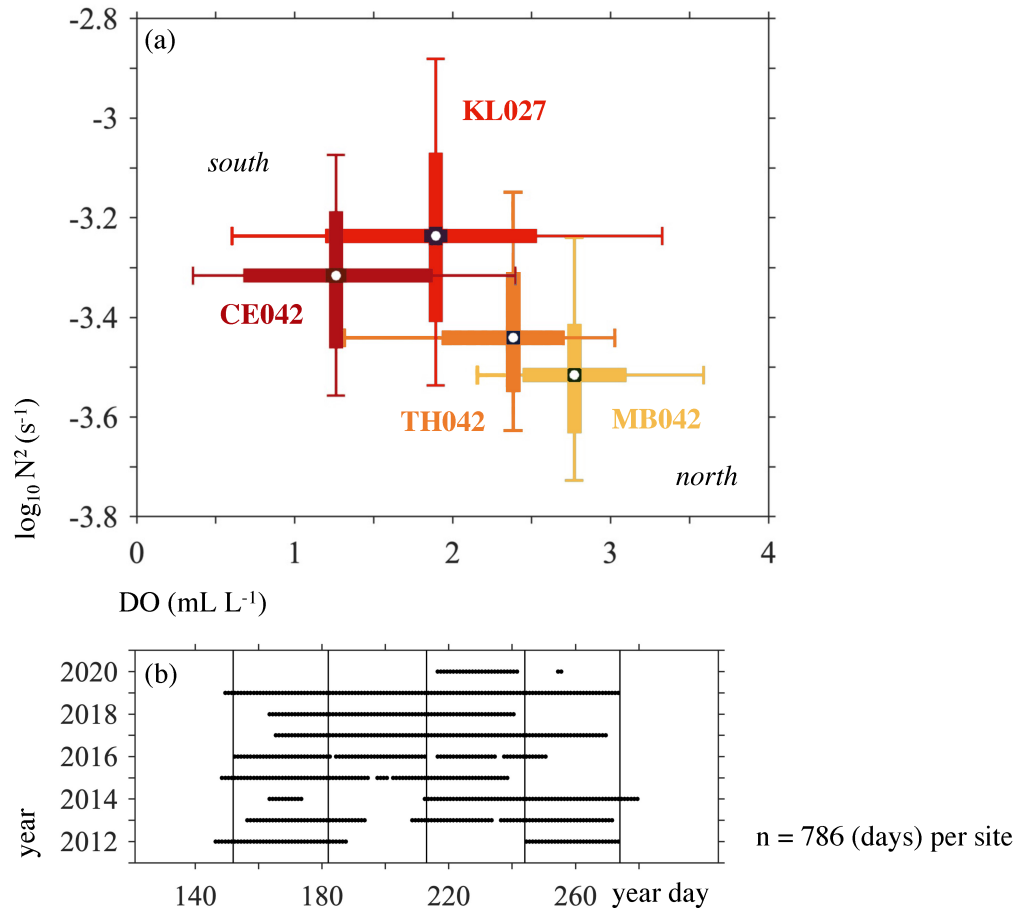


Figure 4.9: OCNMS mid-shelf sites subsurface DO and stratification. This figure presents daily averages of observed DO and calculated buoyancy frequency (N^2). Data shown represents times when top-bottom density and bottom DO were available, at the same time, for all four sites (CE042, KL027, TH042 and MB042). This requirement yields 786 days of data per site, with the coverage shown in (b). Statistics for the daily averages of DO and N^2 are presented for each mooring (a): the median (white circle), the 25th - 75th percentile (thick lines); and 10th/90th percentile (end dashes). Sites CE042 (dark red), TH042 (orange), MB042 (yellow) are all at the same approximate depth (42m), while KL027 (red) is shallower (27m).

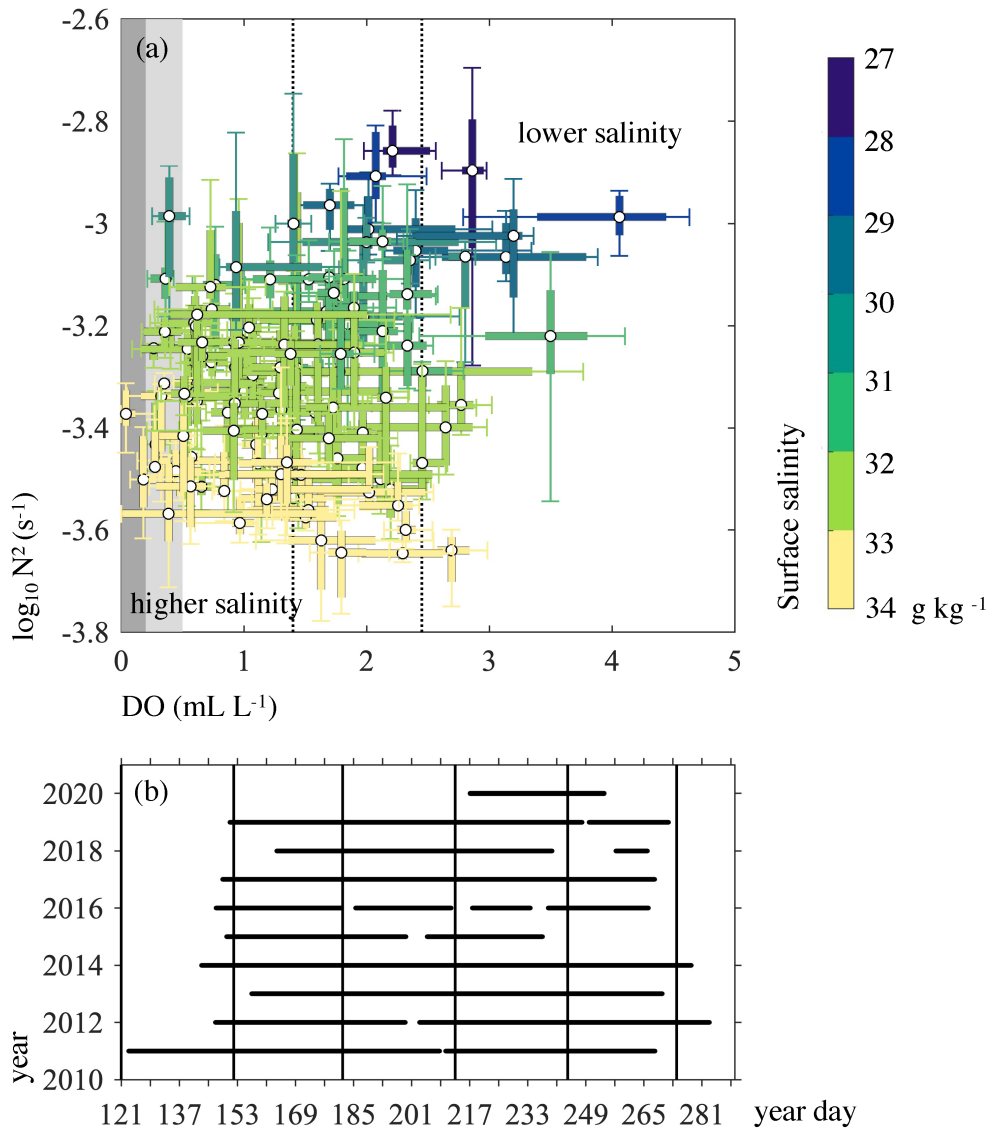


Figure 4.10: CE042 subsurface DO and stratification. This figure presents summary statistics of observed DO and calculated buoyancy frequency (N^2) at CE042. Data shown represents times when top-bottom density and bottom DO were available, at the same time, at CE042 with coverage shown in (b). Summary statistics were calculated using N^2 and DO at 8-day increments for all deployments, which provides a total of $N = 134$ (sets of 8-day data). Each N^2 and DO set are colored by median surface salinity during the 8-day span (a). Summary statistics are the same as Figure 4.9. Mild and intermediate hypoxia are marked with a vertical dashed line; severe hypoxia is shaded light grey and suboxia shaded dark grey.

4.4.2 Anomalous summertime T-S-DO conditions

Temperature-salinity (T-S) relationships at mid-shelf (~ 42 m, CE042) indicate summer water properties in 2016 - 2019 were different to those in 2011 - 2015 and 2020 (Figure 4.11). The spread of T-S data shown for June and September are impacted by changes in wind stress and transitions to (and out of) each upwelling season (Figure 4.11a & d), but a shift in T-S is evident after 2015 in all months shown (June – September; Figure 4.11). Water at CE042 between 2016 - 2019 appears to be “spicier” (warmer and saltier) than prior years and “returns” to pre-2015 values in 2020 (Figure 4.11a-d). Note the 2020 deployment was shorter than other years. This altered T-S water mass is unusual as mid- Washington shelf water properties – for years 2004 and prior – showed little to no alongcoast or interannual variability and only a weak relationship to local wind stress (as shown in analysis by Hickey et al. 2016).

We explored the anomalous T-S by comparing mooring data for different years against a baseline (see section 4.2.1.3 for details). Results of the statistical tests and data analyzed are shown in Figure 4.12, and yellow shading marks years/variables that are classified as different from the baseline. While statistically significant high DO is present at CE042 in the summer of 2015, statistically significant low DO is present from 2017 – 2019 (Figure 4.12a). The temperature record demonstrates a statistically significant high temperature for the years 2014 – 2020; warmest in 2015 and 2019 (Figure 4.12e). Statistically significant low salinity present in years 2014 and 2015, is followed by a statistically significant high salinity in years 2016 – 2019 (Figure 4.12d). Across years,

statistically significant high spiciness corresponds to low DO and vice versa (Figure 4.12a & b).

During the time from 2014 – 2019 the CCS experienced a unique set of oceanographic conditions, which are also reflected in OCNMS shelf mooring data. From 2014 – 2016, the northeast Pacific experienced a high-temperature anomaly, which has been characterized as the largest Marine Heat Wave (MHW) on record (DiLorenzo & Mantua 2016). A strong El Niño event also developed in 2015, with a poleward expansion of warm water (DiLorenzo & Mantua 2016; Jacox et al. 2016). Then a second MHW formed in the north Pacific in 2019, which has been characterized as the second largest MHW on record by the end of 2020 (Weber et al. 2021). The OCNMS temperature record at CE042 demonstrates statistically significant high temperature for the years 2014 – 2020; warmest in 2015 and 2019 (Figure 4.12e). This is not surprising given the CCS has experienced anomalously high temperature anomalies since 2014 (Thompson et al. 2018; Zaba et al. 2020), and MHW conditions in 2015 and 2019.

A salinity anomaly also formed in the central North Pacific in 2015, advected to the source waters of the California Current, and by 2017 a high salinity anomaly was observed in water offshore California (Thompson et al. 2018 & 2019; Ren and Rudnick 2021). The statistically significant high salinity anomaly appears earlier (in 2016) on the Washington shelf in OCNMS mooring data than observed off California (in 2017; see Thompson et al. 2018 & 2019; Ren and Rudnick 2021), and both statistically significant high salinity anomalies are present through 2019 offshore (Thompson et al. 2018 & 2019; Ren and Rudnick 2021) and OCNMS (this study) data.

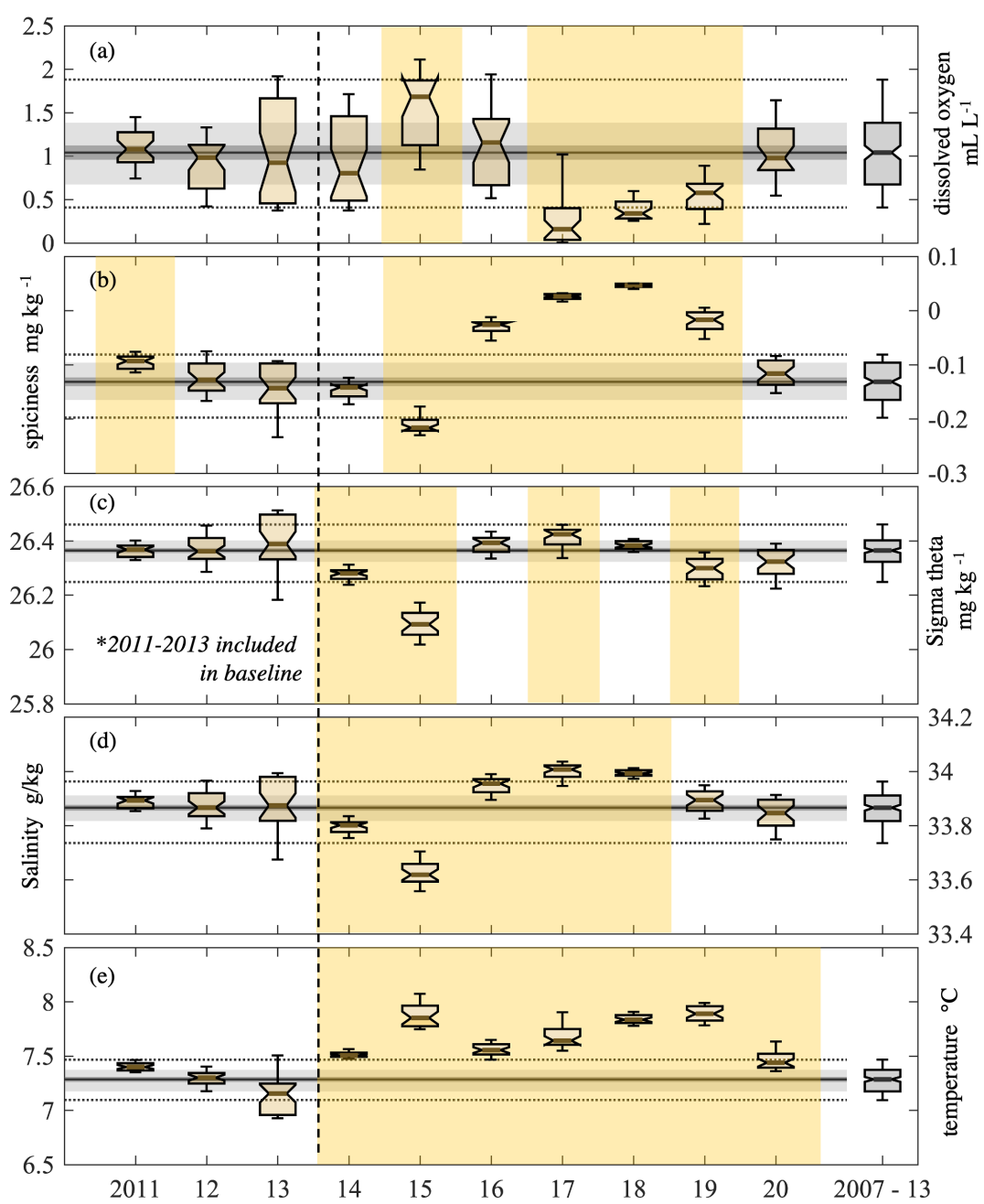


Figure 4.12: Summary statistics for CE042 bottom data. This figure presents August data for years 2011 – 2020 (yellow, notched-boxes). Baseline summary statistics (grey, notched-boxes) represent August data for 2007 – 2013. Baseline summary statistics are also stretched across each subplot for reference: grey dashed lines represent the 90th/10th percentiles; dark grey lines represent the 50th percentile; and light grey shading represents 75th/25th percentiles. Vertical, yellow shading marks groups with mean ranks that tested significantly different than the baseline.

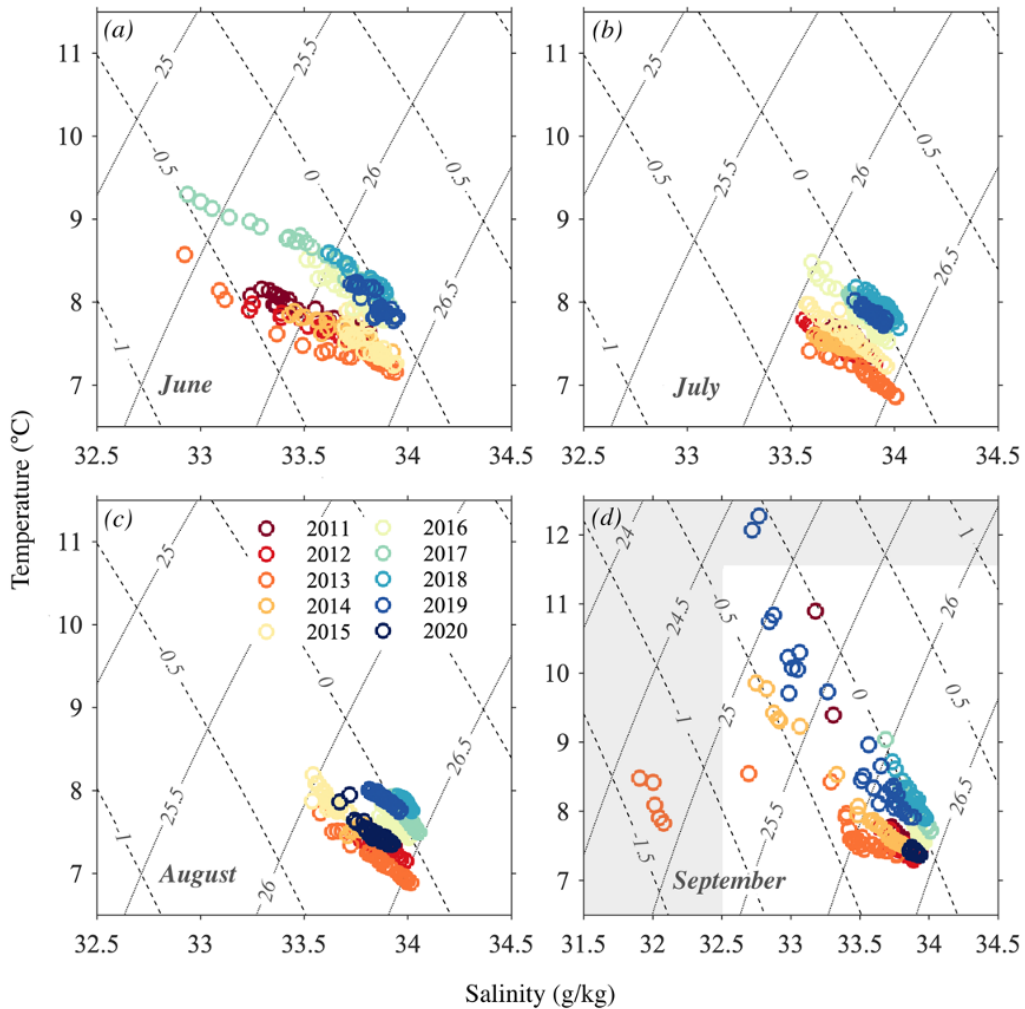


Figure 4.11: Near-bottom temperature and salinity. This figure presents daily averaged data for near-bottom temperature and Salinity at CE042. Black contours represent constant sigma-theta (dotted) and constant (dashed) spiciness. Data were separated by month: June (a), July (b), August (c) and September (d) and colored by year (see subplot c for legend). Grey shading in (d) highlights the difference in x- and y-axis scale from other subplots (a-c).

Anomalous T-S relationship (Figure 4.11) and the statistical tests (Figure 4.12) indicate that a different water mass (or water masses) are present in 2016 – 2019. Across

years, high spiciness corresponds to low DO and vice versa (Figure 4.12a & b); consistent with conditions frequently observed in the CCS. However, the conditions in 2016 - 2019 are slightly different in that a high salinity anomaly is present in the surface California Current. This is different because typically, the sluggish surface California Current transports fresh (mainly Pacific Subarctic Upper Water, PSUW) water equatorward, while the California Undercurrent transports PEW poleward (Hickey 1979). These two water masses are often thought to dominate the offshore water masses, and make up the majority of water that is upwelled to the shelf (Hickey 1979). The advection of low-oxygen PEW water by the California Undercurrent has often been pointed to as a cause of decreasing coastal DO which co-occurs with an increase in spiciness (e.g. Bograd et al. 2008; Pierce et al. 2012; Meinvielle and Johnson 2013), and changes in relative proportion of PEW has pointed to change in community composition in the CCS (McClatchie et al. 2010; Schroeder et al. 2019). However, if ENPCW were present in the surface California Current from 2016 - 2019, then it becomes difficult to solely accredit an increase in spiciness to an increase in amount of PEW present across the slope; As an increase in spiciness can *also* be from an increase in ENPCW present. Both water masses, ENPCW and PEW, are characterized by high salinity, high temperature and low DO levels (Lynn and Simpson 1987), therefore increased presence of either would correspond to an increase in spiciness and lower DO levels. One key difference is that ENPCW is typically low in nutrients (Lynn and Simpson 1987; Talley et al. 2011), which may result in lower productivity, and introduction of water with different nutrient properties may have supported different plankton communities (Bograd et al.

2019; Bernal and McGowan 1981; Chelton 1981; McClatchie 2014; Ren and Rudnick 2021). Ultimately this data clearly shows that a spicier water mass (warmer and saltier) was present during 2016-2019 coincident with the exceptionally low DO conditions on the shelf, however further work is needed to understand the source of this water mass as with our limited data, it could be explained by an increase in PEW or ENPCW water.

4.4.3 Variability of bottom water T-S-DO

To explore multiple deployment years, we provide a summary of bottom salinity and DO from the northern- and southern-most sites for each August from 2011 – 2020 (Figure 4.13). We observe DO variation along the north-south gradient and a spatial difference in both the median salinity experienced and salinity variance is present. A higher (but less variable) bottom salinity is present the south, at CE042, when compared to the northern-most site, MB042, which is located near the Strait of Juan de Fuca (Figures 4.1 & 4.13a). Higher bottom DO values are from the northern site (MB042) and minimum DO concentrations occur in the south (at CE042; 4.13b). Median concentrations of DO at CE042 are each below $1.4 \text{ ml } L^{-1}$ every August from 2011 – 2020, except for 2015; in 2015 all sites experienced elevated DO levels.

We hypothesize that the wind forcing and proximity to the Juan de Fuca Canyon and Strait of Juan de Fuca all combine to impact the observed water type present, DO levels and presence of hypoxia at the northern-most site, MB042. The orientation of site MB042 on a more narrow section of shelf (Figure 2.1) near the Juan de Fuca Canyon *and* Strait of Juan de Fuca, results in higher variability of water mass pres-

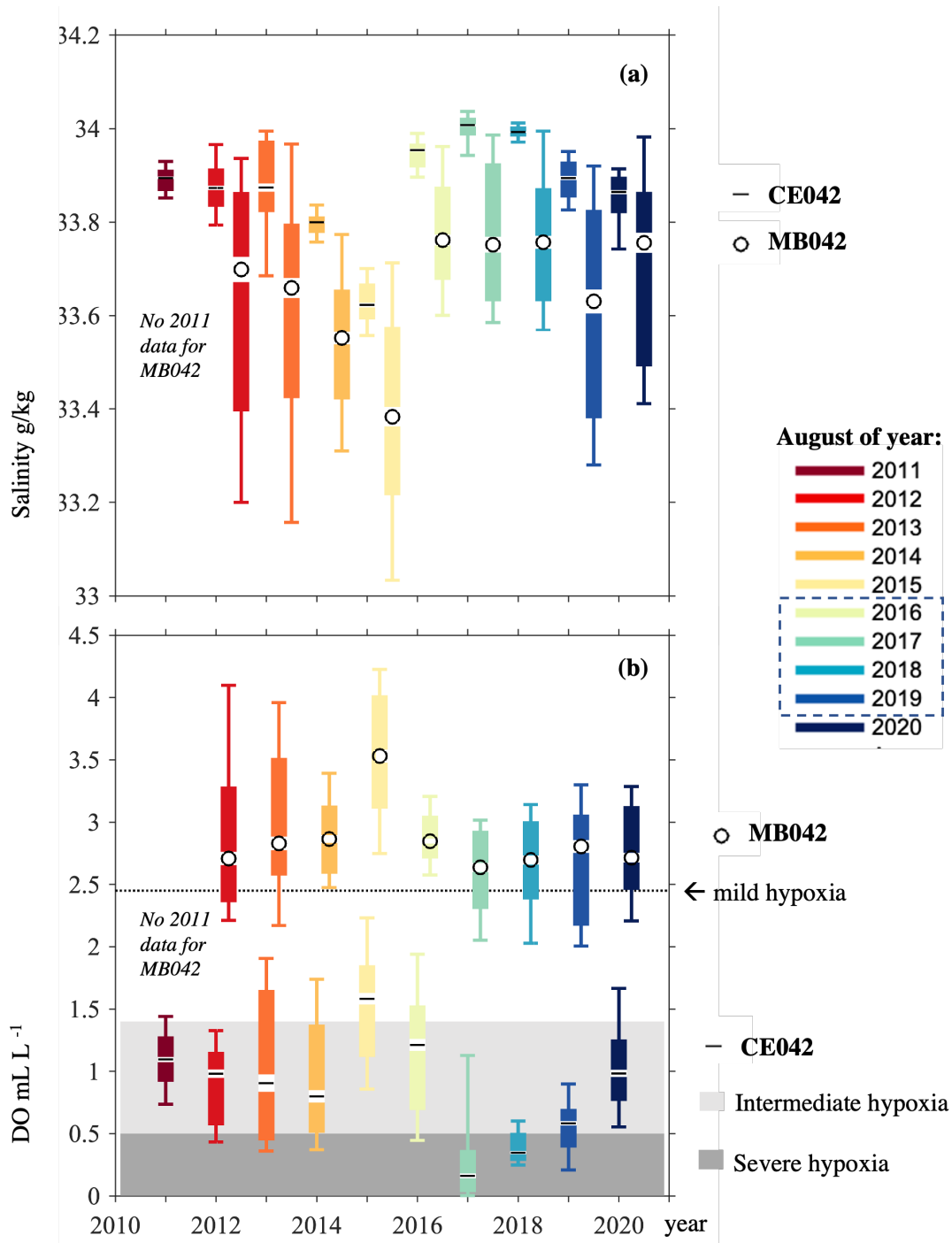


Figure 4.13: August near-bottom DO and salinity. This figure presents time-series data for DO (a) and Salinity (b) at MB042 and CE042. Each August of every year (2011 – 2020) have 744 hours of data included except for: (1) MB042/2011 ($n = 0$); (2) CE042/2015 ($n = 612/ 25.5$ days of hourly data); and (3) CE042/2020 ($n = 705; 29.4$ days of hourly data). Statistics for each year are presented: 10th/25th/50th/75th/90th percentiles. The notched-mean is white, while the median is marked with a dash (CE042) or a circle (MB042).

ence (as compared to CE042). Strong mixing inherent to canyons (Lueck and Osborn 1985; Kunze et al. 2002; Wain et al 2013; Zhao et al. 2012) and strong exchange with the Salish Sea (Bretschneider et al. 1985; Geyer and Cannon 1982; Sutherland et al. 2011; Thomson et al. 2007; MacCready et al. 2020) likely maintains elevated DO levels at MB042, and to a lesser extent at TH042. In addition, retention time at MB042 is likely less due to the narrow shelf. It is likely that mixing in the surface and bottom are stronger in the northern-most sites as compared to the southern-most sites, which could be examined further by combining regional model data with OCNMS mooring data. The southern-most site, CE042, is also located near the Quinault Canyon, but unlike the Juan de Fuca Canyon, the connection with an estuarine system is not as direct. It is likely that during upwelling events, that the proximity to the Quinault Canyon, facilitates transport of water from deeper depths to the shelf and enhanced mixing at the sill. It is not clear how the Quinault Canyon contributes to - and interacts with - shelf hypoxia during different wind forcing scenarios. Regional fishing knowledge suggest that hypoxic events (and fish kills) worsen when winds relax (or remain low) off Cape Elizabeth (personal communication with Ervin Joe Schumacker). It is unclear whether it is low DO water masses that are mobilized during relaxation events, or if the POC (and respiration signal) spreads out across the shelf during relaxation events (e.g., Hales et al. 2006).

4.4.4 Timing of spring transition and river flow

Impacts to coastal ecology are anticipated as flow modifications and climate change alter the timing and volume of freshwater input to estuaries and continental shelves. Warming temperatures impact the hydrologic cycle, and in snowmelt-dominated hydrologic systems (e.g., PNW river basins) warming temperatures directly affects snow accumulation and melt (Hamlet et al. 2005); Studies indicate changes since the mid-20th century include shifts toward earlier spring streamflow (Stewart et al. 2005), lower spring snowpack (Mote et al. 2018), and lower summer stream flow (Fritze et al. 2011). For example, trends of earlier freshet dates and reduced flows are present in the Columbia River record (Bottom et al. 2005). At the time of publication, Curry and Zwiers (2018) show that while a spring peak freshet flow has never been observed outside April – July at the Fraser River (Hope gauge), the timing of spring freshets in the Fraser River (and widespread decreases in snow-to-rain ratios) are an area of active research. During the years we analyzed (1991 - 2020) peak flows occur on average in May at the Columbia River and in May/June at the Fraser River. These results are consistent with the trend observed since the 1900s at the Columbia River (at Dalles), where the peak flow at has shifted from late June to late May, with earlier freshet dates are attributed to human alteration of the flow cycle and earlier snow melt (Bottom et al. 2005) and fall within the Fraser River range described by Curry and Zwiers (2018). These shifts in freshet peak add complexity to understanding shelf biogeochemical change and associated ecological impacts. Historically, the arrival

of large freshet volumes from the Columbia River (and Fraser River) and strong upwelling favorable winds typically all occurred around the same time, in June. However, there is also a recent trend for earlier spring transition dates (Bograd and Lynn 2002; Bograd et al. 2002; García-Reyes and Largier 2010; 2012; Logerwell et al. 2003) and changes in wind strength and persistence (Sydeman et al. 2014; Wang et al. 2015; Rykaczewski et al. 2015; García-Reyes et al. 2015). The de-synchronizing of peak flow and upwelling have implications for ecology (e.g., salmonids see Bottom et al. 2005). While most northern rivers have reduced summer flows, trends towards drier summers have additional implications for water temperature (in streams, rivers and estuaries and on the shelf) and changes in summertime flow (e.g., Lammers et al. 2007; Chegwiddden et al. 2017; Pacific Climate Impacts Consortium, 2022). We hypothesize that reduced summer flows have a negative impact on shelf biogeochemistry (lower DO and lower saturation states), especially when following a large peak freshet (e.g., 2017) that likely result in retention of additional POC and build a respiration signal earlier in the season. However, this question needs to be further investigated with use of a numerical model combined with observational data.

Hickey and Banas (2008) outline how freshwater presence maintains high productivity characteristic to the PNW. This high productivity maintains a high standing stock of particulate organic carbon (POC) (e.g., Hales et al. 2006), which builds a respiration signal in the water column and at the sediment/water interface and contribute to the formation of hypoxia (Diaz and Rosenberg 2008; Rabalais et al. 2010). On the PNW shelf, it has been demonstrated that the combination of high river flow and strong

upwelling supports high levels of nutrients in coastal zone (N, P, Si) and micronutrients to the portions of the Washington and Oregon where the plume covered (Bottom et al. 2005; Hickey and Banas 2008; Jay et al. 2009). Presence of freshwater has also been shown to maintain productivity and shift the location of productivity (and POC). For example, the Columbia River plume increases cross-shelf export, which shifts primary productivity from the inner shelf to the outer shelf and slope and likely impacts spatial variability of carbon production and export (Banas et al. 2009). On the outer shelf and slope export of carbon is easier (in the vertical). This has the potential to reduce DO levels in water that will later be transported to the shelf during upwelling. In addition, the Fraser River and inland Salish Sea rivers have been shown to amplify regional primary productivity by providing some terrigenous nutrients, but on a much larger scale Davis et al. (2014) show these rivers drive persistent estuarine circulation in the Strait of Juan de Fuca which can effectively double the input of oceanic nitrogen back to the shelf. Based on model results reported by Davis et al. (2014), this nitrogen flux to the coastal ocean is comparable to that supplied by local wind-driven upwelling on the Washington shelf. However, because the model results include complete shutdown of the exchange between the Salish Sea and the coastal ocean, it is not clear what a shift in peak river flow would mean for shelf productivity and a subsequent hypoxic volume. Prior studies have used observations (Hales et al. 2006; Connolly et al. 2010), incubation experiments (Adams et al. 2013), and high-resolution models (Siedlecki et al. 2015) to understand the impact of respiration on PNW shelf oxygen. There is a consensus that the respiration signal builds over a season, and results in lower DO later

in the summer. However, it is not clear how extreme river flows (e.g., 2011 and 2017) modify the respiration signal, or what changes occur if the timing of peak river flow occurs during downwelling conditions (e.g., 2017). It is also not clear what impact lateral trapping has on the development of hypoxia. For instance, in other EBUS (e.g., the Benguela system, see Flynn et al. 2020; Rixen et al. 2021), it is hypothesized that hydrographic fronts limit lateral exchange and contribute to nutrient trapping (and hypoxia). A similar process can occur in the PNW, with upwelling and/or river plume fronts (e.g., Banas et al. 2009; Giddings and MacCready 2017).

The timing and volume of river flow are both important, especially when combined with wind events. In the summer the Columbia River plume tends southward and offshore when the rotational tendency and ambient flow are in the same direction. However, under certain wind and discharge conditions, the plume can reverse direction. In particular, during strong downwelling-favorable winds, the plume travels northward, tightly hugging the coastline. If we compare two large water years in the Columbia River (2011 and 2017), we can see that they have different summertime DO levels (Figure 4.5). We hypothesize that the timing of the 2017 (versus 2011) Columbia River flow contributed to the anomalous hypoxia in 2017. In 2011, peak discharge in the Columbia River occurred in June, which took place after the spring transition (April), and flows remained above normal into the summer. While in 2017, the peak flow took place in March, before the spring transition (April), and above normal flows were not observed in the summer. In 2011, if the Columbia River plume spent most of the spring/summer in a southward position, this would likely reduce or reverse exchange during this period

leading to less ocean nutrient delivery. In 2017, the Columbia River discharge was above normal and peaked earlier than the spring transition; during downwelling favorable conditions. These conditions (wind + discharge) met criteria (outlined by García-Berdeal et al. 2002; Hickey et al. 2009) for the Columbia River plume to spend the majority of April in a northward position. Although we have no mooring data to corroborate this, we hypothesize that the northward position of the plume resulted in additional nutrient delivery to the shelf. While 2011 vs 2017 were different at the deeper moorings (lower DO in 2017), these were the worst two years for the shallow site (CE015). Future work to better understand the impact of timing of peak flow with the spring transition is necessary. Further, additional work should be performed to better understand how the inner (15m) versus middle (27-42m) shelf responds to freshwater input. These questions can be explored by incorporating Ocean Observatories Initiative (OOI) shelf mooring data located to the north and south of the Columbia River, in conjunction with a numerical model.

As outlined in section 4.4.2, during the time from 2014 – 2019 the CCS experienced a unique set of oceanographic conditions, and during 2017 - 2019 tragic shelf DO levels (ranging from severe to anoxic conditions) were present off Washington in OCNMS mooring data. Upwelling controls variability in the spring/summer (Hickey et al. 2006), with the efficiency (and depth) of upwelling based upon magnitude/persistence of upwelling winds (e.g. Hickey et al. 2006) and the local cross-shelf wind profile (Jacox and Edwards 2012), as well as other physical characteristics like local stratification, bottom slope, and shelf width (Allen et al. 1995), and coastline shape (Barth et al.

2000; Pickett and Paduan 2003). To better understand shelf conditions, the timing of transitions to the upwelling season (spring transition) and out of the upwelling season (fall transition) are both important. In the PNW, physical and biological estimates for spring (and fall) transitions exist (e.g., "physical" transitions, Pierce and Barth (2022); and "biological" transitions, Peterson et al. 2014). Both are important when trying to understand shelf DO and ecological impact. Based on winds off Oregon, as defined by Pierce and Barth (2022), the 2017 spring transition in the PNW (physical transition) is in April, if we adjust the metric to include winds at N41 (the timing is similar off Washington). However, if a biological metric developed by Peterson et al. (2014) is implemented, which considers warm- (versus cold-) water species presence, the *biological* spring transition takes place in June 2017. This transition occurs after a long period of warm-water species presence (from 30 September 2014 through 21 June 2017) (NOAA Fisheries 2022). Incorporation of the biological transition is important, as the aforementioned extended period of warm-water species presence was unprecedented in the biological transition record developed by Peterson et al. (2014) (and maintained, see NOAA Fisheries 2022), and likely further complicated the multi-stressor environment for species like salmonids and flatfish. Some studies suggest a lack of planktivorous fish would cause more organic matter to reach shelf sediments (e.g., Bakun and Weeks 2004) therefore building a stronger respiration signal. Global climate models suggest that changes in upwelling will likely be dependent on latitude, with intensification of CCS upwelling in the spring (especially in the southern CCS), followed by significant weakening of upwelling during the summer months (especially in the northern CCS)

(e.g., García-Reyes et al. 2015; Rykaczewski et al. 2015; Wang et al. 2015). The juxtaposition of changing winds and upwelling seasonality with modified river discharge pose large challenges for ecology of the CCS, and communities that rely upon it. A better understanding of summer conditions is especially necessary to better understand potential outcomes of a below normal discharge year that also features weak wind forcing. Interdisciplinary work that synthesizes multiple stressors are necessary to better understand and manage ecosystems across the CCS.

4.5 Conclusions

Natural variability inherent to EBUS alongside uncertainties in present and future trends in upwelling seasonality, coastal warming and stratification, primary production and biogeochemistry of source waters each pose large challenges to the climate response across EBUS and within each system itself (Sydeman et al. 2014; García-Reyes et al. 2015; Rykaczewski et al. 2015; Varela et al. 2015; Wang et al. 2015; Bindoff et al. 2019). A step towards better understanding drivers of multiple stressor interactions includes analysis of subsurface observations to identify relationships and trends in shelf waters. In this work we focus on the physical dynamics which influence shelf DO in the northern CCS (off Washington, Figure 4.1) in attempt to better understand the physical dynamics that influenced the extreme low DO observed in the summers of 2017 - 2019. From this work we found significant interannual variability in DO, with the 2016-2019 low DO period is statistically associated with spicier water potentially suggesting

a link between source waters impacted by the El Niño and MHW presence and shelf DO. Further, given the very, very low North Pacific Gyre Oscillation (NPGO) index in 2017 (Thompson et al. 2018) and demonstrated relationships between DO levels in the PNW and the NPGO (e.g., Peterson et al. 2013), addition of other North Pacific climate information (e.g., NPGO and the North Pacific High) may help improve our ability to understand (and forecast) freshwater input and shelf biogeochemistry. When compared to records presented by Connolly et al. (2010) and Peterson et al. (2013), which collectively span a historical period of summer upwelling from 1950 – 1986 and more recent period from 1998 – 2012, summertime hypoxic exposure appears to have worsened on the Washington shelf. However, 2011 – 2020 shows significant interannual variability without a clear downward trend. Continued data collection in OCNMS (and across the CCS regions) will aid in determining a temporal DO trend, and clarify if the 2017 – 2019 were anomalous or an example of what future decades may hold in store. We also observed a north-south trend with lower DO in the south, which can be explained by several hypotheses, ranging from shelf width to canyons to stratification. However, the relationship between stratification, surface salinity and DO is complex. Within periods with similar surface salinity, more stratification is related to lower DO, *but* overall higher stratification is caused by lower surface salinity and is associated with higher DO. This likely demonstrates a complex relationship between the presence of river water and mixing driven by downwelling. Additional work to further assess the impact of timing of the Columbia and Fraser Rivers with wind events is important to

understand DO and carbonate chemistry off Washington, and help make predictions for future climate conditions.

Chapter 5

Summary

Chapter 2: Observations of shelf hypoxia off northern California.

Moorings placed over the central CCS shelf from the mid- to inner- shelf exhibit complex and temporally varying DO trends. At the deeper, mid-shelf site, GF, two distinct modes of variability are seen where upwelling relates to DO decline and relaxation events with increasing DO levels. During the second mode at GF, it seems like the opposite occurs: upwelling relates to an increase in DO levels; relaxation events to declining DO levels. These observations paired with the relationship between spice and DO levels during the first mode at GF suggest water mass variability is driving DO trends (at least over the deeper sections of shelf, i.e., GF). During the second mode at GF, we hypothesize that either: (1) a local respiration signal was established and, during the second mode, shelf waters are lower in DO level than source waters, but the signal is still dominated by advection; (2) weaker winds lead to upwelling from shallower depths. It is clear that the DO-spice covariance over the first mode is strong, and then DO-stratification vary over

the second mode at GF. At the shallower inner-shelf sites, and for the entire time-series, upwelling relates to DO decline and relaxation events with increasing DO levels.

Stratification reduces vertical mixing, precluding diffusive fluxes of DO from the surface layer. As the upwelling season continues and shifts to the relaxation season, a respiration signal likely builds up across the shelf and may explain why the lowest DO levels occur later in the summer. The spatial variations in hypoxia that we observed in this study region, and differences between this region and other upwelling regions, is likely to be explained by differences in oxygen demand (sediment demand plus delivery of POC to sub-thermocline waters), differences in stratification (surface heating, freshwater influences, wind stress), and flow-path history of waters at that site. We hypothesize that later in the spring/summer (during the relaxation season) DO levels on the shelf are likely to be lower than the water being upwelled to the shelf. In this scenario, when upwelling circulation starts, the near-bottom mid-shelf environment may be freshened by higher-DO water advected to the shelf during upwelling, while the lower-DO water present at the mid-shelf may be advected shoreward. This would result in a drop in DO values at inner-shelf sites (e.g., BH) but increasing DO levels at mid-shelf sites like (GF). The importance of source water is clear in the first half at GF and the overall trend and second half shows the importance of local drawdown. These are consistent with other parts of the CCS. For example Adams et al. (2013) found later in the upwelling season shelf DO levels were lower than DO levels in newly upwelled water. The inner-shelf on the other hand shows less clear trends and more temporal variability pointing to a complex mosaic of shelf DO levels. Future work should involve velocity measurements

to better understand the direction of flow during upwelling and relaxation events.

Based on the mooring data we explored, it seems like DO levels off northern California are higher than those observed off Washington. It is not yet clear why hypoxia off northern California is less severe than in the PNW, but it likely relates to a combination of forcing mechanisms that explain the mismatch in productivity. We hypothesize that the wind strength likely plays a role in alleviating the respiration signal by: (1) reducing the respiration signal on the shelf; (2) shifting carbon export to the outer shelf/slope; and (3) changing retention time and ventilation of shelf waters (e.g., Botsford et al. 2006; Yokomizo et al. 2010; Stone et al. 2020). This idea is corroborated by the lowest DO levels at all three sites were observed outside the core upwelling season (e.g., the period of coldest water temperatures and strongest upwelling-favorable winds; not during the months of April and May). We also think the role of river plumes may play an important role in the expression of hypoxia in different regions of the CCS (and during different freshwater input scenarios within a subregion). For instance, lower freshwater to San Francisco Bay would result in less extreme density anomalies and thus weaker shelf stratification. However, more work is needed to explore the mismatch between shelf DO levels observed in the central versus northern CCS.

Our study region features a characteristic strong upwelling season and, in 2015, negligible freshwater influence. During the upwelling season, low runoff is typical but the freshwater input was exacerbated by drought conditions in 2015. With literature pointing to an increase in warming that will magnify the frequency of both droughts and floods in California, these data present one bookend of the shelf hypoxia story for

this subregion. Although discharge from San Francisco Bay (and the Sacramento-San Joaquin Delta) is already a particularly complex puzzle with several end users, a better understanding of freshwater impacts to shelf chemistry may help with ecosystem management in the coastal zone. In a system like San Francisco Bay, where freshwater discharge is heavily regulated (from the Delta and from industrial and municipal discharge sources), managers may have a lever to help modulate coastal hypoxia and acidification. Although, a development of this metric would require collection of additional time-series observations and require a modeling study to further quantify the impact of San Francisco Bay outflow on retention within the Gulf.

While open-ocean waters are experiencing deoxygenation, at present upwelling source waters hover near the threshold for intermediate hypoxia and are often below the threshold for mild hypoxia. The presence of more persistent hypoxia and intermediate to severe hypoxic events over the shelf is achieved by local oxygen uptake over the shelf. At the deeper site, GF, the lowest DO levels were observed after the upwelling season and during relaxation events, pointing to an important role of local DO draw-down. Upwelling regions with broader shelves and stronger stratification may be prone to more severe and/or persistent hypoxia (e.g., Monterio et al. 2011) – and within these regions, it has been suggested that most severe hypoxia has potential to occur within bays (e.g., Largier 2020). Linking observations with numerical modeling has the potential to describe the mosaic of oxygen variability more fully across upwelling shelves and may elucidate how short duration hypoxic events may be exacerbated by global deoxygenation. This is critical to assessment, evaluation, and management responses to

increased occurrences of hypoxia due to deoxygenation of source waters.

Chapter 3: Seasonality of near-bottom dissolved oxygen over a submarine bank off northern California.

From 2014 to 2018 we monitored DO concentrations over a submarine bank located at the shelf break off northern California. We observed seasonal variability. The similarity of seasonal patterns across years (2014 - 2018), especially in temperature, is interesting given the unique set of oceanographic conditions the CCS experienced from 2014 – 2019. Overall, with the onset of upwelling, near-bottom water becomes cooler and saltier, and DO levels decrease. Although the coolest water occurs early in the upwelling season, the minimum in DO levels occur later, towards the end of the upwelling season and often during the relaxation season. Deviations from the seasonal trend observed are likely attributed to a combination of physical and biogeochemical processes working together. Specifically, we hypothesize that the interplay of wind-driven mixing and surface productivity may help explain interannual differences, but additional work is needed to separate these signals. At Cordell Bank, DO concentrations were often below the threshold of mild hypoxia (2.45 ml/L), but only one instance of intermediate hypoxia was observed (1.4 to 2.45 ml/L) during the relaxation season (July 2017). A step towards better understanding drivers of DO variability (and multi-stressor interactions) includes analysis of subsurface observations to identify relationships and trends in shelf waters. Continued monitoring at Cordell Bank, and incorporation of this mooring data set with long term time-series, may help make management decisions and/or predictions

for future climate conditions. Finally, observed DO is also lower than expected using two end-member source waters (PEW and PSUW) thus pointing to the likely importance of local drawdown (and potentially presence of more than two source water masses).

Chapter 4: Interannual variability in shelf hypoxia off the Washington coast

Natural variability inherent to EBUS alongside uncertainties in present and future trends in upwelling seasonality, coastal warming and stratification, primary production and biogeochemistry of source waters each pose large challenges to the climate response across EBUS and within each system itself (Sydeman et al. 2014; García-Reyes et al. 2015; Rykaczewski et al. 2015; Varela et al. 2015; Wang et al. 2015; Bindoff et al. 2019). A step towards better understanding drivers of multiple stressor interactions includes analysis of subsurface observations to identify relationships and trends in shelf waters. In this work we focus on the physical dynamics which influence shelf DO in the northern CCS (off Washington, Figure 4.1) in attempt to better understand the physical dynamics that influenced the extreme low DO observed in the summers of 2017 - 2019. From this work we found significant interannual variability in DO, with the 2016-2019 low DO period is statistically associated with spicier water potentially suggesting a link between source waters impacted by the El Niño and MHW presence and shelf DO. Further, given the very, very low North Pacific Gyre Oscillation (NPGO) index in 2017 (Thompson et al. 2018) and demonstrated relationships between DO levels in the PNW and the NPGO (e.g., Peterson et al. 2013), addition of other North Pacific climate information (e.g., NPGO and the North Pacific High) may help improve our

ability to understand (and forecast) freshwater input and shelf biogeochemistry. When compared to records presented by Connolly et al. (2010) and Peterson et al. (2013), which collectively span a historical period of summer upwelling from 1950 – 1986 and more recent period from 1998 – 2012, summertime hypoxic exposure appears to have worsened on the Washington shelf. However, 2011 – 2020 shows significant interannual variability without a clear downward trend. Continued data collection in OCNMS (and across the CCS regions) will aid in determining a temporal DO trend, and clarify if the 2017 – 2019 were anomalous or an example of what future decades may hold in store. We also observed a north-south trend with lower DO in the south, which can be explained by several hypotheses, ranging from shelf width to canyons to stratification. However, the relationship between stratification, surface salinity and DO is complex. Within periods with similar surface salinity, more stratification is related to lower DO, *but* overall higher stratification is caused by lower surface salinity and is associated with higher DO. This likely demonstrates a complex relationship between the presence of river water and mixing driven by downwelling. Additional work to further assess the impact of timing of the Columbia and Fraser Rivers with wind events is important to understand DO and carbonate chemistry off Washington, and help make predictions for future climate conditions.

A note on DO levels observed across the central CCS

As part of this work we monitored DO levels across the shelf off northern California: (1) at a mid-shelf site (~54m) in the Gulf of the Farallones, offshore San Francisco

Bay, and within the more stratified upwelling shadow south of Point Reyes; (2) at two shallower sites, (~ 18 and 30m), to the north and south of Point Reyes (Figure 2.1); and (3) at two sites over a submarine bank (Cordell Bank) located at the shelf-break off northern California (Figure 3.1). Results from these moorings showed different exposure to hypoxia. This demonstrates that while source water variability may set the initial condition for water parcels being modified over the shelf, the spatial patterns of flow, stratification, ventilation and respiration are the factors that account for the lowest and most persistent hypoxic events observed in shelf habitats. The different exposures to hypoxic stress at these three sites represent very different - yet connected - habitats: north of the Point Reyes headland, south of the headland, and along the shelf-edge (over a submarine bank). Recognition of spatial heterogeneity in physical dynamics that influence DO levels, will surely prove to be more complex when high-frequency observations are available from more locations. Further, large-scale deoxygenation shifts in source waters will likely result in shifting distributions of shelf hypoxia. For example, if source water DO levels dropped by $1\text{ ml } L^{-1}$ then the mode at Gulf of the Farallones mooring could be expected to drop from 1.7 to $0.7\text{ ml } L^{-1}$ and severe hypoxia will be commonplace. This is critical to assessment, evaluation and management responses to increased occurrences of hypoxia due to deoxygenation of source waters.

Reference List

- Adams, Katherine A., John A. Barth, and Francis Chan. “Temporal Variability of Near-Bottom Dissolved Oxygen during Upwelling off Central Oregon.” *Journal of Geophysical Research: Oceans* 118, no. 10 (2013): 4839–54. <https://doi.org/10.1002/jgrc.20361>.
- Alford, Matthew H., and Parker MacCready. “Flow and Mixing in Juan de Fuca Canyon, Washington.” *Geophysical Research Letters* 41, no. 5 (2014): 1608–15. <https://doi.org/10.1002/2013GL058967>.
- Allen, J. S., P. A. Newberger, and J. Federiuk. “Upwelling Circulation on the Oregon Continental Shelf. Part I: Response to Idealized Forcing.” *Journal of Physical Oceanography* 25, no. 8 (August 1, 1995): 1843–66. [https://doi.org/10.1175/1520-0485\(1995\)025<1843:UCOTOC>2.0.CO;2](https://doi.org/10.1175/1520-0485(1995)025<1843:UCOTOC>2.0.CO;2).
- Allen, S. E., and B. M. Hickey. “Dynamics of Advection-Driven Upwelling over a Shelf Break Submarine Canyon.” *Journal of Geophysical Research: Oceans* 115, no. C8 (2010). <https://doi.org/10.1029/2009JC005731>.
- Arellano, Beatriz, and David Rivas. “Coastal Upwelling Will Intensify along the Baja California Coast under Climate Change by Mid-21st Century: Insights from a GCM-Nested Physical-NPZD Coupled Numerical Ocean Model.” *Journal of Marine Systems* 199 (November 1, 2019): 103207. <https://doi.org/10.1016/j.jmarsys.2019.103207>.
- Austin, Jay A., and John A. Barth. “Variation in the Position of the Upwelling Front on the Oregon Shelf.” *Journal of Geophysical Research: Oceans* 107, no. C11 (2002): 1-1-1–15. <https://doi.org/10.1029/2001JC000858>.
- Bakun, Andrew, and Craig S. Nelson. “The Seasonal Cycle of Wind-Stress Curl in Subtropical Eastern Boundary Current Regions.” *Journal of Physical Oceanography* 21, no. 12 (December 1, 1991): 1815–34. [https://doi.org/10.1175/1520-0485\(1991\)021<1815:TSCOWS>2.0.CO;2](https://doi.org/10.1175/1520-0485(1991)021<1815:TSCOWS>2.0.CO;2).

- Bakun, Andrew, and Scarla J. Weeks. "Greenhouse Gas Buildup, Sardines, Submarine Eruptions and the Possibility of Abrupt Degradation of Intense Marine Upwelling Ecosystems." *Ecology Letters* 7, no. 11 (2004): 1015–23. <https://doi.org/10.1111/j.1461-0248.2004.00665.x>.
- Banas, N. S., P. MacCready, and B. M. Hickey. "The Columbia River Plume as Cross-Shelf Exporter and along-Coast Barrier." *Continental Shelf Research, Physics of Estuaries and Coastal Seas: Papers from the PECS 2006 Conference*, 29, no. 1 (January 15, 2009): 292–301. <https://doi.org/10.1016/j.csr.2008.03.011>.
- Barth, John A, Stephen D Pierce, and Robert L Smith. "A Separating Coastal Upwelling Jet at Cape Blanco, Oregon and Its Connection to the California Current System." *Deep Sea Research Part II: Topical Studies in Oceanography* 47, no. 5 (May 1, 2000): 783–810. [https://doi.org/10.1016/S0967-0645\(99\)00127-7](https://doi.org/10.1016/S0967-0645(99)00127-7).
- Beardsley, R. C., C. E. Dorman, C. A. Friehe, L. K. Rosenfeld, and C. D. Winant. "Local Atmospheric Forcing during the Coastal Ocean Dynamics Experiment: 1. A Description of the Marine Boundary Layer and Atmospheric Conditions over a Northern California Upwelling Region." *Journal of Geophysical Research: Oceans* 92, no. C2 (1987): 1467–88. <https://doi.org/10.1029/JC092iC02p01467>.
- Beardsley, R. C., and S. J. Lentz. "The Coastal Ocean Dynamics Experiment Collection: An Introduction." *Journal of Geophysical Research: Oceans* 92, no. C2 (1987): 1455–63. <https://doi.org/10.1029/JC092iC02p01455>.
- Belmecheri, Soumaya, Flurin Babst, Eugene R. Wahl, David W. Stahle, and Valerie Trouet. "Multi-Century Evaluation of Sierra Nevada Snowpack." *Nature Climate Change* 6, no. 1 (January 2016): 2–3. <https://doi.org/10.1038/nclimate2809>.
- Bernal, Patricio A., and John A. McGowan. "Advection and Upwelling in the California Current." In *Coastal Upwelling*, 381–99. American Geophysical Union (AGU), 1981. <https://doi.org/10.1029/CO001p0381>.

- Bindoff, Nathaniel L, William W L Cheung, James G Kairo, Javier Arístegui, Valeria A Guinder, Robert Hallberg, Nathalie Hilmi, et al. “Changing Ocean, Marine Ecosystems, and Dependent Communities.” IPCC Special Report on the Ocean and Cryosphere in a Changing Climate, 2019.
- Bograd, Steven J., Mercedes Pozo Buil, Emanuele Di Lorenzo, Carmen G. Castro, Isaac D. Schroeder, Ralf Goericke, Clarissa R. Anderson, Claudia Benitez-Nelson, and Frank A. Whitney. “Changes in Source Waters to the Southern California Bight.” *Deep Sea Research Part II: Topical Studies in Oceanography*, CCE-LTER: Responses of the California Current Ecosystem to Climate Forcing, 112 (February 1, 2015): 42–52. <https://doi.org/10.1016/j.dsr2.2014.04.009>.
- Bograd, Steven J., Carmen G. Castro, Emanuele Di Lorenzo, Daniel M. Palacios, Helen Bailey, William Gilly, and Francisco P. Chavez. “Oxygen Declines and the Shoaling of the Hypoxic Boundary in the California Current.” *Geophysical Research Letters* 35, no. 12 (2008). <https://doi.org/10.1029/2008GL034185>.
- Bograd, Steven J., and Ronald J. Lynn. “Long-Term Variability in the Southern California Current System.” *Deep Sea Research Part II: Topical Studies in Oceanography*, CalCOFI: A Half Century of Physical, Chemical and Biological Research in the California Current System, 50, no. 14 (August 1, 2003): 2355–70. [https://doi.org/10.1016/S0967-0645\(03\)00131-0](https://doi.org/10.1016/S0967-0645(03)00131-0).
- Bograd, Steven J., Isaac D. Schroeder, and Michael G. Jacox. “A Water Mass History of the Southern California Current System.” *Geophysical Research Letters* 46, no. 12 (2019): 6690–98. <https://doi.org/10.1029/2019GL082685>.
- Bograd, Steven, Franklin Schwing, Roy Mendelssohn, and Phaedra Green-Jessen. “On the Changing Seasonality over the North Pacific.” *Geophysical Research Letters* 29, no. 9 (2002): 47-1-47-4. <https://doi.org/10.1029/2001GL013790>.
- Booth, J. A. T., C. B. Woodson, M. Sutula, F. Micheli, S. B. Weisberg, S. J. Bograd, A. Steele, J. Schoen, and L. B. Crowder. “Patterns and Potential Drivers of Declining Oxygen Content along the

- Southern California Coast.” *Limnology and Oceanography* 59, no. 4 (July 2014): 1127–38.
<https://doi.org/10.4319/lo.2014.59.4.1127>.
- Booth, J. Ashley T., Erika E. McPhee-Shaw, Paul Chua, Eric Kingsley, Mark Denny, Roger Phillips, Steven J. Bograd, Louis D. Zeidberg, and William F. Gilly. “Natural Intrusions of Hypoxic, Low PH Water into Nearshore Marine Environments on the California Coast.” *Continental Shelf Research* 45 (August 2012): 108–15. <https://doi.org/10.1016/j.csr.2012.06.009>.
- Bopp, L., L. Resplandy, J. C. Orr, S. C. Doney, J. P. Dunne, M. Gehlen, P. Halloran, et al. “Multiple Stressors of Ocean Ecosystems in the 21st Century: Projections with CMIP5 Models.” *Biogeosciences* 10, no. 10 (October 2, 2013): 6225–45. <https://doi.org/10.5194/bg-10-6225-2013>.
- Bopp, Laurent, Corinne Le Quéré, Martin Heimann, Andrew C. Manning, and Patrick Monfray. “Climate-Induced Oceanic Oxygen Fluxes: Implications for the Contemporary Carbon Budget.” *Global Biogeochemical Cycles* 16, no. 2 (2002): 6-1-6–13. <https://doi.org/10.1029/2001GB001445>.
- Botsford, Louis W., Cathryn A. Lawrence, Edward P. Dever, Alan Hastings, and John Largier. “Effects of Variable Winds on Biological Productivity on Continental Shelves in Coastal Upwelling Systems.” *Deep Sea Research Part II: Topical Studies in Oceanography, The Role of Wind-Driven Flow in Shelf Productivity*, 53, no. 25 (December 1, 2006): 3116–40.
<https://doi.org/10.1016/j.dsr2.2006.07.011>.
- — —. “Wind Strength and Biological Productivity in Upwelling Systems: An Idealized Study.” *Fisheries Oceanography* 12, no. 4–5 (2003): 245–59. <https://doi.org/10.1046/j.1365-2419.2003.00265.x>.
- Bottom, Daniel L., Charles A. Simenstad, Jennifer Burke, Antonio M. Baptista, David A. Jay, Kim K. Jone, Edmundo Casillas, and Michael H. Schiewe. “Salmon at River’s End: The Role of the Estuary in the Decline and Recovery of Columbia River Salmon.” Technical Memorandum NMFS-NWFSC-68. NOAA, 2005.

- Breitberg, Denise, Joseph Salisbury, Joan Bernhard, Wei-Jun Cai, Sam Dupont, Scott Doney, Kristy Kroeker, et al. “And on Top of All That... Coping with Ocean Acidification in the Midst of Many Stressors.” *Oceanography* 25, no. 2 (June 1, 2015): 48–61.
<https://doi.org/10.5670/oceanog.2015.31>.
- Breitburg, Denise, Lisa A. Levin, Andreas Oschlies, Marilaure Grégoire, Francisco P. Chavez, Daniel J. Conley, Véronique Garçon, et al. “Declining Oxygen in the Global Ocean and Coastal Waters.” *Science* 359, no. 6371 (January 5, 2018): eaam7240. <https://doi.org/10.1126/science.aam7240>.
- Bretschneider, D. E., G. A. Cannon, J. R. Holbrook, and D. J. Pashinski. “Variability of Subtidal Current Structure in a Fjord Estuary: Puget Sound, Washington.” *Journal of Geophysical Research: Oceans* 90, no. C6 (1985): 11949–58. <https://doi.org/10.1029/JC090iC06p11949>.
- Brink, Kenneth H., and Allan R. Robinson. *The Global Coastal Ocean - Regional Studies and Syntheses*. Harvard University Press, 2005.
- Bruyère, Cindy L., James M. Done, Greg J. Holland, and Sherrie Fredrick. “Bias Corrections of Global Models for Regional Climate Simulations of High-Impact Weather.” *Climate Dynamics* 43, no. 7 (October 1, 2014): 1847–56. <https://doi.org/10.1007/s00382-013-2011-6>.
- California Department of Water Resources (CDEC). “Water Year 2017: What a Difference a Year Makes.” California Natural Resources Agency, State of California, 2017.
- Capotondi, Antonietta, Michael Alexander, Nicholas Bond, Enrique Curchitser, and James Scott. “Enhanced Upper Ocean Stratification with Climate Change in the CMIP3 Models.” *Journal of Geophysical Research (Oceans)* 117 (April 1, 2012): 4031. <https://doi.org/10.1029/2011JC007409>.
- Chan, F., J. A. Barth, C. A. Blanchette, R. H. Byrne, F. Chavez, O. Cheriton, R. A. Feely, et al. “Persistent Spatial Structuring of Coastal Ocean Acidification in the California Current System.” *Scientific Reports* 7, no. 1 (May 31, 2017): 2526. <https://doi.org/10.1038/s41598-017-02777-y>.

- Chan, F., J. A. Barth, J. Lubchenco, A. Kirincich, H. Weeks, W. T. Peterson, and B. A. Menge. "Emergence of Anoxia in the California Current Large Marine Ecosystem." *Science* 319, no. 5865 (February 15, 2008): 920–920. <https://doi.org/10.1126/science.1149016>.
- Chan, Francis, John A. Barth, Kristy J. Kroeker, Jane Lubchenco, and Bruce A. Menge. "The Dynamics and Impact of Ocean Acidification and Hypoxia: Insights from Sustained Investigations in the Northern California Current Large Marine Ecosystem." *Oceanography* 32, no. 3 (2019): 62–71.
- Chapman, David C., and Steven J. Lentz. "Acceleration of a Stratified Current over a Sloping Bottom, Driven by an Alongshelf Pressure Gradient." *Journal of Physical Oceanography* 35, no. 8 (August 1, 2005): 1305–17. <https://doi.org/10.1175/JPO2744.1>.
- Chavez, Francisco P., and Monique Messié. "A Comparison of Eastern Boundary Upwelling Ecosystems." *Progress in Oceanography*, Eastern Boundary Upwelling Ecosystems: Integrative and Comparative Approaches, 83, no. 1 (December 1, 2009): 80–96. <https://doi.org/10.1016/j.pocean.2009.07.032>.
- Chavez, Francisco, J. Timothy Pennington, Reiko Michisaki, Marguerite Blum, Gabriela Chavez, Jules Friederich, Brent Jones, et al. "Climate Variability and Change: Response of a Coastal Ocean Ecosystem." *Oceanography* 30, no. 4 (December 1, 2017): 128–45. <https://doi.org/10.5670/oceanog.2017.429>.
- Chegwidden, O. S., B. Nijssen, D. E. Rupp, and P. W. Mote. "Hydrologic Response of the Columbia River System to Climate Change." Zenodo, September 19, 2017. <https://doi.org/10.5281/zenodo.854763>.
- Chelton, D., Patricio Bernal, and J. McGowan. "Large-Scale Interannual Physical and Biological Interaction in the California Current (El Nino)." *Journal of Marine Research* 40 (January 1, 1982).
- Chelton, Dudley B., Robert L. Bernstein, Alan Bratkovich, and P. Michael Kosro. "The Central California Coastal Circulation Study." *Eos, Transactions American Geophysical Union* 68, no. 1 (1987): 1–13. <https://doi.org/10.1029/EO068i001p00001>.

- Connolly, T. P., B. M. Hickey, S. L. Geier, and W. P. Cochlan. “Processes Influencing Seasonal Hypoxia in the Northern California Current System.” *Journal of Geophysical Research: Oceans* 115, no. C3 (2010). <https://doi.org/10.1029/2009JC005283>.
- Connolly, Thomas P., and Barbara M. Hickey. “Regional Impact of Submarine Canyons during Seasonal Upwelling.” *Journal of Geophysical Research: Oceans* 119, no. 2 (2014): 953–75. <https://doi.org/10.1002/2013JC009452>.
- Connolly, Thomas P., Barbara M. Hickey, Igor Shulman, and Richard E. Thomson. “Coastal Trapped Waves, Alongshore Pressure Gradients, and the California Undercurrent*.” *Journal of Physical Oceanography* 44, no. 1 (January 1, 2014): 319–42. <https://doi.org/10.1175/JPO-D-13-095.1>.
- Crawford, William R., and M. Angelica Peña. “Declining Oxygen on the British Columbia Continental Shelf.” *Atmosphere-Ocean* 51, no. 1 (February 1, 2013): 88–103. <https://doi.org/10.1080/07055900.2012.753028>.
- Crawford, William R., and Richard K. Dewey. “Turbulence and Mixing: Sources of Nutrients on the Vancouver Island Continental Shelf.” *Atmosphere-Ocean* 27, no. 2 (June 1, 1989): 428–42. <https://doi.org/10.1080/07055900.1989.9649345>.
- Crouch, J., R.R. Heim Jr., and C. Fenimore. “Regional Climate, United States [in ‘State of the Climate in 2011’].” *Bull. Amer. Meteor. Soc.* 93, 2012.
- Curry, Charles L., and Francis W. Zwiers. “Examining Controls on Peak Annual Streamflow and Floods in the Fraser River Basin of British Columbia.” *Hydrology and Earth System Sciences* 22, no. 4 (April 16, 2018): 2285–2309. <https://doi.org/10.5194/hess-22-2285-2018>.
- Davis, Kristen A., Neil S. Banas, Sarah N. Giddings, Samantha A. Siedlecki, Parker MacCready, Evelyn J. Lessard, Raphael M. Kudela, and Barbara M. Hickey. “Estuary-Enhanced Upwelling of Marine Nutrients Fuels Coastal Productivity in the U.S. Pacific Northwest.” *Journal of Geophysical Research: Oceans* 119, no. 12 (2014): 8778–99. <https://doi.org/10.1002/2014JC010248>.

- Davis, Russ E., Mark D. Ohman, Daniel L. Rudnick, and Jeff T. Sherman. "Glider Surveillance of Physics and Biology in the Southern California Current System." *Limnology and Oceanography* 53, no. 5part2 (2008): 2151–68. https://doi.org/10.4319/lo.2008.53.5_part_2.2151.
- Deutsch, Curtis, Steven Emerson, and LuAnne Thompson. "Physical-Biological Interactions in North Pacific Oxygen Variability." *Journal of Geophysical Research: Oceans* 111, no. C9 (2006). <https://doi.org/10.1029/2005JC003179>.
- Dever, E. P. "Subtidal Velocity Correlation Scales on the Northern California Shelf." *Journal of Geophysical Research: Oceans* 102, no. C4 (1997): 8555–71. <https://doi.org/10.1029/96JC03451>.
- — —. "Wind-Forced Cross-Shelf Circulation on the Northern California Shelf." *Journal of Physical Oceanography* 27, no. 8 (August 1, 1997): 1566–80. [https://doi.org/10.1175/1520-0485\(1997\)027<1566:WFCSCO>2.0.CO;2](https://doi.org/10.1175/1520-0485(1997)027<1566:WFCSCO>2.0.CO;2).
- Dever, E. P., C. E. Dorman, and J. L. Largier. "Surface Boundary-Layer Variability off Northern California, USA, during Upwelling." *Deep Sea Research Part II: Topical Studies in Oceanography, The Role of Wind-Driven Flow in Shelf Productivity*, 53, no. 25 (December 1, 2006): 2887–2905. <https://doi.org/10.1016/j.dsr2.2006.09.001>.
- Dever, E. P., and S. J. Lentz. "Heat and Salt Balances over the Northern California Shelf in Winter and Spring." *Journal of Geophysical Research: Oceans* 99, no. C8 (1994): 16001–17. <https://doi.org/10.1029/94JC01228>.
- Di Lorenzo, Emanuele, and Nathan Mantua. "Multi-Year Persistence of the 2014/15 North Pacific Marine Heatwave." *Nature Climate Change* 6, no. 11 (November 2016): 1042–47. <https://doi.org/10.1038/nclimate3082>.
- Diaz, Robert J., and Rutger Rosenberg. "Spreading Dead Zones and Consequences for Marine Ecosystems." *Science* 321, no. 5891 (August 15, 2008): 926–29. <https://doi.org/10.1126/science.1156401>.

- Diaz, Robert, and Rutger Rosenberg. "Marine Benthic Hypoxia: A Review of Its Ecological Effects and the Behavioural Response of Benthic Macrofauna." *Oceanography and Marine Biology. An Annual Review [Oceanogr. Mar. Biol. Annu. Rev.]* 33, (January 1, 1995): 245–303.
- Doney, Scott C., D. Shallin Busch, Sarah R. Cooley, and Kristy J. Kroeker. "The Impacts of Ocean Acidification on Marine Ecosystems and Reliant Human Communities." *Annual Review of Environment and Resources* 45, no. 1 (2020): 83–112. <https://doi.org/10.1146/annurev-environ-012320-083019>.
- Doney, Scott C., Victoria J. Fabry, Richard A. Feely, and Joan A. Kleypas. "Ocean Acidification: The Other CO₂ Problem." *Annual Review of Marine Science* 1, no. 1 (2009): 169–92. <https://doi.org/10.1146/annurev.marine.010908.163834>.
- Dorman, Clive E., and Clinton D. Winant. "Buoy Observations of the Atmosphere along the West Coast of the United States, 1981–1990." *Journal of Geophysical Research* 100, no. C8 (1995): 16029. <https://doi.org/10.1029/95JC00964>.
- Dracup, John A., and Ercan Kahya. "The Relationships between U.S. Streamflow and La Niña Events." *Water Resources Research* 30, no. 7 (1994): 2133–41. <https://doi.org/10.1029/94WR00751>.
- Dussin, R., E.N. Curchitser, C.A. Stock, and N. Van Oostende. "Biogeochemical Drivers of Changing Hypoxia in the California Current Ecosystem." *Deep Sea Research Part II: Topical Studies in Oceanography* 169–170 (November 2019): 104590. <https://doi.org/10.1016/j.dsr2.2019.05.013>.
- Echevin, Vincent, Katerina Goubanova, Ali Belmadani, and Boris Dewitte. "Sensitivity of the Humboldt Current System to Global Warming: A Downscaling Experiment of the IPSL-CM4 Model." *Climate Dynamics* 38, no. 3 (February 1, 2012): 761–74. <https://doi.org/10.1007/s00382-011-1085-2>.
- Edson, James B., Venkata Jampana, Robert A. Weller, Sebastien P. Bigorre, Albert J. Plueddemann, Christopher W. Fairall, Scott D. Miller, Larry Mahrt, Dean Vickers, and Hans Hersbach. "On the

- Exchange of Momentum over the Open Ocean.” *Journal of Physical Oceanography* 43, no. 8 (August 1, 2013): 1589–1610. <https://doi.org/10.1175/JPO-D-12-0173.1>.
- Emerson, Steven, Sabine Mecking, and Jeffrey Abell. “The Biological Pump in the Subtropical North Pacific Ocean: Nutrient Sources, Redfield Ratios, and Recent Changes.” *Global Biogeochemical Cycles* 15, no. 3 (2001): 535–54. <https://doi.org/10.1029/2000GB001320>.
- Emerson, Steven, Yutaka W. Watanabe, Tsuneo Ono, and Sabine Mecking. “Temporal Trends in Apparent Oxygen Utilization in the Upper Pycnocline of the North Pacific: 1980–2000.” *Journal of Oceanography* 60, no. 1 (February 1, 2004): 139–47. <https://doi.org/10.1023/B:JOCE.0000038323.62130.a0>.
- Enns, T., P. F. Scholander, and E. D. Bradstreet. “Effect of Hydrostatic Pressure on Gases Dissolved in Water.” ACS Publications. American Chemical Society, May 1, 2002. World. <https://doi.org/10.1021/j100886a005>.
- Feely, Richard A., Remy R. Okazaki, Wei-Jun Cai, Nina Bednaršek, Simone R. Alin, Robert H. Byrne, and Andrea Fassbender. “The Combined Effects of Acidification and Hypoxia on PH and Aragonite Saturation in the Coastal Waters of the California Current Ecosystem and the Northern Gulf of Mexico.” *Continental Shelf Research* 152 (January 1, 2018): 50–60. <https://doi.org/10.1016/j.csr.2017.11.002>.
- Feely, Richard A., Christopher L. Sabine, J. Martin Hernandez-Ayon, Debby Ianson, and Burke Hales. “Evidence for Upwelling of Corrosive ‘Acidified’ Water onto the Continental Shelf.” *Science* 320, no. 5882 (June 13, 2008): 1490–92. <https://doi.org/10.1126/science.1155676>.
- Feely, Richard A., Christopher L. Sabine, Kitack Lee, Will Berelson, Joanie Kleypas, Victoria J. Fabry, and Frank J. Millero. “Impact of Anthropogenic CO₂ on the CaCO₃ System in the Oceans.” *Science* 305, no. 5682 (July 16, 2004): 362–66. <https://doi.org/10.1126/science.1097329>.

- Feely, Richard, Scott Doney, and Sarah Cooley. "Ocean Acidification: Present Conditions and Future Changes in a High-CO₂ World." *Oceanography* 22, no. 4 (December 1, 2009): 36–47.
<https://doi.org/10.5670/oceanog.2009.95>.
- Fewings, Melanie R., Libe Washburn, Clive E. Dorman, Christopher Gotschalk, and Kelly Lombardo. "Synoptic Forcing of Wind Relaxations at Pt. Conception, California." *Journal of Geophysical Research: Oceans* 121, no. 8 (2016): 5711–30. <https://doi.org/10.1002/2016JC011699>.
- Flament, P. "A State Variable for Characterizing Water Masses and Their Diffusive Stability: Spiciness." *Progress in Oceanography* 54, no. 1–4 (July 2002): 493–501.
[https://doi.org/10.1016/S0079-6611\(02\)00065-4](https://doi.org/10.1016/S0079-6611(02)00065-4).
- Flynn, R. F., J. Granger, J. A. Veitch, S. Siedlecki, J. M. Burger, K. Pillay, and S. E. Fawcett. "On-Shelf Nutrient Trapping Enhances the Fertility of the Southern Benguela Upwelling System." *Journal of Geophysical Research: Oceans* 125, no. 6 (2020): e2019JC015948.
<https://doi.org/10.1029/2019JC015948>.
- Foreman, M.G.G., D.K. Lee, J. Morrison, S. Macdonald, D. Barnes, and I.V. Williams. "Simulations and Retrospective Analyses of Fraser Watershed Flows and Temperatures." *Atmosphere-Ocean* 39, no. 2 (June 1, 2001): 89–105. <https://doi.org/10.1080/07055900.2001.9649668>.
- Fritze, Holger, Iris T. Stewart, and Edzer Pebesma. "Shifts in Western North American Snowmelt Runoff Regimes for the Recent Warm Decades." *Journal of Hydrometeorology* 12, no. 5 (October 1, 2011): 989–1006. <https://doi.org/10.1175/2011JHM1360.1>.
- Gan, Jianping, and J. S. Allen. "A Modeling Study of Shelf Circulation off Northern California in the Region of the Coastal Ocean Dynamics Experiment 2. Simulations and Comparisons with Observations." *Journal of Geophysical Research: Oceans* 107, no. C11 (2002): 5-1-5–21.
<https://doi.org/10.1029/2001JC001190>.
- — —. "A Modeling Study of Shelf Circulation off Northern California in the Region of the Coastal Ocean Dynamics Experiment: Response to Relaxation of Upwelling Winds." *Journal of*

- Geophysical Research: Oceans* 107, no. C9 (2002): 6-1-6–31.
<https://doi.org/10.1029/2000JC000768>.
- — —. “Modeling Upwelling Circulation off the Oregon Coast.” *Journal of Geophysical Research: Oceans* 110, no. C10 (2005). <https://doi.org/10.1029/2004JC002692>.
- García Berdeal, I., B. M. Hickey, and M. Kawase. “Influence of Wind Stress and Ambient Flow on a High Discharge River Plume.” *Journal of Geophysical Research: Oceans* 107, no. C9 (2002): 13-1-13–24. <https://doi.org/10.1029/2001JC000932>.
- Garcia, Herncin E., and Louis I. Gordon. “Oxygen Solubility in Seawater: Better Fitting Equations.” *Limnology and Oceanography* 37, no. 6 (1992): 1307–12.
<https://doi.org/10.4319/lo.1992.37.6.1307>.
- García-Reyes, M., and J. Largier. “Observations of Increased Wind-Driven Coastal Upwelling off Central California.” *Journal of Geophysical Research: Oceans* 115, no. C4 (2010).
<https://doi.org/10.1029/2009JC005576>.
- García-Reyes, M., and J. L. Largier. “Seasonality of Coastal Upwelling off Central and Northern California: New Insights, Including Temporal and Spatial Variability.” *Journal of Geophysical Research: Oceans* 117, no. C3 (2012). <https://doi.org/10.1029/2011JC007629>.
- García-Reyes, Marisol, William J. Sydeman, David S. Schoeman, Ryan R. Rykaczewski, Bryan A. Black, Albertus J. Smit, and Steven J. Bograd. “Under Pressure: Climate Change, Upwelling, and Eastern Boundary Upwelling Ecosystems.” *Frontiers in Marine Science* 2 (2015).
<https://www.frontiersin.org/article/10.3389/fmars.2015.00109>.
- Gentemann, Chelle L., Melanie R. Fewings, and Marisol García-Reyes. “Satellite Sea Surface Temperatures along the West Coast of the United States during the 2014–2016 Northeast Pacific Marine Heat Wave.” *Geophysical Research Letters* 44, no. 1 (2017): 312–19.
<https://doi.org/10.1002/2016GL071039>.

- Gershunov, Alexander, Tim P. Barnett, and Daniel R. Cayan. "North Pacific Interdecadal Oscillation Seen as Factor in ENSO-Related North American Climate Anomalies." *Eos, Transactions American Geophysical Union* 80, no. 3 (1999): 25–30. <https://doi.org/10.1029/99EO00019>.
- Geyer, W. R., and G. A. Cannon. "Sill Processes Related to Deep Water Renewal in a Fjord." *Journal of Geophysical Research: Oceans* 87, no. C10 (1982): 7985–96. <https://doi.org/10.1029/JC087iC10p07985>.
- Giddings, S. N., and P. MacCready. "Reverse Estuarine Circulation Due to Local and Remote Wind Forcing, Enhanced by the Presence of Along-Coast Estuaries." *Journal of Geophysical Research: Oceans* 122, no. 12 (2017): 10184–205. <https://doi.org/10.1002/2016JC012479>.
- Giddings, S. N., P. MacCready, B. M. Hickey, N. S. Banas, K. A. Davis, S. A. Siedlecki, V. L. Trainer, R. M. Kudela, N. A. Pelland, and T. P. Connolly. "Hindcasts of Potential Harmful Algal Bloom Transport Pathways on the Pacific Northwest Coast." *Journal of Geophysical Research: Oceans* 119, no. 4 (2014): 2439–61. <https://doi.org/10.1002/2013JC009622>.
- Giorgio, Paul del, and Peter Williams. *Respiration in Aquatic Ecosystems*. OUP Oxford, 2005.
- Grantham, Brian A., Francis Chan, Karina J. Nielsen, David S. Fox, John A. Barth, Adriana Huyer, Jane Lubchenco, and Bruce A. Menge. "Upwelling-Driven Nearshore Hypoxia Signals Ecosystem and Oceanographic Changes in the Northeast Pacific." *Nature* 429, no. 6993 (June 2004): 749–54. <https://doi.org/10.1038/nature02605>.
- Gruber, Nicolas, Claudine Hauri, Zouhair Lachkar, Damian Loher, Thomas L. Frölicher, and Gian-Kasper Plattner. "Rapid Progression of Ocean Acidification in the California Current System." *Science* 337, no. 6091 (July 13, 2012): 220–23. <https://doi.org/10.1126/science.1216773>.
- Hales, Burke, Lee Karp-Boss, Alexander Perlin, and Patricia A. Wheeler. "Oxygen Production and Carbon Sequestration in an Upwelling Coastal Margin." *Global Biogeochemical Cycles* 20, no. 3 (2006). <https://doi.org/10.1029/2005GB002517>.

- Halle, Christopher M., and John L. Largier. "Surface Circulation Downstream of the Point Arena Upwelling Center." *Continental Shelf Research* 31, no. 12 (August 15, 2011): 1260–72. <https://doi.org/10.1016/j.csr.2011.04.007>.
- Hamlet, Alan F., Philip W. Mote, Martyn P. Clark, and Dennis P. Lettenmaier. "Effects of Temperature and Precipitation Variability on Snowpack Trends in the Western United States*." *Journal of Climate* 18, no. 21 (November 1, 2005): 4545–61. <https://doi.org/10.1175/JCLI3538.1>.
- Harris, Katherine E., Michael D. DeGrandpre, and Burke Hales. "Aragonite Saturation State Dynamics in a Coastal Upwelling Zone." *Geophysical Research Letters* 40, no. 11 (2013): 2720–25. <https://doi.org/10.1002/grl.50460>.
- Hickey, B. M. "Coastal Oceanography of Western North America from the Tip of Baja California to Vancouver Island." In *The Sea*, edited by K.H. Brink and A.R. Robinson, 11, Ch. 12:345–93. New York, NY: Wiley and Sons, Inc, 1998.
- — —. "Coastal Submarine Canyons." In P. Muller and D. Henderson (eds.), *Proceedings of the University of Hawaii 'Aha Huliko'a Workshop on Flow Topography Interactions*, p. 95–110. SOEST Special Publication. University of Hawaii, Honolulu, HI.
- Hickey, B. M., R. M. Kudela, J. D. Nash, K. W. Bruland, W. T. Peterson, P. MacCready, E. J. Lessard, et al. "River Influences on Shelf Ecosystems: Introduction and Synthesis." *Journal of Geophysical Research: Oceans* 115, no. C2 (2010). <https://doi.org/10.1029/2009JC005452>.
- Hickey, B., A. MacFadyen, W. Cochlan, R. Kudela, K. Bruland, and C. Trick. "Evolution of Chemical, Biological, and Physical Water Properties in the Northern California Current in 2005: Remote or Local Wind Forcing?" *Geophysical Research Letters* 33, no. 22 (2006). <https://doi.org/10.1029/2006GL026782>.
- Hickey, B., R. McCabe, S. Geier, E. Dever, and N. Kachel. "Three Interacting Freshwater Plumes in the Northern California Current System." *Journal of Geophysical Research: Oceans* 114, no. C2 (2009). <https://doi.org/10.1029/2008JC004907>.

- Hickey, Barbara, and Neil Banas. “Why Is the Northern End of the California Current System So Productive?” *Oceanography* 21, no. 4 (December 1, 2008): 90–107.
<https://doi.org/10.5670/oceanog.2008.07>.
- Hickey, Barbara M. “The California Current System—Hypotheses and Facts.” *Progress in Oceanography* 8, no. 4 (January 1979): 191–279. [https://doi.org/10.1016/0079-6611\(79\)90002-8](https://doi.org/10.1016/0079-6611(79)90002-8).
— — —. “The Response of a Steep-Sided, Narrow Canyon to Time-Variable Wind Forcing.” *Journal of Physical Oceanography* 27, no. 5 (May 1, 1997): 697–726. [https://doi.org/10.1175/1520-0485\(1997\)027<0697:TROASS>2.0.CO;2](https://doi.org/10.1175/1520-0485(1997)027<0697:TROASS>2.0.CO;2).
- Hickey, Barbara M., and Nancy E. Pola. “The Seasonal Alongshore Pressure Gradient on the West Coast of the United States.” *Journal of Geophysical Research: Oceans* 88, no. C12 (1983): 7623–33.
<https://doi.org/10.1029/JC088iC12p07623>.
- Hoegh-Guldberg, Ove, and John F. Bruno. “The Impact of Climate Change on the World’s Marine Ecosystems.” *Science* 328, no. 5985 (June 18, 2010): 1523–28.
<https://doi.org/10.1126/science.1189930>.
- Hofmann, A. F., E. T. Peltzer, P. M. Walz, and P. G. Brewer. “Hypoxia by Degrees: Establishing Definitions for a Changing Ocean.” *Deep Sea Research Part I: Oceanographic Research Papers* 58, no. 12 (December 1, 2011): 1212–26. <https://doi.org/10.1016/j.dsr.2011.09.004>.
- Howard, Evan M., Hartmut Frenzel, Fayçal Kessouri, Lionel Renault, Daniele Bianchi, James C. McWilliams, and Curtis Deutsch. “Attributing Causes of Future Climate Change in the California Current System With Multimodel Downscaling.” *Global Biogeochemical Cycles* 34, no. 11 (2020): e2020GB006646. <https://doi.org/10.1029/2020GB006646>.
- Huyer, Adriana. “Coastal Upwelling in the California Current System.” *Progress in Oceanography* 12, no. 3 (January 1, 1983): 259–84. [https://doi.org/10.1016/0079-6611\(83\)90010-1](https://doi.org/10.1016/0079-6611(83)90010-1).
- Huyer, Adriana, P. Michael Kosro, Steven J. Lentz, and Robert C. Beardsley. “Poleward Flow in the California Current System.” In *Poleward Flows Along Eastern Ocean Boundaries*, edited by S. J.

- Neshyba, Ch. N. K. Mooers, R. L. Smith, and R. T. Barber, 142–59. *Coastal and Estuarine Studies*. New York, NY: Springer New York, 1989. https://doi.org/10.1007/978-1-4613-8963-7_12.
- Jacox, M. G., and C. A. Edwards. “Upwelling Source Depth in the Presence of Nearshore Wind Stress Curl.” *Journal of Geophysical Research: Oceans* 117, no. C5 (2012). <https://doi.org/10.1029/2011JC007856>.
- Jacox, Michael G., Michael A. Alexander, Samantha Siedlecki, Ke Chen, Young-Oh Kwon, Stephanie Brodie, Ivonne Ortiz, et al. “Seasonal-to-Interannual Prediction of North American Coastal Marine Ecosystems: Forecast Methods, Mechanisms of Predictability, and Priority Developments.” *Progress in Oceanography* 183 (April 1, 2020): 102307. <https://doi.org/10.1016/j.pocean.2020.102307>.
- Jacox, Michael G., Steven J. Bograd, Elliott L. Hazen, and Jerome Fiechter. “Sensitivity of the California Current Nutrient Supply to Wind, Heat, and Remote Ocean Forcing.” *Geophysical Research Letters* 42, no. 14 (2015): 5950–57. <https://doi.org/10.1002/2015GL065147>.
- Jacox, Michael G., Elliott L. Hazen, Katherine D. Zaba, Daniel L. Rudnick, Christopher A. Edwards, Andrew M. Moore, and Steven J. Bograd. “Impacts of the 2015–2016 El Niño on the California Current System: Early Assessment and Comparison to Past Events.” *Geophysical Research Letters* 43, no. 13 (2016): 7072–80. <https://doi.org/10.1002/2016GL069716>.
- Jay, David A., Jiayi Pan, Philip M. Orton, and Alexander R. Horner-Devine. “Asymmetry of Columbia River Tidal Plume Fronts.” *Journal of Marine Systems* 78, no. 3 (October 2009): 442–59. <https://doi.org/10.1016/j.jmarsys.2008.11.015>.
- Johnstone, J.M., and N. Mantua. “La Niña Impacts on Pacific Northwest Climate in Spring: 2011 and the Historical Record. Paper Presented at 2nd Annual Pacific Northwest Climate Science Conference.” Presented at the 2nd Annual Pacific Northwest Climate Science Conference, University of Washington, Seattle, Washington, USA. Seattle, WA, USA, 2011.

- Kahya, Ercan, and John A. Dracup. "U.S. Streamflow Patterns in Relation to the El Niño/Southern Oscillation." *Water Resources Research* 29, no. 8 (1993): 2491–2503.
<https://doi.org/10.1029/93WR00744>.
- Kämpf, Jochen, and Piers Chapman. "The California Current Upwelling System." In *Upwelling Systems of the World: A Scientific Journey to the Most Productive Marine Ecosystems*, edited by Jochen Kämpf and Piers Chapman, 97–160. Cham: Springer International Publishing, 2016.
https://doi.org/10.1007/978-3-319-42524-5_4.
- Kaplan, David M., Chris Halle, Jeff Paduan, and John L. Largier. "Surface Currents during Anomalous Upwelling Seasons off Central California." *Journal of Geophysical Research: Oceans* 114, no. C12 (2009). <https://doi.org/10.1029/2009JC005382>.
- Kaplan, David M., and John Largier. "HF Radar-Derived Origin and Destination of Surface Waters off Bodega Bay, California." *Deep Sea Research Part II: Topical Studies in Oceanography, The Role of Wind-Driven Flow in Shelf Productivity*, 53, no. 25 (December 1, 2006): 2906–30.
<https://doi.org/10.1016/j.dsr2.2006.07.012>.
- Keeling, Ralph F., Arne Körtzinger, and Nicolas Gruber. "Ocean Deoxygenation in a Warming World." *Annual Review of Marine Science* 2, no. 1 (2010): 199–229.
<https://doi.org/10.1146/annurev.marine.010908.163855>.
- Krause, Jeffrey W., Mark A. Brzezinski, John L. Largier, Heather M. McNair, Michael Maniscalco, Kay D. Bidle, Andrew E. Allen, and Kimberlee Thamatrakoln. "The Interaction of Physical and Biological Factors Drives Phytoplankton Spatial Distribution in the Northern California Current." *Limnology and Oceanography* 65, no. 9 (September 2020): 1974–89.
<https://doi.org/10.1002/lno.11431>.
- Kudela, Raphael, Neil Banas, John Barth, Elizabeth Frame, David Jay, John Largier, Evelyn Lessard, Tawnya Peterson, and Andrea Vander Woude. "New Insights into the Controls and Mechanisms of

- Plankton Productivity in Coastal Upwelling Waters of the Northern California Current System.” *Oceanography* 21, no. 4 (December 1, 2008): 46–59. <https://doi.org/10.5670/oceanog.2008.04>.
- Kunze, Eric, Leslie K. Rosenfeld, Glenn S. Carter, and Michael C. Gregg. “Internal Waves in Monterey Submarine Canyon.” *Journal of Physical Oceanography* 32, no. 6 (June 1, 2002): 1890–1913. [https://doi.org/10.1175/1520-0485\(2002\)032<1890:IWIMSC>2.0.CO;2](https://doi.org/10.1175/1520-0485(2002)032<1890:IWIMSC>2.0.CO;2).
- Lammers, Richard B., Jonathan W. Pundsack, and Alexander I. Shiklomanov. “Variability in River Temperature, Discharge, and Energy Flux from the Russian Pan-Arctic Landmass: RUSSIAN RIVER TEMPERATURE.” *Journal of Geophysical Research: Biogeosciences* 112, no. G4 (December 2007): n/a-n/a. <https://doi.org/10.1029/2006JG000370>.
- Landry, M. R., and B. M. Hickey. *Coastal Oceanography of Washington and Oregon*. Elsevier, 1989.
- Largier, J. L., B. A. Magnell, and C. D. Winant. “Subtidal Circulation over the Northern California Shelf.” *Journal of Geophysical Research: Oceans* 98, no. C10 (1993): 18147–79. <https://doi.org/10.1029/93JC01074>.
- Largier, J.L., C.A. Lawrence, M. Roughan, D.M. Kaplan, E.P. Dever, C.E. Dorman, R.M. Kudela, et al. “WEST: A Northern California Study of the Role of Wind-Driven Transport in the Productivity of Coastal Plankton Communities.” *Deep Sea Research Part II: Topical Studies in Oceanography* 53, no. 25–26 (December 2006): 2833–49. <https://doi.org/10.1016/j.dsr2.2006.08.018>.
- Largier, John L. “Considerations in Estimating Larval Dispersal Distances from Oceanographic Data.” *Ecological Applications* 13, no. sp1 (2003): 71–89. [https://doi.org/10.1890/1051-0761\(2003\)013\[0071:CIELDD\]2.0.CO;2](https://doi.org/10.1890/1051-0761(2003)013[0071:CIELDD]2.0.CO;2).
- Largier, John, Eric Wolanski, Jorg Imberger, and Malcolm Heron. “The Importance of Retention Zones in the Dispersal of Larvae.” *American Fisheries Society Symposium* 2004 (January 1, 2004): 105–22.

- Lentz, Steven J. “A Heat Budget for the Northern California Shelf during CODE 2.” *Journal of Geophysical Research: Oceans* 92, no. C13 (1987): 14491–509.
<https://doi.org/10.1029/JC092iC13p14491>.
- Lentz, Steven J., and David C. Chapman. “The Importance of Nonlinear Cross-Shelf Momentum Flux during Wind-Driven Coastal Upwelling.” *Journal of Physical Oceanography* 34, no. 11 (November 1, 2004): 2444–57. <https://doi.org/10.1175/JPO2644.1>.
- Lentz, Steven J., and Melanie R. Fewings. “The Wind- and Wave-Driven Inner-Shelf Circulation.” *Annual Review of Marine Science* 4, no. 1 (2012): 317–43. <https://doi.org/10.1146/annurev-marine-120709-142745>.
- Levin, L A, W Ekau, A J Gooday, F Jorissen, J J Middelburg, S W A Naqvi, C Neira, N N Rabalais, and J Zhang. “Effects of Natural and Human-Induced Hypoxia on Coastal Benthos,” 2009, 36.
- Levin, Lisa A. “Manifestation, Drivers, and Emergence of Open Ocean Deoxygenation.” *Annual Review of Marine Science* 10, no. 1 (2018): 229–60. <https://doi.org/10.1146/annurev-marine-121916-063359>.
- Levin, Lisa A., and Denise L. Breitburg. “Linking Coasts and Seas to Address Ocean Deoxygenation.” *Nature Climate Change* 5, no. 5 (May 2015): 401–3. <https://doi.org/10.1038/nclimate2595>.
- Levin, Lisa A., and Nadine Le Bris. “The Deep Ocean under Climate Change.” *Science (New York, N.Y.)* 350, no. 6262 (November 13, 2015): 766–68. <https://doi.org/10.1126/science.aad0126>.
- Logerwell, E.a., N. Mantua, P.w. Lawson, R.c. Francis, and V.n. Agostini. “Tracking Environmental Processes in the Coastal Zone for Understanding and Predicting Oregon Coho (Oncorhynchus Kisutch) Marine Survival.” *Fisheries Oceanography* 12, no. 6 (2003): 554–68.
<https://doi.org/10.1046/j.1365-2419.2003.00238.x>.
- Lohan, Maeve C., and Kenneth W. Bruland. “Elevated Fe(II) and Dissolved Fe in Hypoxic Shelf Waters off Oregon and Washington: An Enhanced Source of Iron to Coastal Upwelling Regimes.”

Environmental Science & Technology 42, no. 17 (September 1, 2008): 6462–68.

<https://doi.org/10.1021/es800144j>.

Lueck, Rolf G., and Thomas R. Osborn. “Turbulence Measurements in a Submarine Canyon.”

Continental Shelf Research 4, no. 6 (January 1, 1985): 681–98. [https://doi.org/10.1016/0278-4343\(85\)90036-6](https://doi.org/10.1016/0278-4343(85)90036-6).

Lund, Jay, Josue Medellin-Azuara, John Durand, and Kathleen Stone. “Lessons from California’s 2012–

2016 Drought.” *Journal of Water Resources Planning and Management* 144, no. 10 (October 1, 2018): 04018067. [https://doi.org/10.1061/\(ASCE\)WR.1943-5452.0000984](https://doi.org/10.1061/(ASCE)WR.1943-5452.0000984).

Lynn, Ronald J., Steven J. Bograd, Teresa K. Chereskin, and Adriana Huyer. “Seasonal Renewal of the

California Current: The Spring Transition off California.” *Journal of Geophysical Research: Oceans* 108, no. C8 (2003). <https://doi.org/10.1029/2003JC001787>.

Lynn, Ronald J., and James J. Simpson. “The California Current System: The Seasonal Variability of Its

Physical Characteristics.” *Journal of Geophysical Research: Oceans* 92, no. C12 (1987): 12947–66. <https://doi.org/10.1029/JC092iC12p12947>.

MacCready, P., R. M. McCabe, S. A. Siedlecki, M. Lorenz, S. N. Giddings, J. Bos, S. Albertson, N. S.

Banas, and S. Garnier. “Estuarine Circulation, Mixing, and Residence Times in the Salish Sea.” *Journal of Geophysical Research: Oceans* 126, no. 2 (2021): e2020JC016738.

<https://doi.org/10.1029/2020JC016738>.

MacCready, Parker, Neil S. Banas, Barbara M. Hickey, Edward P. Dever, and Yonggang Liu. “A Model

Study of Tide- and Wind-Induced Mixing in the Columbia River Estuary and Plume.” *Continental Shelf Research, Physics of Estuaries and Coastal Seas: Papers from the PECS 2006 Conference*, 29, no. 1 (January 15, 2009): 278–91. <https://doi.org/10.1016/j.csr.2008.03.015>.

Magnell, Bruce. “Circulation on the Northern California Shelf and Slope : Final Report of the Northern

California Coastal Circulation Study /, by Bruce A Magnell et al. | The Online Books Page.”

- Camarillo, California: U.S. Dept. of the Interior, Minerals Management Service, Pacific Outer Continental Shelf Region, 1991.
- Mazzini, Piero L. F., Craig M. Risien, John A. Barth, Stephen D. Pierce, Anatoli Erofeev, Edward P. Dever, P. Michael Kosro, Murray D. Levine, R. Kipp Shearman, and Michael F. Vardaro. “Anomalous Near-Surface Low-Salinity Pulses off the Central Oregon Coast.” *Scientific Reports* 5, no. 1 (November 26, 2015): 17145. <https://doi.org/10.1038/srep17145>.
- McCabe, Ryan M., Barbara M. Hickey, Raphael M. Kudela, Kathi A. Lefebvre, Nicolaus G. Adams, Brian D. Bill, Frances M. D. Gulland, Richard E. Thomson, William P. Cochlan, and Vera L. Trainer. “An Unprecedented Coastwide Toxic Algal Bloom Linked to Anomalous Ocean Conditions.” *Geophysical Research Letters* 43, no. 19 (2016): 10,366–10,376. <https://doi.org/10.1002/2016GL070023>.
- McClatchie, S., R. Goericke, R. Cosgrove, G. Auad, and R. Vetter. “Oxygen in the Southern California Bight: Multidecadal Trends and Implications for Demersal Fisheries.” *Geophysical Research Letters* 37, no. 19 (2010). <https://doi.org/10.1029/2010GL044497>.
- McDougall, T. J., D. R. Jackett, F. J. Millero, R. Pawlowicz, and P. M. Barker. “A Global Algorithm for Estimating Absolute Salinity.” *Ocean Science* 8, no. 6 (December 21, 2012): 1123–34. <https://doi.org/10.5194/os-8-1123-2012>.
- Mecking, Sabine, Chris Langdon, Richard A. Feely, Christopher L. Sabine, Curtis A. Deutsch, and Dong-Ha Min. “Climate Variability in the North Pacific Thermocline Diagnosed from Oxygen Measurements: An Update Based on the U.S. CLIVAR/CO₂ Repeat Hydrography Cruises: NORTH PACIFIC OXYGEN VARIABILITY.” *Global Biogeochemical Cycles* 22, no. 3 (September 2008): n/a-n/a. <https://doi.org/10.1029/2007GB003101>.
- Meinville, M., and Gregory C. Johnson. “Decadal Water-Property Trends in the California Undercurrent, with Implications for Ocean Acidification.” *Journal of Geophysical Research: Oceans* 118, no. 12 (2013): 6687–6703. <https://doi.org/10.1002/2013JC009299>.

- Melton, Christopher, Libe Washburn, and Chris Gotschalk. “Wind Relaxations and Poleward Flow Events in a Coastal Upwelling System on the Central California Coast.” *Journal of Geophysical Research: Oceans* 114, no. C11 (2009). <https://doi.org/10.1029/2009JC005397>.
- Moffitt, Sarah E., Russell A. Moffitt, Wilson Sauthoff, Catherine V. Davis, Kathryn Hewett, and Tessa M. Hill. “Paleoceanographic Insights on Recent Oxygen Minimum Zone Expansion: Lessons for Modern Oceanography.” *PLOS ONE* 10, no. 1 (January 28, 2015): e0115246. <https://doi.org/10.1371/journal.pone.0115246>.
- Monteiro, Pedro M S, Boris Dewitte, Mary I Scranton, Aurélien Paulmier, and Anja K van der Plas. “The Role of Open Ocean Boundary Forcing on Seasonal to Decadal-Scale Variability and Long-Term Change of Natural Shelf Hypoxia.” *Environmental Research Letters* 6, no. 2 (April 1, 2011): 025002. <https://doi.org/10.1088/1748-9326/6/2/025002>.
- Mote, Philip W., Sihan Li, Dennis P. Lettenmaier, Mu Xiao, and Ruth Engel. “Dramatic Declines in Snowpack in the Western US.” *Npj Climate and Atmospheric Science* 1, no. 1 (March 2, 2018): 1–6. <https://doi.org/10.1038/s41612-018-0012-1>.
- NOAA. “The California Current Marine Heatwave Tracker - Blobtracker | Integrated Ecosystem Assessment.” The California Current Marine Heatwave Tracker - Blobtracker, 2022. <https://www.integratedecosystemassessment.noaa.gov/regions/california-current/california-current-marine-heatwave-tracker-blobtracker>.
- Ono, T., T. Midorikawa, Y. W. Watanabe, K. Tadokoro, and T. Saino. “Temporal Increases of Phosphate and Apparent Oxygen Utilization in the Subsurface Waters of Western Subarctic Pacific from 1968 to 1998.” *Geophysical Research Letters* 28, no. 17 (2001): 3285–88. <https://doi.org/10.1029/2001GL012948>.
- Pacific Climate Impacts Consortium. “Timing & Volume of River Flow - Environmental Reporting BC.” Long-term Change in Timing & Volume of River Flow in B.C. Province of British Columbia. Accessed January 1, 2022. <https://www.env.gov.bc.ca/soe/indicators/climate-change/rivers.html>.

- Pauly, D., and V. Christensen. "Primary Production Required to Sustain Global Fisheries." *Nature* 374, no. 6519 (March 1995): 255–57. <https://doi.org/10.1038/374255a0>.
- Peterson, William, Jennifer Fisher, Jay Peterson, Cheryl Morgan, Brian Burke, and Kurt Fresh. "Applied Fisheries Oceanography: Ecosystem Indicators of Ocean Conditions Inform Fisheries Management in the California Current." *Oceanography* 27, no. 4 (December 1, 2014): 80–89. <https://doi.org/10.5670/oceanog.2014.88>.
- Peterson, W.T., and NOAA Fisheries. "Local Biological Indicators | NOAA Fisheries." Biological conditions experienced by juvenile salmon entering the northern California Current., April 28, 2022. West Coast. <https://www.fisheries.noaa.gov/west-coast/science-data/local-biological-indicators>.
- Pickett, Mark H., and Jeffrey D. Paduan. "Ekman Transport and Pumping in the California Current Based on the U.S. Navy's High-Resolution Atmospheric Model (COAMPS)." *Journal of Geophysical Research: Oceans* 108, no. C10 (2003). <https://doi.org/10.1029/2003JC001902>.
- Pierce, Stephen D, and John A Barth. "Combined Plot of All Years, Cumulative Wind Stress." Wind stress, cumulative wind stress, and spring transition dates: data products for Oregon upwelling-related research, 2022. <http://shadow.ceoas.oregonstate.edu/damp/windstress/2017.html>.
- Pierce, Stephen D., John A. Barth, R. Kipp Shearman, and Anatoli Y. Erofeev. "Declining Oxygen in the Northeast Pacific." *Journal of Physical Oceanography* 42, no. 3 (March 1, 2012): 495–501. <https://doi.org/10.1175/JPO-D-11-0170.1>.
- Pitcher, Grant C., Arturo Aguirre-Velarde, Denise Breitburg, Jorge Cardich, Jacob Carstensen, Daniel J. Conley, Boris Dewitte, et al. "System Controls of Coastal and Open Ocean Oxygen Depletion." *Progress in Oceanography* 197 (September 1, 2021): 102613. <https://doi.org/10.1016/j.pocean.2021.102613>.

- Poon, Ying-Keung, and Ole Secher Madsen. "A Two-Layer Wind-Driven Coastal Circulation Model." *Journal of Geophysical Research: Oceans* 96, no. C2 (1991): 2535–48.
<https://doi.org/10.1029/90JC02286>.
- Pozo Buil, Mercedes, and Emanuele Di Lorenzo. "Decadal Changes in Gulf of Alaska Upwelling Source Waters." *Geophysical Research Letters* 42, no. 5 (2015): 1488–95.
<https://doi.org/10.1002/2015GL063191>.
- — —. "Decadal Dynamics and Predictability of Oxygen and Subsurface Tracers in the California Current System." *Geophysical Research Letters* 44, no. 9 (2017): 4204–13.
<https://doi.org/10.1002/2017GL072931>.
- Pozo Buil, Mercedes, Michael G. Jacox, Jerome Fiechter, Michael A. Alexander, Steven J. Bograd, Enrique N. Curchitser, Christopher A. Edwards, Ryan R. Rykaczewski, and Charles A. Stock. "A Dynamically Downscaled Ensemble of Future Projections for the California Current System." *Frontiers in Marine Science* 8 (2021).
<https://www.frontiersin.org/article/10.3389/fmars.2021.612874>.
- Pringle, James M., and Edward P. Dever. "Dynamics of Wind-Driven Upwelling and Relaxation between Monterey Bay and Point Arena: Local-, Regional-, and Gyre-Scale Controls." *Journal of Geophysical Research: Oceans* 114, no. C7 (2009). <https://doi.org/10.1029/2008JC005016>.
- Rabalais, N. N., R. J. Díaz, L. A. Levin, R. E. Turner, D. Gilbert, and J. Zhang. "Dynamics and Distribution of Natural and Human-Caused Hypoxia." *Biogeosciences* 7, no. 2 (February 12, 2010): 585–619. <https://doi.org/10.5194/bg-7-585-2010>.
- Redmond, Kelly T., and Roy W. Koch. "Surface Climate and Streamflow Variability in the Western United States and Their Relationship to Large-Scale Circulation Indices." *Water Resources Research* 27, no. 9 (1991): 2381–99. <https://doi.org/10.1029/91WR00690>.

- Ren, Alice S., Fei Chai, Huijie Xue, David M. Anderson, and Francisco P. Chavez. “A Sixteen-Year Decline in Dissolved Oxygen in the Central California Current.” *Scientific Reports* 8, no. 1 (December 2018). <https://doi.org/10.1038/s41598-018-25341-8>.
- Ren, Alice S., and Daniel L. Rudnick. “Temperature and Salinity Extremes from 2014-2019 in the California Current System and Its Source Waters.” *Communications Earth & Environment* 2, no. 1 (March 19, 2021): 1–9. <https://doi.org/10.1038/s43247-021-00131-9>.
- Rixen, Tim, Niko Lahajnar, Tarron Lamont, Rolf Koppelman, Bettina Martin, Justus E. E. van Beusekom, Claire Siddiqui, Keshnee Pillay, and Luisa Meiritz. “Oxygen and Nutrient Trapping in the Southern Benguela Upwelling System.” *Frontiers in Marine Science* 8 (2021). <https://www.frontiersin.org/article/10.3389/fmars.2021.730591>.
- Roquet, F., G. Madec, Trevor J. McDougall, and Paul M. Barker. “Accurate Polynomial Expressions for the Density and Specific Volume of Seawater Using the TEOS-10 Standard.” *Ocean Modelling* 90 (June 2015): 29–43. <https://doi.org/10.1016/j.ocemod.2015.04.002>.
- Rosenfeld, L.K. “CODE-1: Moored Array and Large-Scale Data Report.” Technical Report. WHOI-85-35, 1983.
- Roughan, Moninya, Newell Garfield, John Largier, Edward Dever, Clive Dorman, Dwight Peterson, and Jeff Dorman. “Transport and Retention in an Upwelling Region: The Role of across-Shelf Structure.” *Deep Sea Research Part II: Topical Studies in Oceanography*, The Role of Wind-Driven Flow in Shelf Productivity, 53, no. 25 (December 1, 2006): 2931–55. <https://doi.org/10.1016/j.dsr2.2006.07.015>.
- Ryan, J. P., R. M. Kudela, J. M. Birch, M. Blum, H. A. Bowers, F. P. Chavez, G. J. Doucette, et al. “Causality of an Extreme Harmful Algal Bloom in Monterey Bay, California, during the 2014–2016 Northeast Pacific Warm Anomaly.” *Geophysical Research Letters* 44, no. 11 (2017): 5571–79. <https://doi.org/10.1002/2017GL072637>.

- Rykaczewski, Ryan R., John P. Dunne, William J. Sydeman, Marisol García-Reyes, Bryan A. Black, and Steven J. Bograd. “Poleward Displacement of Coastal Upwelling-Favorable Winds in the Ocean’s Eastern Boundary Currents through the 21st Century.” *Geophysical Research Letters* 42, no. 15 (2015): 6424–31. <https://doi.org/10.1002/2015GL064694>.
- Ryther, John H. “Photosynthesis and Fish Production in the Sea.” *Science* 166, no. 3901 (1969): 72–76.
- Sanford, Eric, Jacqueline L. Sones, Marisol García-Reyes, Jeffrey H. R. Goddard, and John L. Largier. “Widespread Shifts in the Coastal Biota of Northern California during the 2014–2016 Marine Heatwaves.” *Scientific Reports* 9, no. 1 (December 2019): 4216. <https://doi.org/10.1038/s41598-019-40784-3>.
- Scannell, H. A., G. C. Johnson, L. Thompson, J. M. Lyman, and S. C. Riser. “Subsurface Evolution and Persistence of Marine Heatwaves in the Northeast Pacific.” *Geophysical Research Letters* 47, no. 23 (2020): e2020GL090548. <https://doi.org/10.1029/2020GL090548>.
- Schmidtko, Sunke, Lothar Stramma, and Martin Visbeck. “Decline in Global Oceanic Oxygen Content during the Past Five Decades.” *Nature* 542, no. 7641 (February 2017): 335–39. <https://doi.org/10.1038/nature21399>.
- Schroeder, Isaac D., Jarrod A. Santora, Steven J. Bograd, Elliott L. Hazen, Keith M. Sakuma, Andrew M. Moore, Christopher A. Edwards, Brian K. Wells, and John C. Field. “Source Water Variability as a Driver of Rockfish Recruitment in the California Current Ecosystem: Implications for Climate Change and Fisheries Management.” *Canadian Journal of Fisheries and Aquatic Sciences* 76, no. 6 (June 2019): 950–60. <https://doi.org/10.1139/cjfas-2017-0480>.
- Send, Uwe. “Vorticity and Instability during Flow Reversals on the Continental Shelf.” *Journal of Physical Oceanography* 19, no. 10 (October 1, 1989): 1620–33. [https://doi.org/10.1175/1520-0485\(1989\)019<1620:VAIDFR>2.0.CO;2](https://doi.org/10.1175/1520-0485(1989)019<1620:VAIDFR>2.0.CO;2).

- Send, Uwe, Robert C. Beardsley, and Clinton D. Winant. "Relaxation from Upwelling in the Coastal Ocean Dynamics Experiment." *Journal of Geophysical Research: Oceans* 92, no. C2 (1987): 1683–98. <https://doi.org/10.1029/JC092iC02p01683>.
- Send, Uwe, and SungHyun Nam. "Relaxation from Upwelling: The Effect on Dissolved Oxygen on the Continental Shelf: RELAXATION FROM UPWELLING." *Journal of Geophysical Research: Oceans* 117, no. C4 (April 2012): n/a-n/a. <https://doi.org/10.1029/2011JC007517>.
- Siedlecki, S. A., N. S. Banas, K. A. Davis, S. Giddings, B. M. Hickey, P. MacCready, T. Connolly, and S. Geier. "Seasonal and Interannual Oxygen Variability on the Washington and Oregon Continental Shelves." *Journal of Geophysical Research: Oceans* 120, no. 2 (2015): 608–33. <https://doi.org/10.1002/2014JC010254>.
- Siedlecki, Samantha A., Darren Pilcher, Evan M. Howard, Curtis Deutsch, Parker MacCready, Emily L. Norton, Hartmut Frenzel, et al. "Coastal Processes Modify Projections of Some Climate-Driven Stressors in the California Current System." *Biogeosciences* 18, no. 9 (May 11, 2021): 2871–90. <https://doi.org/10.5194/bg-18-2871-2021>.
- Simpson, James J. "On the Exchange of Oxygen and Carbon Dioxide between Ocean and Atmosphere in an Eastern Boundary Current." In *Gas Transfer at Water Surfaces*, edited by Wilfried Brutsaert and Gerhard H. Jirka, 505–14. Water Science and Technology Library. Dordrecht: Springer Netherlands, 1984. https://doi.org/10.1007/978-94-017-1660-4_46.
- Singh, Deepti, Daniel L. Swain, Justin S. Mankin, Daniel E. Horton, Leif N. Thomas, Bala Rajaratnam, and Noah S. Diffenbaugh. "Recent Amplification of the North American Winter Temperature Dipole." *Journal of Geophysical Research: Atmospheres* 121, no. 17 (2016): 9911–28. <https://doi.org/10.1002/2016JD025116>.
- Smith, Robert L. "A Comparison of the Structure and Variability of the Flow Field in Three Coastal Upwelling Regions: Oregon, Northwest Africa, and Peru." In *Coastal Upwelling*, 107–18. American Geophysical Union (AGU), 1981. <https://doi.org/10.1029/CO001p0107>.

- Stewart, Iris T., Daniel R. Cayan, and Michael D. Dettinger. "1136 JOURNAL OF CLIMATE VOLUME 18 Changes toward Earlier Streamflow Timing across Western North America," 2004.
- Stone, Hally B., Neil S. Banas, Parker MacCready, Raphael M. Kudela, and Bridget Ovall. "Linking Chlorophyll Concentration and Wind Patterns Using Satellite Data in the Central and Northern California Current System." *Frontiers in Marine Science* 7 (2020).
<https://www.frontiersin.org/article/10.3389/fmars.2020.551562>.
- Stramma, Lothar, Gregory C. Johnson, Janet Sprintall, and Volker Mohrholz. "Expanding Oxygen-Minimum Zones in the Tropical Oceans." *Science (New York, N.Y.)* 320, no. 5876 (May 2, 2008): 655–58. <https://doi.org/10.1126/science.1153847>.
- Strub, P. T., J. S. Allen, A. Huyer, R. L. Smith, and R. C. Beardsley. "Seasonal Cycles of Currents, Temperatures, Winds, and Sea Level over the Northeast Pacific Continental Shelf: 35°N to 48°N." *Journal of Geophysical Research: Oceans* 92, no. C2 (1987): 1507–26.
<https://doi.org/10.1029/JC092iC02p01507>.
- Strub, P. Ted, P. Michael Kosro, and Adriana Huyer. "The Nature of the Cold Filaments in the California Current System." *Journal of Geophysical Research* 96, no. C8 (1991): 14743.
<https://doi.org/10.1029/91JC01024>.
- Sutherland, David A., Parker MacCready, Neil S. Banas, and Lucy F. Smedstad. "A Model Study of the Salish Sea Estuarine Circulation." *Journal of Physical Oceanography* 41, no. 6 (June 1, 2011): 1125–43. <https://doi.org/10.1175/2011JPO4540.1>.
- Swain, Daniel L., Deepti Singh, Daniel E. Horton, Justin S. Mankin, Tristan C. Ballard, and Noah S. Diffenbaugh. "Remote Linkages to Anomalous Winter Atmospheric Ridging Over the Northeastern Pacific." *Journal of Geophysical Research: Atmospheres* 122, no. 22 (2017): 12,194–12,209. <https://doi.org/10.1002/2017JD026575>.

- — — . “Remote Linkages to Anomalous Winter Atmospheric Ridging Over the Northeastern Pacific.”
Journal of Geophysical Research: Atmospheres 122, no. 22 (2017): 12,194–12,209.
<https://doi.org/10.1002/2017JD026575>.
- Sydeman, W. J., M. García-Reyes, D. S. Schoeman, R. R. Rykaczewski, S. A. Thompson, B. A. Black, and S. J. Bograd. “Climate Change and Wind Intensification in Coastal Upwelling Ecosystems.”
Science 345, no. 6192 (July 4, 2014): 77–80. <https://doi.org/10.1126/science.1251635>.
- Talley, L.D., R.A. Feely, B.M. Sloyan, R. Wanninkhof, M.O. Baringer, J.L. Bullister, C.A. Carlson, et al. “Changes in Ocean Heat, Carbon Content, and Ventilation: A Review of the First Decade of GO-SHIP Global Repeat Hydrography.” *Annual Review of Marine Science* 8, no. 1 (2016): 185–215. <https://doi.org/10.1146/annurev-marine-052915-100829>.
- Talley, Lynne D., George L. Pickard, William J. Emery, and James H. Swift. “Chapter 10 - Pacific Ocean.” In *Descriptive Physical Oceanography (Sixth Edition)*, edited by Lynne D. Talley, George L. Pickard, William J. Emery, and James H. Swift, 303–62. Boston: Academic Press, 2011.
<https://doi.org/10.1016/B978-0-7506-4552-2.10010-1>.
- Thomas, John H. “A Theory of Steady Wind-Driven Currents in Shallow Water with Variable Eddy Viscosity.” *Journal of Physical Oceanography* 5, no. 1 (January 1, 1975): 136–42.
[https://doi.org/10.1175/1520-0485\(1975\)005<0136:ATOSWD>2.0.CO;2](https://doi.org/10.1175/1520-0485(1975)005<0136:ATOSWD>2.0.CO;2).
- Thompson, Andrew R, Sam McClatchie, Robert M Suryan, Jane Dolliver, and Stephanie Loredó. “State of the California Current 2017 – 18: still not quite normal in the north and getting interesting in the south.” 59 (2018): 66.
- Thomson, Richard E., and Maxim V. Krassovski. “Poleward Reach of the California Undercurrent Extension.” *Journal of Geophysical Research: Oceans* 115, no. C9 (2010).
<https://doi.org/10.1029/2010JC006280>.

- Thomson, Richard E., Steven F. Mihály, and Evgueni A. Kulikov. “Estuarine versus Transient Flow Regimes in Juan de Fuca Strait.” *Journal of Geophysical Research: Oceans* 112, no. C9 (2007). <https://doi.org/10.1029/2006JC003925>.
- Trowbridge, John H., and Steven J. Lentz. “The Bottom Boundary Layer.” *Annual Review of Marine Science* 10, no. 1 (2018): 397–420. <https://doi.org/10.1146/annurev-marine-121916-063351>.
- Turi, G., Z. Lachkar, and N. Gruber. “Spatiotemporal Variability and Drivers of $p\text{CO}_2$ and Air–Sea CO_2 Fluxes in the California Current System: An Eddy-Resolving Modeling Study.” *Biogeosciences* 11, no. 3 (February 6, 2014): 671–90. <https://doi.org/10.5194/bg-11-671-2014>.
- United States Geological Survey (USGS). “Explanations for the National Water Conditions,” 2021. https://water.usgs.gov/nwc/explain_data.html.
- Vander Woude, A. J., J. L. Largier, and R. M. Kudela. “Nearshore Retention of Upwelled Waters North and South of Point Reyes (Northern California)—Patterns of Surface Temperature and Chlorophyll Observed in CoOP WEST.” *Deep Sea Research Part II: Topical Studies in Oceanography, The Role of Wind-Driven Flow in Shelf Productivity*, 53, no. 25 (December 1, 2006): 2985–98. <https://doi.org/10.1016/j.dsr2.2006.07.003>.
- Varela, R., I. Álvarez, F. Santos, M. deCastro, and M. Gómez-Gesteira. “Has Upwelling Strengthened along Worldwide Coasts over 1982-2010?” *Scientific Reports* 5, no. 1 (May 8, 2015): 10016. <https://doi.org/10.1038/srep10016>.
- Wain, D. J., M. C. Gregg, M. H. Alford, R.-C. Lien, R. A. Hall, and G. S. Carter. “Propagation and Dissipation of the Internal Tide in Upper Monterey Canyon.” *Journal of Geophysical Research: Oceans* 118, no. 10 (2013): 4855–77. <https://doi.org/10.1002/jgrc.20368>.
- Wang, Daiwei, Tarik C. Gouhier, Bruce A. Menge, and Auroop R. Ganguly. “Intensification and Spatial Homogenization of Coastal Upwelling under Climate Change.” *Nature* 518, no. 7539 (February 2015): 390–94. <https://doi.org/10.1038/nature14235>.

- Ware, Daniel M., and Richard E. Thomson. “Bottom-Up Ecosystem Trophic Dynamics Determine Fish Production in the Northeast Pacific.” *Science* 308, no. 5726 (May 27, 2005): 1280–84.
<https://doi.org/10.1126/science.1109049>.
- Watanabe, Y. W., T. Ono, A. Shimamoto, T. Sugimoto, M. Wakita, and S. Watanabe. “Probability of a Reduction in the Formation Rate of the Subsurface Water in the North Pacific during the 1980s and 1990s.” *Geophysical Research Letters* 28, no. 17 (2001): 3289–92.
<https://doi.org/10.1029/2001GL013212>.
- Weber, Edward D., Toby D. Auth, Simone Baumann-Pickering, Timothy R. Baumgartner, Eric P. Bjorkstedt, Steven J. Bograd, Brian J. Burke, et al. “State of the California Current 2019–2020: Back to the Future With Marine Heatwaves?” *Frontiers in Marine Science* 8 (2021).
<https://www.frontiersin.org/article/10.3389/fmars.2021.709454>.
- Whitney, F. A., and H. J. Freeland. “Variability in Upper-Ocean Water Properties in the NE Pacific Ocean.” *Deep Sea Research Part II: Topical Studies in Oceanography* 46, no. 11 (November 1, 1999): 2351–70. [https://doi.org/10.1016/S0967-0645\(99\)00067-3](https://doi.org/10.1016/S0967-0645(99)00067-3).
- Whitney, Frank A., Steven J. Bograd, and Tsuneo Ono. “Nutrient Enrichment of the Subarctic Pacific Ocean Pycnocline.” *Geophysical Research Letters* 40, no. 10 (2013): 2200–2205.
<https://doi.org/10.1002/grl.50439>.
- Whitney, Frank A., Howard J. Freeland, and Marie Robert. “Persistently Declining Oxygen Levels in the Interior Waters of the Eastern Subarctic Pacific.” *Progress in Oceanography*, Time Series of the Northeast Pacific, 75, no. 2 (October 1, 2007): 179–99.
<https://doi.org/10.1016/j.pocean.2007.08.007>.
- Wilkerson, Frances P., Adria M. Lassiter, Richard C. Dugdale, Albert Marchi, and Victoria E. Hogue. “The Phytoplankton Bloom Response to Wind Events and Upwelled Nutrients during the CoOP WEST Study.” *Deep Sea Research Part II: Topical Studies in Oceanography*, The Role of Wind-

- Driven Flow in Shelf Productivity, 53, no. 25 (December 1, 2006): 3023–48.
<https://doi.org/10.1016/j.dsr2.2006.07.007>.
- Wing, Sr, Lw Botsford, JI Largier, and Le Morgan. “Spatial Structure of Relaxation Events and Crab Settlement in the Northern California Upwelling System.” *Marine Ecology Progress Series* 128 (1995): 199–211. <https://doi.org/10.3354/meps128199>.
- Wing, Stephen R., Louis W. Botsford, Stephen V. Ralston, and John L. Largier. “Meroplanktonic Distribution and Circulation in a Coastal Retention Zone of the Northern California Upwelling System.” *Limnology and Oceanography* 43, no. 7 (1998): 1710–21.
<https://doi.org/10.4319/lo.1998.43.7.1710>.
- Wing, Stephen R., John L. Largier, Louis W. Botsford, and James F. Quinn. “Settlement and Transport of Benthic Invertebrates in an Intermittent Upwelling Region.” *Limnology and Oceanography* 40, no. 2 (1995): 316–29. <https://doi.org/10.4319/lo.1995.40.2.0316>.
- Xu, Zhongfeng, Ying Han, and Zongliang Yang. “Dynamical Downscaling of Regional Climate: A Review of Methods and Limitations.” *Science China Earth Sciences* 62, no. 2 (February 1, 2019): 365–75. <https://doi.org/10.1007/s11430-018-9261-5>.
- Yokomizo, Hiroyuki, Louis W. Botsford, Matthew D. Holland, Cathryn A. Lawrence, and Alan Hastings. “Optimal Wind Patterns for Biological Production in Shelf Ecosystems Driven by Coastal Upwelling.” *Theoretical Ecology* 3, no. 1 (February 1, 2010): 53–63.
<https://doi.org/10.1007/s12080-009-0053-5>.
- Zaba, Katherine D., and Daniel L. Rudnick. “The 2014–2015 Warming Anomaly in the Southern California Current System Observed by Underwater Gliders.” *Geophysical Research Letters* 43, no. 3 (2016): 1241–48. <https://doi.org/10.1002/2015GL067550>.
- Zaba, Katherine D., Daniel L. Rudnick, Bruce D. Cornuelle, Ganesh Gopalakrishnan, and Matthew R. Mazloff. “Volume and Heat Budgets in the Coastal California Current System: Means, Annual

Cycles, and Interannual Anomalies of 2014–16.” *Journal of Physical Oceanography* 50, no. 5 (May 1, 2020): 1435–53. <https://doi.org/10.1175/JPO-D-19-0271.1>.

Zhao, Zhongxiang, Matthew H. Alford, Ren-Chieh Lien, Michael C. Gregg, and Glenn S. Carter.

“Internal Tides and Mixing in a Submarine Canyon with Time-Varying Stratification.” *Journal of Physical Oceanography* 42, no. 12 (December 1, 2012): 2121–42. <https://doi.org/10.1175/JPO-D-12-045.1>.